LOV domain signaling:
A study of LOV–LOV interactions

Dissertation
zur Erlangung des Doktorgrades der Naturwissenschaften
(Dr. rer. nat.)
der Fakultät für Chemie und Pharmazie
der Universität Regensburg

vorgelegt von
Kathrin Magerl
aus
München

im Jahr 2017

Die Arbeit wurde von Prof. Dr. Bernhard Dick angeleitet.
Das Promotionsgesuch wurde am 30.01.2017 eingereicht.
Das Promotionskolloquium fand am 21.04.2017 statt.

Prüfungsausschuss:

Vorsitzender:	Prof. Dr. Arno Pfitzner
1. Gutachter:	Prof. Dr. Bernhard Dick
2. Gutachter:	PD Dr. Tilman Kottke
weiterer Prüfer:	Prof. Dr. Frank-Michael Matysik

List of abbreviations

The following list contains all abbreviations repeatedly used in this thesis except SI units. The standard one or three letter code was used for amino acids and DNA bases.

A. thaliana	*Arbabidopsis thaliana* (At)
BLUF	blue light sensor using flavin adenine dinucleotide
bZIP	basic region leucine zipper
CCD	charge-coupled device
C. reinhardtii	*Chlamydomonas reinhardtii* (Cr)
CRY	cryptochrome
C-terminal	carboxy-terminal
cw	continuous wave
DADS	decay associated difference spectrum
DNA	deoxyribonucleic acid
E. coli	*Escherichia coli*
EDTA	ethylenediaminetetraacetic acid
EPR	electron paramagnetic resonance
eT	electron transfer
FAD	flavin adenine dinucleotide
FbFP	flavin-binding fluorescent protein
FDHW	full duration at half width
FMN	flavin mononucleotide
FP	fluorescent protein
FRET	Förster resonance energy transfer
FWHM	full width at half maximum
GFP	green fluorescent protein
HTH	helix-turn-helix

IR	infrared
LC	lumichrome
LED	light emitting diode
LOV	light-, oxygen-, voltage-sensitive
NHS	N-hydroxysuccinimide
N-terminal	amino-terminal
NWML	nominal molecular weight limit
MALS	multiangle light scattering
MD	molecular dynamics
PAS	PER-ARNT-SIM
PB	phosphate buffer
PCET	proton coupled electron transfer
Phot	phototropin
PMT	photomultiplier tube
pT	proton transfer
PtAureo1a	Aureochrome 1a *Phaeodactylum tricornutum*
RF	riboflavin
R. sphaeroides	*Rhodobacter sphaeroides* (Rs)
SAXS	small angle X-ray scattering
SEC	size exclusion chromatography
STK	serine/threonine kinase
SVD	singular value decomposition
TA	transient absorption
TCSPC	time-correlated single photon counting
TEV	Tobacco etch virus
UPLC	ultra performance liquid chromatography
UV	ultraviolet
UVR-8	UV resistance locus 8
VfAureo1	Aureochrome-1 *Vaucheria frigida*
Vis	visible
WCC	white collar complex

wt	wild type
ZTL	ZEITLUPE

Contents

1 Introduction

Sunlight is prerequisite for life on earth. All life processes depend directly or indirectly on this ever-present energy source. The ability to adapt and respond to environmental light is an evolutionary selection factor and has developed across all kingdoms of life. Light reception in nature is realized by photosensory proteins, which respond to the environmental stimulus light, providing the regulation of metabolic reactions and physiological functions.

The solar radiation reaching the earth's surface peaks in the blue-green range of the spectrum. Due to the optical properties of water, blue light between 420 nm and 500 nm penetrates deepest of all spectral ranges into the oceans, enabling organisms to make use of the light energy also below the sea level [1]. Hence, it is not surprising that many physiological responses in nature are induced only by blue and near ultraviolet (UV) light. First reports of the influence of blue light on plants were given as early as in the 19th century [2]. Amongst others, Julius von Sachs investigated plant growth under different light conditions. He used either colored glass or colored chemical solutions to provide red and blue light and observed differences in the biological plant response depending on the light color he used [3]. A few years later in 1880, Charles Darwin described experiments on phototropism and postulated that it cannot be induced by red light [4]. Over the next 100 years many studies on blue light-induced effects regarding plant growth were performed and a debate about the chromophore molecule responsible for the light absorption between carotenoids and flavins flared up [5]. Since no photoreceptor for blue light had been identified by then, the question could not be answered unambiguously. A milestone in the history of the investigation of blue light reception was the molecular identification of the photoreceptor cryptochrome cry1 from *Arabidopsis thaliana* in 1993 [6]. Only four years later, phototropin was identified in *Arabidopsis thaliana* and was shown to be responsible for phototropism [7, 8]. Since then great process has been made and a lot more blue light photoreceptors have been identified across almost all taxonomic groups.

A great number of physiological functions in nature are triggered by blue light, e.g. photosynthesis [9] and processes related to it like phototropism [7], stomata opening [10], chloroplast relocation [11] and solar tracking of leafs [10], but also phototaxis [12], gametogenesis [13], entrainment of circadian rhythms [14] and many more. The blue light photoreceptors responsible for these processes can be classified into the families of xanthopsins [15], BLUF (blue light using flavin adenin dinucleotide) domains [16], cryptochromes [6], LOV (light-, oxygen-, voltage-sensitive) protein

families [17], phototropins [7] and ZEITLUPEs (ZTL) [18]. Besides this, there are the UV-sensitive UVR-8 (UV resistance locus 8) receptors [19], the red light-sensing phytochromes [20] and rhodopsins [21]. Taken together, the eight photoreceptor families cover almost the entire UV, visible and far-red region of the electromagnetic spectrum.

In general, photoreceptors consist of two components: a chromophore molecule to absorb the light and a protein core to host the chromophore and propagate the signal downstream to an effector domain or a signaling partner. With the exception of xanthopsins, all blue light photoreceptors non-covalently bind flavin as a chromophore, either as flavin mononucleotide (FMN) or flavin adenine dinucleotide (FAD). The excitation of flavin by light represents the key element of the photoreception mechanism.

Phototropins, ZEITLUPEs and LOV domain proteins can be summarized as light-, oxygen-, voltage-sensitive domains. LOV domains, BLUF domains and cryptochromes all share a flavin chromophore, but the photochemistry upon blue light excitation is different. While BLUF domains and cryptochromes perform electron transfer reactions, LOV domains form a covalent bond between flavin and a nearby cysteine - the so-called adduct state - via a triplet state reaction of FMN. In the following the LOV domains which are the main aspect of this work will be described in more detail.

1.1 LOV domains

LOV domains form a subset of the PER-ARNT-SIM (PAS) superfamily and have preserved their structure [22–25]. The LOV core is composed of a central β-scaffold with five antiparallel β-strands (Aβ, Bβ, Gβ, Hβ, Iβ) and four α-helices (Cα, Dα, Eα, Fα) as shown in Figure 1.1.1. Eα and Fα pack against the β-sheet and form a pocket to non-covalently bind the flavin chromophore. The reactive cysteine participating in adduct formation is located on Eα within the highly conserved sequence GXNCRFL(Q). The LOV core is flanked by variable N- and/or C-terminal extensions, which are often helical. These flanking regions are thought to act as connective elements that propagate light-induced signals from the LOV core to effector domains or interacting partner proteins.

Most LOV domains non-covalently bind FMN as a chromophor, in some cases they harbor FAD. FMN and FAD are the biologically active forms of riboflavin. They exhibit a very rich photochemistry and can act as one- or two-electron redox reagents [26]. The chemical versatility is linked to the fact that flavins can switch between three different oxidation states: the fully oxidized form (ox), the one-electron reduced, semiquinone form (sq) and the fully reduced, hydroquinone (hq) form (see Figure 1.1.2A). Nature makes use of these attributes in the form of various flavoen-

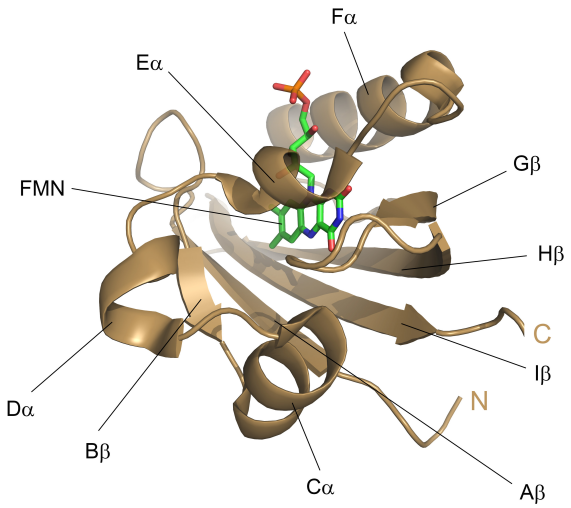

Figure 1.1.1 PAS-fold of LOV domains exemplified by the crystal structure of the LOV1 domain from *C. reinhardtii* phototropin (PDB 1N9L). The central anti-parallel β-scaffold is linked by a helical connector, together forming the binding pocket of FMN. The LOV core is shown in cartoon representation in brown, the FMN chromophore in stick representation in green. The nitrogen atoms of FMN are colored blue, the oxygens red and phosphorus orange.

zymes, which are involved in the four major energy metabolism systems: photosynthesis, aerobic respiration, denitrification and sulfur respiration [27].

In the dark state the flavin chromophore of LOV domains in the fully oxidized form strongly absorbs in the blue region of the spectrum. The absorption bands are centered around 450 nm ($S_0 \rightarrow S_1$ transition), 360 nm ($S_0 \rightarrow S_2$) and 280 nm ($S_0 \rightarrow S_3$). The flavin chromophore is non-covalently bound in the LOV binding pocket via hydrogen bonds leading to a characteristic vibrational fine-structure of the absorption bands (Figure 1.1.2C) [17]. Blue light excitation induces covalent bond formation of FMN-C4a with the thiol group of a nearby, conserved cysteine. This so-called adduct state represents the active, signaling state and is strictly conserved among all currently characterized LOV domains. Adduct formation is accompanied by a change of the absorption spectrum resulting in a peak centered at 390 nm as can be seen in Figure 1.1.2C. Adduct formation is reversible in the dark. The flavin-cysteine bond breaks on the timescale of seconds to hours [28, 29]. The photocycle of LOV domains has been extensively investigated, but still some details remain unclear. A consensus exists, however, that upon blue light absorption FMN gets excited into the singlet state and subsequently undergoes intersystem crossing to the triplet state, LOV_{715} (numbers indicate the absorption maximum of the particular intermediate), within ns to µs. From there, the covalent bond between FMN-C4a and the sulfur group of a nearby cysteine is formed resulting in the adduct state (LOV_{390}) [30]. A scheme of the LOV photocycle is shown in Figure 1.1.2B.

Several mechanistic proposals for the adduct formation have been debated in the literature, including an ionic mechanism, a concerted mechansim and a radical pair

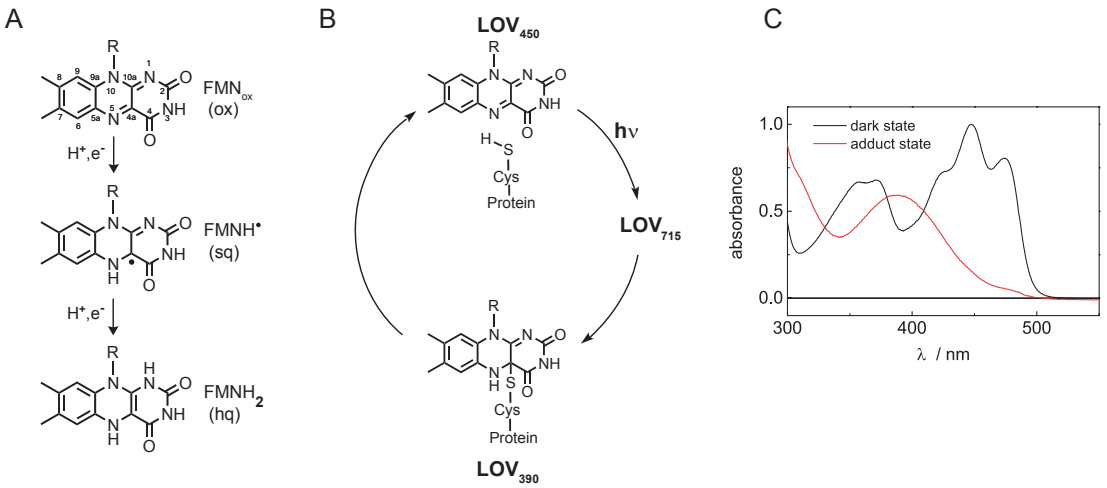

Figure 1.1.2 A: Structures of the fully oxidized state of FMN (ox), the one-electron reduced neutral semiquinone radical FMNH$^\bullet$ (sq) and the fully reduced $FMNH_2$ (hq). **B:** Scheme of the LOV photocycle. Upon absorption of blue light, LOV_{450} gets excited in the singlet state and subsequently undergoes intersystem crossing to the triplet state (LOV_{715}) from which the adduct state is formed (LOV_{390}). LOV_{390} reverts back to LOV_{450} in the dark. **C:** Steady-state UV/Vis spectra of the dark state (black line) and the adduct state (red line) of LOV domains in the range of 300 nm to 550 nm. Panel **A** and **B** are taken from [31].

mechanism [32–34]. The latter one seems to be most likely. According to this, LOV_{715} initiates either concerted or sequential electron and proton transfer from the reactive cysteine resulting in the formation of the biradical pair FMNH$^\bullet$ $^\bullet$SCys which subsequently combines to yield the adduct [35, 36]. However, although indications of the neutral semiquinone radical of FMN could be detected in a LOV domain of *C. reinhardtii*, there is so far no unequivocal proof that these are intermediates in the photocycle [37].

Adduct formation is just the primary step in LOV domain signaling. Protonation of FMN-N5 due to adduct formation induces the flip of the amide side chain of a nearby, conserved glutamine located on Iβ to adjust hydrogen-bonding interactions [38–42]. This in turn leads to further changes in the hydrogen-bonding network within the LOV core, transducing the light trigger into a physiological signal [43, 44]. The signal is propagated from the flavin chromophore to the β-scaffold, from where it can be further transferred to adjacent N- and C-terminal elements like linkers or flanking helices. Alteration of the dynamics and the structure of these elements influences the oligomeric state and the activity of output modules [42, 45]. Recently, a bioinformatics study on 6700 LOV domains identified 119 clusters of associated domains including so far unidentified effectors such as regulators for G protein signaling and lipases [46]. This emphasizes the high modularity of LOV domains which allows them to control many processes in nature but also makes them suitable for applications in the field of optogenetics, fluorescence microscopy or singlet oxygen production.

1.2 Aim of this work

LOV domains have been investigated in great detail for more than 15 years. Much knowledge has been attained regarding the structure, function and signaling of LOV domains. The LOV pardigm which is strictly conserved across all kingdoms of life, offers already today various application possibilities. But nevertheless, still open questions remain to be answered, e.g. the mechanism of adduct formation and the details of signal transduction and the communication with interaction partners.
This thesis addresses some of these questions. It has two main objectives: at first, engineering the flavin photochemistry in a LOV domain towards efficient electron and proton transfer and, secondly, the investigation of intermolecular interactions of LOV domains in dependence of light activation. The questions addressed were, how can the flavin photochemistry be tuned towards efficient electron and proton transfer instead of adduct formation? Which factors influence the flavin reactivity and what is the underlying mechanism? Can we follow LOV-LOV interactions via Förster resonance energy transfer? Which role do intermolecular interactions of LOV domains play in signaling?

Taken together, primary and secondary signaling events of LOV domains were investigated to further extend the knowledge about these photosensory domains. The results are presented in the following chapters, which consist of publications already submitted and under review process and of yet unpublished data.

In **chapter 2** the LOV1 domain of *C. reinhardtii* was used as a template to mutationally induce efficient electron transfer towards flavin instead of the naturally occurring adduct formation. The photocycle of CrLOV1 wild type has already been investigated previously so that the impact of the mutations can be analyzed in great detail. A single point mutation in the LOV core, F41Y, was sufficient to switch from adduct formation towards electron transfer in CrLOV1 under aerobic conditions, although the reactive Cys was present. This allows for deductions regarding the wild type adduct mechanism, which is still not fully understood. Furthermore, the knowledge how to switch the flavin reactivity inside the LOV core may come in useful for LOV-based applications.

The flavin photochemistry of LOV domains is also subject of **chapter 3**. By using a mutational approach the naturally non-photoreducible and photo-inactive fluorescent reporter protein iLOV has been engineered towards efficient photoreduction under aerobic conditions. The introduction of aspartate as a proton donor into the LOV core does not only allow for efficient photoreduction of FMN but also has implications for the presence of natural electron transfer pathways in LOV domains. The ability to tune the flavin photochemistry inside a LOV core could also contribute to the development and design of novel photoreceptor-based tools for optogenetics or imaging technologies.

It becomes more and more apparent that blue light-dependent LOV-LOV interactions play a major role in LOV protein signaling. Oligomeric state changes of the

LOV domain from *R. sphaeroides* and of the LOV1 domain from *C. reinhardtii* were investigated by size exclusion chromatography and Förster resonance energy transfer. The results are presented in **chapter 4**. Using fluorescence spectroscopy offers the great advantage that the interactions could be followed to the nM range, but labeling of the LOV domains required for FRET on the other hand entails some experimental difficulties. The results on RsLOV extend the knowledge about the oligomeric state changes revealed so far for this short LOV domain, while the results on CrLOV further confirm this LOV domains' divergence compared to LOV1 domains from higher plants.

The experimental methods used in this thesis are described in detail in chapter 5. And completing this thesis, the results are summarized in chapter 6.

2 Electron transfer in mutated LOV domains of *C.reinhardtii*

2.1 Introduction

LOV domains undergo a photocycle upon blue light excitation. The FMN is excited in the singlet state and subsequently undergoes intersystem crossing to the excited triplet state. On a timescale of 100 ns up to 5 µs a covalent bond is formed between the C4(a) atom of FMN and a nearby Cys [30]. This flavin-cysteinyl adduct represents the active, signaling state of the protein. The signaling chain continues with conformational changes of the protein, presumably a flip of a Gln in the binding pocket [41], inducing downstream signaling in the effector domain of Phot. The adduct fully reverts in the dark on the timescale of seconds to hours depending on the particular LOV domain [28, 29]. Several mechanistic proposals for this adduct formation have been debated in the literature [32–34]. Of these, a radical pair mechanism seems to be most likely: the triplet state of FMN initiates electron and proton transfer, or a sequence of electron and proton transfer, from the reactive Cys resulting in the biradical pair $FMNH^{\bullet}$ $^{\bullet}SCys$ which subsequently combines to yield the adduct [35, 36]. However, although the neutral semiquinone radical of FMN could be detected in a LOV domain of *C. reinhardtii*, there is so far no unequivocal proof that these are intermediates in the photocycle [37, 47].

In contrast, proton coupled electron transfer (PCET) [48] from a conserved Tyr to the excited singlet state of FAD is the primary photochemical reaction in BLUF domains [49, 50]. It is believed that formation of the signaling state is completed by a rearrangement of the hydrogen bond network. There is still some debate as to which specific amino acids are involved, e.g. rotation of a Gln or a Trp [51–54]. cryptochromes also perform a photoreduction of the FAD cofactor via an electron transfer after light activation. In this case a conserved Trp triad is involved as electron donor. Some details, especially the oxidation state of the FAD in the dark state, are still under debate [45].

LOV domains, BLUF domains and CRY exhibit only a low similarity at the sequence level. Regarding their different primary activation mechanisms the question arises whether the different reactions of flavin in these domains are determined by individual amino acids or governed by the whole protein environment.

Some work has been published already to address this topic. Mutational studies on BLUF domains unraveled that replacing the electron donor Tyr by the inert amino acids Phe or Ala abolishes the photoinduced electron transfer completely, and instead formation of the excited triplet state of FAD was observed [55]. After substitution of the Tyr with Trp the electron transfer remains active, forming a radical pair with Trp instead of Tyr [56]. Additionaly, it has been shown recently that the redox potential of FAD and Tyr as well as the pK_a value of Tyr can be tuned by using fluorinated Tyr, which in turn has a large influence on the reaction kinetics of electron and proton transfer [57, 58]. A different approach was adopted by Suzuki and co-workers. By sequence alignment of two crystal structures they identified the position in a BLUF domain that corresponds to that of the Cys in LOV domains regarding the distance and orientation with respect to the flavin chromophore. They placed a Cys into this position in BLUF and inactivated the electron donor Tyr via a mutation to Phe. In this mutant the UV/Vis and IR spectra taken after photoexcitation strongly resemble those of the LOV adduct state [59].

In contrast, the formation of stable and long-lived flavin radicals was observed under aerobic and anaerobic conditions in the presence and absence of external electron donors in LOV domains when replacing the reactive Cys by Ser, Gly or Ala [36, 47, 60]. However, so far LOV domains could not be made to follow an alternative reaction type other than adduct formation as long as the reactive Cys is present, albeit there is some tolerance about the position of this Cys as shown in a mutational study on the LOV2 domain of *A. sativa* [29]. These authors presented several alternative locations of the reactive Cys within the binding pocket of the LOV domain which were still photocycling.

Very recently, Yee *et al.* demonstrated that the LOV domain VVD and the artificial construct YF1 are capable of transducing the light-induced signal downstream within the protein although the reactive Cys is lacking, identifying the neutral semiquinone radical as the signaling state [61]. Analogously, some BLUF domains do not require the formation of a radical intermediate to retain their biological function [62]. These findings lead to the hypothesis that the primary reaction of these photoreceptors is not decisive for the initial activation of the proteins but rather modulates second order events of the signaling process. Gaining more knowledge how to manipulate the photoreactivity of a flavin chromophore inside a protein core and hence being able to control the timescales of activation via switching between different mechanisms within the same domain structure could therefore contribute substantially to the design and engineering of optogenetic tools and reporter proteins in living cells.

In the following chapter, we succeeded in changing the reaction type of FMN in the LOV1 domain of *C. reinhardtii* via substitution of Phe41 with the electron donor amino acid Tyr. Upon blue-light excitation, the F41Y mutant does not form a flavin-cysteinyl adduct characteristic for LOV domains but performs an electron transfer with the introduced Tyr even though the reactive Cys57 is present. When additionally mutating this Cys to Ala or Ser the quantum yield and protonation state of the

intermediate flavin radicals can be tuned. We present spectroscopic data in combination with MD simulations to unravel the primary FMN photochemistry, identify radical species participating in the reaction and discuss structural changes, hydrogen bond rearrangements and solvent accessibility in the proteins. These results allow us to propose key parameters important for an electron transfer to occur in LOV domains.

2.2 Results

2.2.1 Photoreaction of *Cr*LOV1-F41Y

Phe41 was substituted isosterically with Tyr in *Cr*LOV1 in order to investigate the influence of an electron donor amino acid in the protein core on the photoreactivity of the chromophore FMN. The F41Y mutant was expressed and purified like the wild type (wt) as a soluble, green protein in solution.
The steady-state UV/Vis spectrum of *Cr*LOV1-F41Y (Figure 2.2.1) exhibits the typical fine structured absorption bands with maxima at 473 nm, 445 nm, 368 nm and 352 nm, blue-shifted by 3 nm compared to the wt. The absorption band in the UVA is a good indicator for the hydrogen bonding network and the polarity in the FMN binding pocket [63, 64]. The high spectral similarity between *Cr*LOV1-F41Y and *Cr*LOV1 wt indicates that the mutation did not lead to major structural changes within the protein. In contrast to *Cr*LOV1 wt, the steady-state UV/Vis spectrum of *Cr*LOV1-F41Y does not change upon blue light illumination, meaning no adduct is formed in this mutant.

To further investigate the behavior of *Cr*LOV1-F41Y upon blue light excitation, transient absorption (TA) spectroscopy in the µs timerange was applied. Figure 2.2.2 shows difference absorption spectra of *Cr*LOV1-F41Y at 200 ns and 4.9 µs after

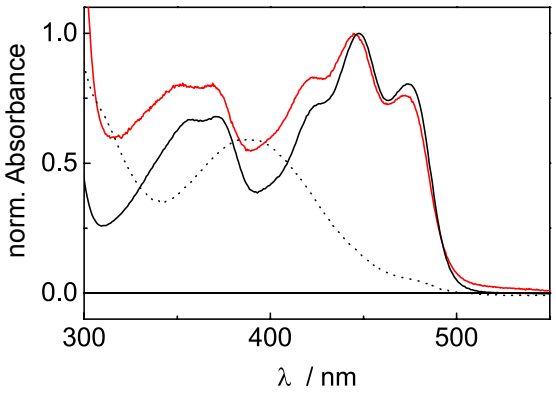

Figure 2.2.1 Comparison of the steady-state UV/Vis spectra of *Cr*LOV1 wt in the dark (black line) and in the adduct state (dotted line) and of *Cr*LOV1-F41Y (red line). The steady-state UV/Vis spectrum of *Cr*LOV1-F41Y does not change upon blue light illumination.

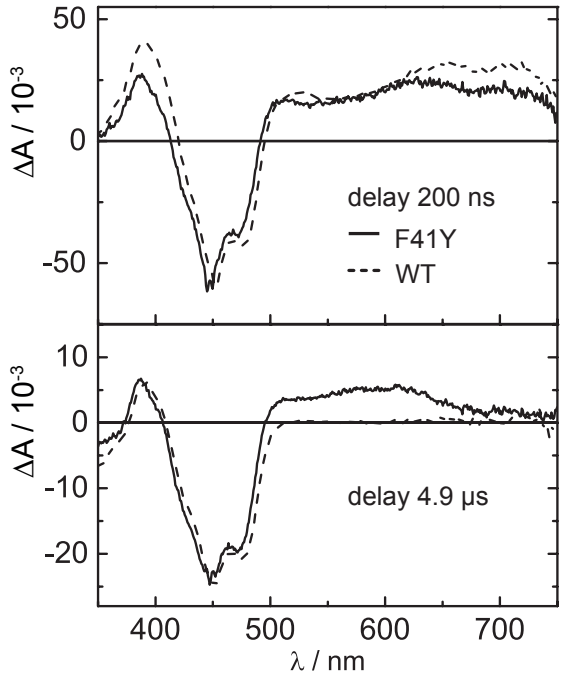

Figure 2.2.2 Difference absorption spectra extracted from a TA measurement recorded with a 10 µs time window of *Cr*LOV1-F41Y (solid line) 200 ns and 4.9 µs after laser excitation. Spectra of *Cr*LOV1 wt (dotted line) are shown for comparison. The noise level of the data was reduced by singular value decomposition (SVD) and all spectra were scaled to the same minimum at 447 nm.

laser excitation. For comparison, previously published spectra of *Cr*LOV1 wt are included [47]. All spectra are scaled to the same minimum at 447 nm. The negative absorption band at around 450 nm corresponds to the ground state bleach of the oxidized FMN, FMNox. Positive absorption signals are detected for *Cr*LOV1-F41Y from 493–745 nm and below 415 nm in Figure 2.2.2 after 200 ns. The wt exhibits a similar spectrum blue-shifted by 5 nm. After 4.9 µs, a positive band can be detected at 374–407 nm and above 493 nm up to 660 nm in the case of *Cr*LOV1-F41Y. The positive absorption band above 660 nm almost decayed to zero at this time delay. The difference spectrum of *Cr*LOV1 wt in Figure 2.2.2 after 4.9 µs is characterized by the positive absorption of the adduct state at 376-409 nm and the ground state bleach. Above 500 nm, no absorption signals contribute to the spectrum.

We performed global lifetime analysis of the TA data (see chapter 5, subsection 5.5.2), two lifetime components were sufficient for a good fit. Figure 2.2.3 shows the two decay associated difference spectra (DADS) corresponding to decay time constants of $\tau_1 = 1.3\,\mu s$ and $\tau_2 > 10\,\mu s$. The first DADS (D_1) exhibits positive signals above 490 nm and below 420 nm next to the negative ground state bleach of FMNox. The broad absorption band with the typical structure in the range 650 to 700 nm can be associated with the excited triplet state of FMN [65]. The triplet decay time of *Cr*LOV1-F41Y is almost the same as in *Cr*LOV1 wt, which was reported to be 1.16 µs [47]. The second DADS (D_2) is non-decaying within the observed

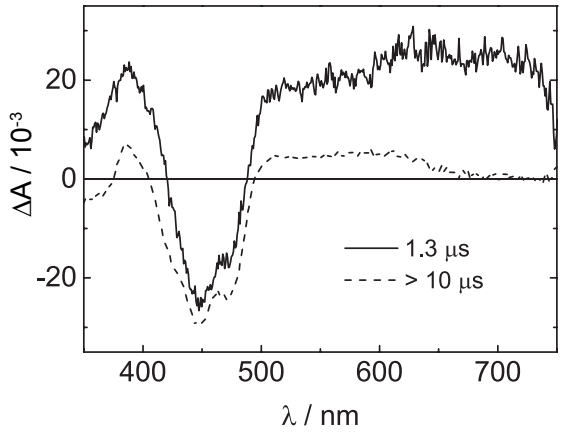

Figure 2.2.3 DADS obtained from global lifetime analysis of *Cr*LOV1-F41Y. The first DADS (solid line) decays with a time constant of 1.3 µs, while the second DADS (dashed line) is non-decaying within the measured time window of 10 µs.

streak window of 10 µs. This D_2 has positive absorption in the range of 375 nm to 403 nm and from 495 nm to 670 nm, resembling the spectrum of the neutral semiquinone radical $FMNH^\bullet$ [65, 66]. The spectrum of this radical in the LOV environment is known from photochemical reduction experiments of *Cr*LOV1-C57G with EDTA or β-mercaptoethanol [60, 67–69]. Comparison of these spectra with D_2 of *Cr*LOV1-F41Y revealed a significant difference in the range 500-530 nm, indicating an additional species contributing to D_2. $FMNH^\bullet$ is formed by electron transfer to FMN, leading to the radical anion $FMN^{\bullet-}$ which is subsequently protonated. In the photoreduction experiment with *Cr*LOV1-C57G the electron was donated by β-mercaptoethanol. The cation of this donor or its decay products do not absorb in the visible spectral range and protonation of $FMN^{\bullet-}$ is complete in this steady state experiment. In the case of *Cr*LOV1-F41Y, however, the electron is most probably donated by Tyr41. The initially produced tyrosine radical cation usually deprotonates quickly to the neutral radical. On the other hand, protonation of the radical anion $FMN^{\bullet-}$ can be a slow process on the µs timescale. Hence we considered the following species for a possible contribution to D_2: $FMNH^\bullet$, $FMN^{\bullet-}$ and $TyrO^\bullet$.
We then tried to fit the observed D_2 (black line, Figure 2.2.4) to a linear combination of reference spectra of FMNox, $FMNH^\bullet$, $FMN^{\bullet-}$ minus FMNox and $TyrO^\bullet$ (for description how these reference spectra were generated see chapter 5, subsubsection 5.5.2.1). A fit to the reference spectrum of $FMNH^\bullet$ minus FMNox (figure 2.2.4, green line) did not lead to reasonable agreement, as did a fit including also the reference spectrum of $FMN^{\bullet-}$ minus FMNox (blue line, figure 2.2.4). However, the linear combination of FMNox, $FMNH^\bullet$ and $FMN^{\bullet-}$ minus FMNox yields a good description of D_2 in the range $\lambda > 500$ nm (magenta line, figure 2.2.4). The difference between this linear combination and $D_2 < 500$ nm corresponds to the red spectrum shown in figure 2.2.4, inset. The peak with maxima at 397 nm and 413 nm resembles the spectrum of $TyrO^\bullet$ minus TyrOH. The tyrosyl radical spectrum in aqueous solution shows a narrow absorption peak at 408 nm with a shoulder at 391 nm [70].

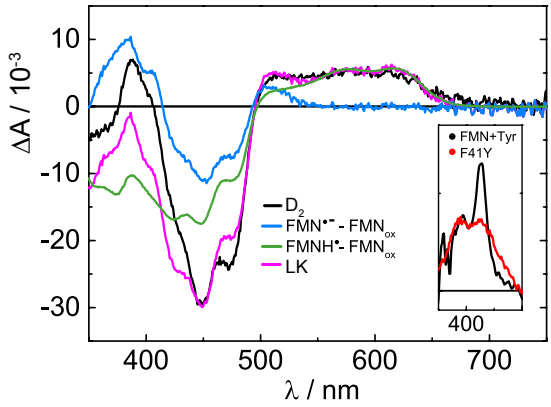

Figure 2.2.4 D_2 of *Cr*LOV1-F41Y (black line) compared to the linear combination (LK) of the reference difference spectra (purple line) for the species $FMNH^{\bullet}$ minus FMNox (green line) and $FMN^{\bullet-}$ minus FMNox (blue line). **Inset:** The reference spectrum of the $TyrO^{\bullet}$ radical (black line) compared to the difference between D_2 and the sum of the flavin radical species, i.e. the black and the purple lines from the main plot (red line). The $TyrO^{\bullet}$ reference spectrum (black line), generated with FMN and Tyr, was red-shifted by 9 nm for better comparison.

It is shown as the black spectrum in the inset in figure 2.2.4, red-shifted by 6 nm for better comparison. It is evident from the spectra that the peak at 397 nm of the red spectrum is in good agreement with the reference spectrum of $TyrO^{\bullet}$. The different shape of the second peak at 413 nm can be explained by the fact that the reference spectrum of $FMN^{\bullet-}$ minus FMNox was generated with CrLOV1/C57S which has a spectral shift of the ground state bleach compared to CrLOV1/F41Y. We conclude that electron transfer in *Cr*LOV1-F41Y occurs from Tyr41 to FMN, and that the flavin radical anion is still not completely protonated after 10 µs.

2.2.2 Additional mutation of the reactive Cys57

No evidence for adduct formation was found in *Cr*LOV1-F41Y although the reactive Cys is still present. To elucidate, whether this Cys57 is participating in the observed electron transfer reaction of *Cr*LOV1-F41Y, we additionally replaced the reactive Cys with the polar amino acid serine and the unpolar amino acids alanine and glycine. The UV/Vis spectra (Figure 2.2.5) are in good agreement with the UV/Vis spectrum of *Cr*LOV1 wt indicating an intact hydrogen bonding network around the FMN.

We performed TA measurements at pH 8.0 on a 20 µs time window with *Cr*LOV1-F41Y/C57A and on a 50 µs time window with *Cr*LOV1-F41Y/C57S. The data were analyzed by global lifetime analysis using two exponential functions for each data set. The D_1 displayed in Figure 2.2.6A decay with time constants of 1.7 µs for *Cr*LOV1-F41Y/C57A and 2.8 µs for *Cr*LOV1-F41Y/C57S, i.e. they are associated with the decay of the excited triplet state of FMN. D_2 of *Cr*LOV1-F41Y/C57S decays within 28.0 µs, while the C57A mutant is non-decaying within the measured time window

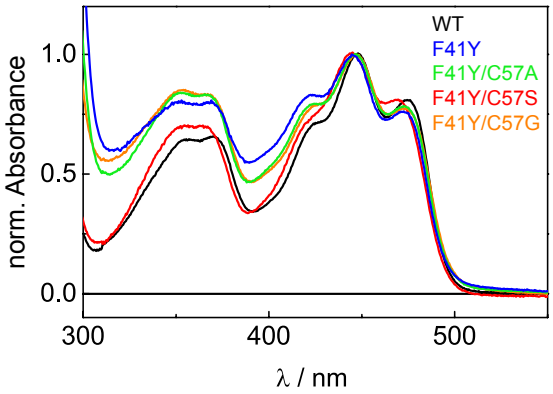

Figure 2.2.5 UV/Vis spectra of the *Cr*LOV1-F41Y mutants measured in the range of 300-600 nm.

(Figure 2.2.6B). Both DADS in Figure 2.2.6B exhibit similar spectral features of $FMNH^{\bullet}$ like *Cr*LOV1-F41Y. Interestingly, the spectral signatures of the radicals appear not only in the D_2, but also in the D_1 exemplified by subtraction of the D_1 of the C57G mutant which is entirely due to triplet absorption (see Figure 2.2.6C). The $FMNH^{\bullet}$ absorption varies significantly between the different mutants in the range of 540 nm to 655 nm. The highest amplitude can be

found in *Cr*LOV1-F41Y/C57S, followed by *Cr*LOV1-F41Y/C57A and *Cr*LOV1-F41Y. Furthermore, the positive absorption below 405 nm differs between CrLOV1-F41Y/C57S and CrLOV1-F41Y/C57A, being more intense in the latter one with a shoulder at 398 nm. In combination with the pronounced peak around 500 nm in *Cr*LOV1-F41Y/C57A, these spectral features are characteristic for the FMN radical anion, $FMN^{\bullet-}$.

A fit of the linear combination of the aforementioned reference spectra revealed contributions of $FMNH^{\bullet}$, FMNox, $FMN^{\bullet-}$ and $TyrO^{\bullet}$ to the D_2 of *Cr*LOV1-F41Y/C57S. In contrast, D_2 of *Cr*LOV1-F41Y/C57A could be well described using a linear combination of $FMNH^{\bullet}$, FMNox and $FMN^{\bullet-}$. Including the $TyrO^{\bullet}$ spectrum did not improve the fit. The results from spectral fitting indicate that the introduced Tyr41 is quite likely the terminal amino acid of the electron transfer chain and therefore the electron donor, since the spectrum of $TyrO^{\bullet}$ needs to be taken into account to fit the D_2 of *Cr*LOV1-F41Y and *Cr*LOV1-F41Y/C57S. Only in the case of *Cr*LOV1-F41Y/C57A we could not establish the contribution of $TyrO^{\bullet}$ via spectral fitting of D_2. But in this mutant, the $FMN^{\bullet-}$ features are more pronounced compared to the other F41Y mutants, which has a strong absorption in the same spectral region as the $TyrO^{\bullet}$ radical.

The photophysical behavior of *Cr*LOV1-F41Y/C57G is different compared to the other F41Y mutants investigated. Analysis of a 100 µs TA dataset results in two DADS (Figure 2.2.7). D_1 exhibits the typical spectral features of the FMN triplet state and decays with $\tau = 28.0$ µs, prolonged by a factor of 10 compared to the corresponding DADS of the other F41Y mutants. D_2 is non-decaying within the measured streak window and the spectrum exhibits high similarity with D_1. This

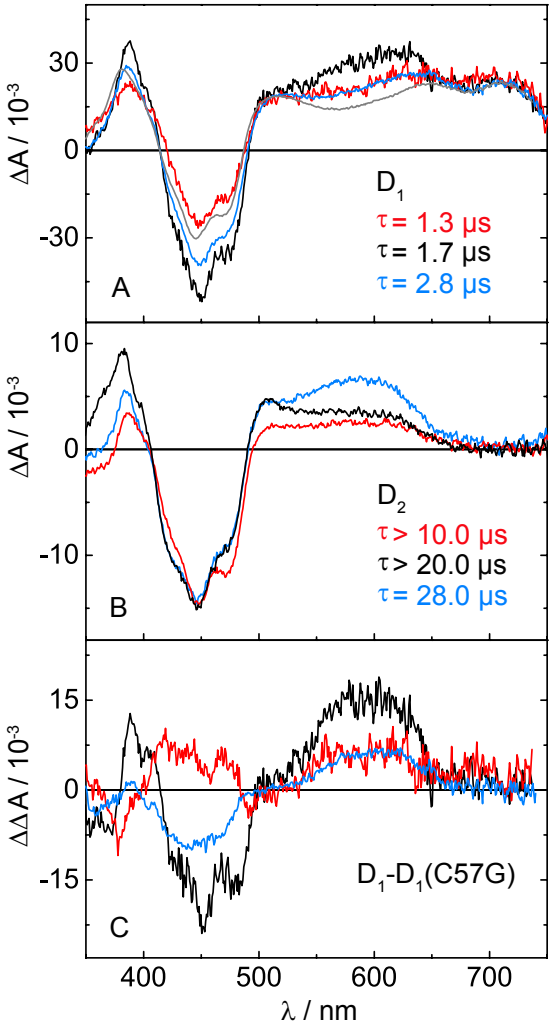

Figure 2.2.6 DADS obtained from the global lifetime analysis for *Cr*LOV1-F41Y/C57S (blue line) and *Cr*LOV1-F41Y/C57A (black line). The DADS in **A** decay with a time constant of 2.8 µs and 1.7 µs. The DADS of *Cr*LOV1-F41Y (red line) and of *Cr*LOV1-C57G (gray line) are shown for comparison. The spectrum of *Cr*LOV1-C57G corresponds to the pure triplet transient absorption. **B:** The second DADS of *Cr*LOV1-F41Y/C57S decays with a time constant of 28.0 µs, while the one of *Cr*LOV1-F41Y/C57A is non-decaying within the measured streak window of 20 µs. The DADS were scaled to the same minimum at 447 nm. **C:** The D_1 of panel A after subtraction of the D_1 of *Cr*LOV1-C57G.

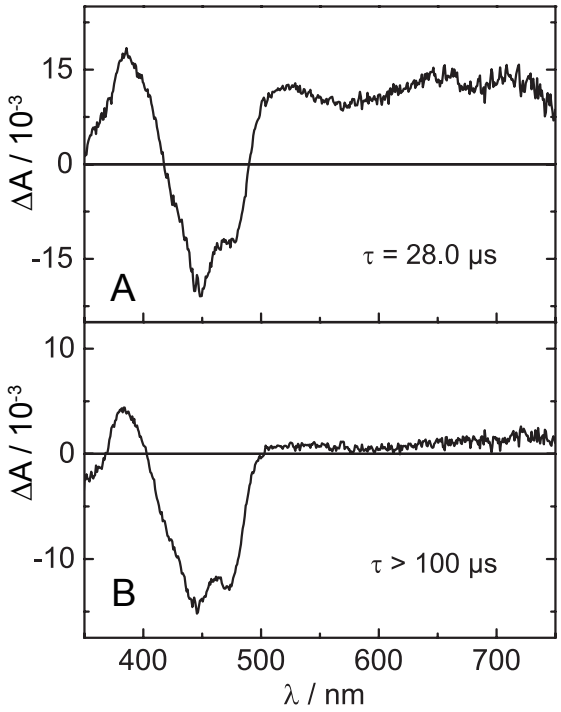

Figure 2.2.7 DADS of *Cr*LOV1 F41Y C57G obtained by global lifetime analysis. **A:** D_1 decaying with a rate constant of 28.0 μs **B:** D_2 non-decaying within 100.0 μs.

component has an amplitude of approx. 10 % of the faster decaying component. In *Cr*LOV1-F41Y/C57G no spectral evidence for FMN radicals can be observed. These findings suggest a biphasic triplet decay like already observed in the case of *Cr*LOV1-C57G [47] indicating the presence of an additional quenching channel. The same has been reported for Pp2FbFP L30M, a LOV domain based singlet oxygen sensitizer [71]. It has been suggested that two distinct triplet states are formed in those proteins which can be divergently quenched by oxygen due to varying accessibility of molecular oxygen into the binding pocket. Glycine is the least sterically demanding natural amino acid. This allows for more space in the binding pocket and therefore increased flexibility of the chromophore.

2.2.3 pH influence

Our TA data show, that mainly the protonated $FMNH^{\bullet}$ can be observed upon blue light excitation of the *Cr*LOV1-F41Y mutants. In order to identify the proton donor in this reaction we increased the pH of the buffer solutions up to 11.0 and repeated the TA measurements. Figure 2.2.8 compares the D_2 at different pH values of the respective *Cr*LOV1-F41Y mutants resulting from analysis of the TA data.

All three F41Y mutants form the neutral radical $FMNH^{\bullet}$ even at strongly basic pH, albeit with a reduced yield. The strongest decrease of approx. 50 % can be observed

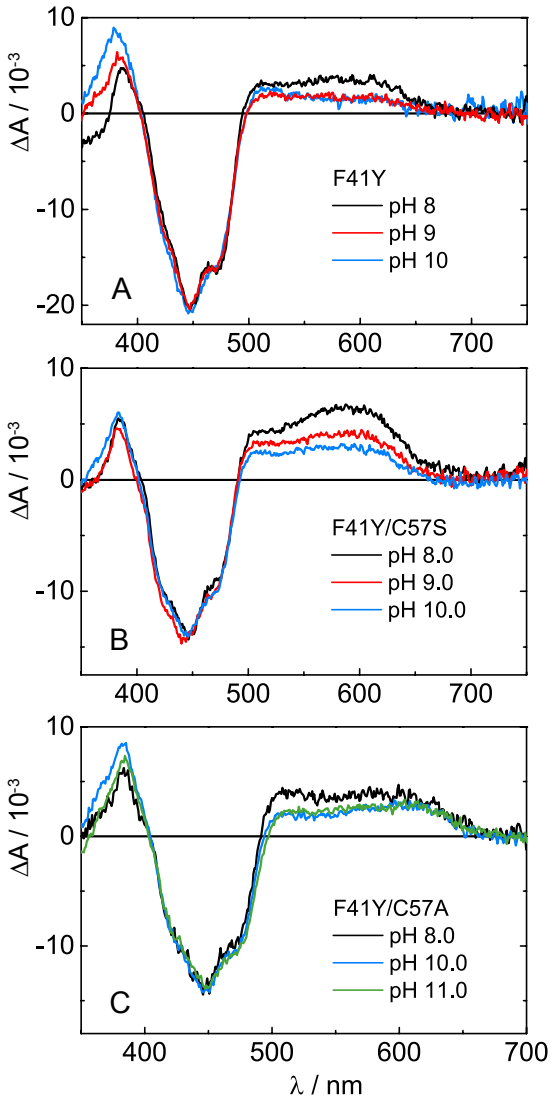

Figure 2.2.8 Comparison of the D_2 of *Cr*LOV1-F41Y (**A**), F41Y/C57S (**B**) and F41Y/C57A (**C**) at pH 8.0, 9.0, 10.0 and 11.0, respectively.

in the case of *Cr*LOV1-F41Y/C57S (Figure 2.2.8B). In the D_2 of *Cr*LOV1-F41Y and *Cr*LOV1-F41Y/C57A (Figure 2.2.8A and C) the spectral features of $FMN^{\bullet-}$ become more pronounced with increasing pH including the absorption bands around 500 nm and below 400 nm. The fact that $FMNH^{\bullet}$ can still be observed at strongly basic pH indicates that the proton donor must be protonated as well up to a pH of 10.0-11.0. Therefore, protonation by the solvent is not possible but must be performed by an amino acid of the LOV core. According to the crystal structure of *Cr*LOV1 (pdb 1N9L) as well as our MD simulations, the only proton donor in the binding pocket of the *Cr*LOV1-F41Y mutants is Tyr41. In the case of *Cr*LOV1-F41Y also Cys57 is possible. The pK_a value of free Cys is 8.18 and the one of Tyr is 10.07. However, the pK_a values of amino acids can be significantly shifted by the protein environment

[72]. Hence, we calculated the pK_a value of Tyr41 in the *Cr*LOV1-F41Y mutants using the H^{++} program v3.2 [73] resulting in pK_a values of 11.45 (F41Y/C57S) and >12 (F41Y, F41Y/C57A). Cys57 in *Cr*LOV1-F41Y has a calculated pK_a of 10.9 and is thus also strongly shifted towards a more basic value. We conclude that Tyr41 is the proton donor in *Cr*LOV1-F41Y/C57A and C57S. In the case of *Cr*LOV1-F41Y, however, we can not exclude Cys57 as a possible proton donor. It should be noted that the accessibility of the solvent molecules into the binding pocket should be considered within the context of protonation. This will be discussed in subsection 2.2.5.

2.2.4 Decay of the S_1 state suggests electron transfer via the excited singlet state

The TA data of the *Cr*LOV1-F41Y mutants provide evidence for the occurrence of an electron transfer reaction. Next to the observation of FMN and Tyr radical species, the triplet decay times obtained are as short as in *Cr*LOV1 wt indicating a quenching of the excited FMN triplet state. The only exception is *Cr*LOV1-F41Y/C57G in which no radical species could be detected in the µs timerange and the triplet decay is prolonged compared to the other F41Y mutants. Determination of the S_1 decay times (Table 2.1), however, yields a biexponential decay behavior for all *Cr*LOV1-F41Y mutants, including *Cr*LOV1-F41Y/C57G. In all F41Y mutants one decay time corresponds to the expected value for *Cr*LOV1 (i.e. 3 ns for wt and 4.5-5 ns for photo-inactive *Cr*LOV1 mutants) while the second S_1 decay time is a component that is faster than the time resolution of our apparatus (ca. 1 ns). This indicates, that the CrLOV1-F41Y mutants can adopt at least two conformations to account for the biexponential decay behavior.

Furthermore, the fluorescence quantum yields, Φ_F, of the *Cr*LOV1-F41Y mutants were determined (Table 2.1). The fluorescence of the photoinactive mutants C57S, C57A and C57G are strongly quenched from $\Phi_F = 0.30$, 0.30 and 0.25 to $\Phi_F = 0.18$ (F41Y/C57S), 0.15 (F41Y/C57A), and 0.10 (F41Y/C57G) when additionally introducing Tyr41. The wt and the F41Y mutant have similar values of 0.16 and 0.14, respectively. We conclude from our measurements of Φ_F and the S_1 decay times that both, the photoactive C57 and the extra tyrosine, provide quenching channels that do not exist in the photoinactive mutants. This could be enhanced ISC to the triplet state, but might also indicate that some fraction of the electron transfer occurs from the singlet state.

To check this, we analyzed the sum of all DADS of each particular F41Y mutant. The sum of all DADS corresponds to the initial situation before any µs-processes occur and will be named hereafter t_0 spectra. They are shown in Figure 2.2.9A. All spectra were scaled to the same value at 715 nm. At this wavelength exclusively the FMN triplet state absorbs and no other species contribute to the spectrum. As a reference, the t_0 spectrum of *Cr*LOV1 C57G is included. It is known from a previous

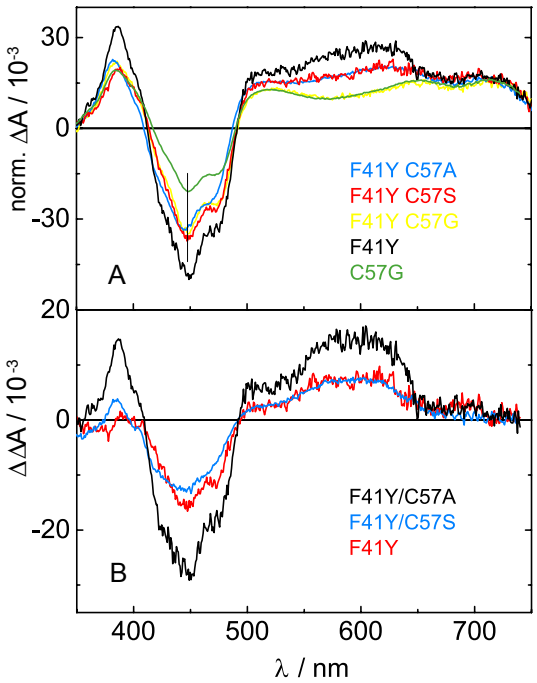

Figure 2.2.9 A: Sum for all DADS of *Cr*LOV1-F41Y, *Cr*LOV1-F41Y/C57S, *Cr*LOV1-F41Y/C57G and *Cr*LOV1-F41Y/C57A referring to the spectra at t_0 before any µs processes occur. The corresponding spectrum of *Cr*LOV1-C57G representing the pure triplet spectrum of FMN in the *Cr*LOV1 core is shown for comparison. **B:** Difference spectra obtained by subtracting the reference spectrum of *Cr*LOV1-C57G from the t_0 spectrum of each F41Y mutant in **A**. The difference spectra show characteristic features of FMN radical species.

study, that this spectrum refers to the pure triplet spectrum of FMN in the *Cr*LOV1 core [47]. When comparing this reference spectrum with the t_0 spectra of *Cr*LOV1-F41Y, F41Y/C57S and F41Y/C57A significant differences become apparent in the range of 500 nm to 660 nm and below 410 nm (see Figure 2.2.9A). Subtraction of the C57G reference spectrum from the t_0 spectra of *Cr*LOV1-F41Y, F41Y/C57S and F41Y/C57A yields the spectra in Figure 2.2.9B, which show characteristic features of the flavin radical spectra described above. Since these spectra can already be observed at t_0, the radical species in *Cr*LOV1-F41Y, *Cr*LOV1-F41Y/C57S and *Cr*LOV1-F41Y/C57A can not be formed exclusively via a triplet state reaction. Thus, the electron transfer in these mutants must occur to some extent in the excited singlet state of FMN. The t_0 spectrum of *Cr*LOV1-F41Y/C57G on the other hand is very similar to that of *Cr*LOV1-C57G except for the spectral range of the ground state bleach. This means, that if *Cr*LOV1-F41Y/C57G performs an electron transfer via the excited singlet state, as suggested by the fluorescence data, the radical is not stabilized and probably recombines on a faster timescale than formation of the triplet state occurs.

Table 2.1 Fluorescence quantum yields, Φ_F, and S_1 decay times of all F41Y mutants. The fluorescence lifetimes were determined using time correlated single photon counting with excitation at $\lambda = 376\,nm$ and detection at $\lambda = 510\,nm$. Values for CrLOV1 wt and CrLOV1-C57S are taken from Holzer *et al.* [74].

	τ_1/ns	τ_2/ns	Φ_f
F41Y	3.0 (∼50 %)	0.9 (∼50 %)	0.14
WT[a]	2.9	-	0.16
F41Y/C57A	3.4 (∼50 %)	1.2 (∼50 %)	0.15
C57A	4.5	-	0.30
F41Y/C57S	3.6 (∼65 %)	1.0 (∼35 %)	0.18
C57S[a]	4.6	-	0.30
F41Y/C57G	4.3 (∼80 %)	0.9 (∼20 %)	0.10
C57G	4.5	-	0.25

[a] values shown for comparison.

2.2.5 Molecular Dynamics Simulations

The microenvironment surrounding the FMN chromophore and its interactions with the protein is of crucial importance. The photoreactivity of riboflavin is strongly affected by its hydrogen bond network [63, 75]. Ivan Stambolic kindly performed 20 ns MD simulations of *Cr*LOV1-F41Y using the dark state crystal structure of *Cr*LOV1 wt (pdb 1N9L) as a starting structure [76]. The MD data reveal that substitution of Phe41 with Tyr has only minor influence on the overall structure of *Cr*LOV1-F41Y. Small perturbations occur around Tyr41 but the hydrogen bonding network built around FMN C2(=O), N3(H) and C4(=O) including Asn89 and Asn99 remains intact. Tyr41 can form a hydrogen bond with FMN C4(=O) as well as with FMN N5 instead of Gln120, which is rotated away from FMN. A close-up view of the binding pocket of the 20 ns simulation structure of *Cr*LOV1-F41Y in comparison with the dark state crystal structure of the wild type is shown in Figure 2.2.10.

Figure 2.2.11A and B shows the structures of *Cr*LOV1-F41Y/C57S and *Cr*LOV1-F41Y/C57A. In *Cr*LOV1-F41Y/C57S the hydrogen bond network between Asn89, Asn99 and FMN C2(=O), N3(H) and C4(=O) remains intact. In this case, the distance between Tyr41 and FMN C4(=O) is small enough to form a hydrogen bond, while direct interaction with FMN N5 like in *Cr*LOV1-F41Y is quite unlikely. Instead, FMN N5 can form a hydrogen bond with the polar side chain of Ser57.
In the case of CrLOV1-F41Y/C57A (Figure 2.2.11B) the hydrogen bond network on the polar side of FMN is changed and does not include Asn99. Asn89 in turn, can form a hydrogen bond with N3(H) and C4(=O) of FMN. The introduced Tyr41 is very close to the FMN and well stabilized in this mutant, with possible hydrogen bonds to FMN N5, C4(=O) and Asn89. Since Ala57 cannot form hydrogen bonds, Tyr41 is the only amino acid in the close proximity of FMN which can

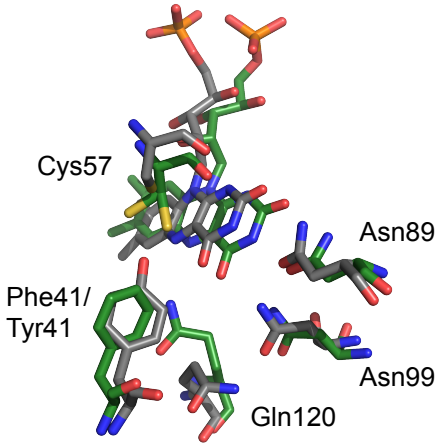

Figure 2.2.10 Superposition of the 20 ns MD simulation structure of *Cr*LOV1-F41Y (gray) with the dark state crystal structure of *Cr*LOV1 wt (green) visualized with PyMOL [77]. The mutation F41Y does not cause significant perturbations of the *Cr*LOV1 structure except for Gln120, which is rotated away from FMN.

make a connection with FMN N5. In both mutants, *Cr*LOV1-F41Y/C57S and *Cr*LOV1-F41Y/C57A, Gln120 is rotated away from FMN, not interacting with the chromophore.

In contrast, FMN N5 does not participate in hydrogen bond interactions in *Cr*LOV1-F41Y/C57G (Figure 2.2.11C). The distance between Tyr41 and FMN C4(=O) and FMN N5 is approx. 5 Å and therefore larger than in the other F41Y mutants. Furthermore, the hydrogen bond network between FMN and Asn89 and Asn99 is changed compared to *Cr*LOV1 wt. Asn89 can interact with FMN N3(H) and C4(=O), but due to a rotation of Asn99 no interaction between this asparagine and FMN is possible. Gln120 is interacting with C4(=O) instead.

Figure 2.2.11D and E compares the distances between Tyr41-OH and either FMN N5 (D) or FMN O4 (E) of the distinct F41Y mutants. The distances between Tyr41 and FMN N5 vary strongly between the different mutants from around 3.0 Å for *Cr*LOV1-F41Y to 5.0 Å for *Cr*LOV1-F41Y/C57G. The distances of *Cr*LOV1-F41Y/C57A and C57S are broadly distributed with a maximum at 3.0-4.0 Å. The distances between Tyr41 OH and FMN O4 on the other hand are almost equal in all F41Y mutants between 2.7 and 3.0 Å (Figure 2.2.11E).
Furthermore, the dihedral angle distributions between Tyr41-CE2, FMN - (C5a-C4a) and Tyr41 - CE1 of all *Cr*LOV1 F41Y mutants were determined from the 20 ns MD trajectories (figure). The distribution curves are broad in all cases with varying

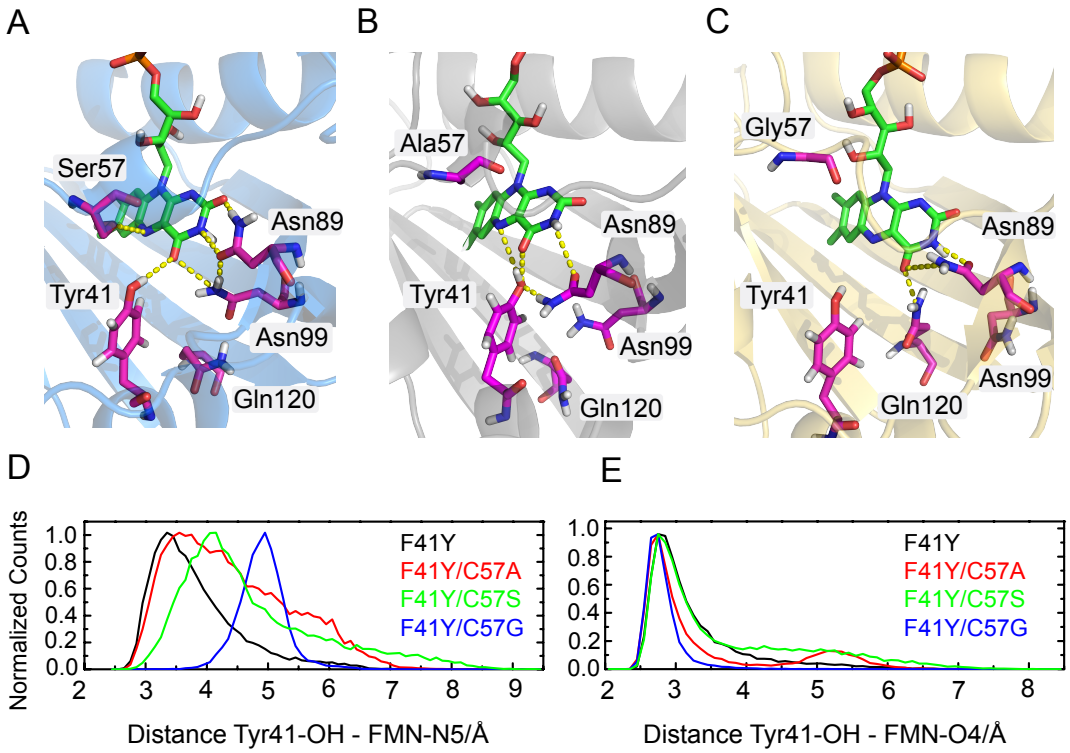

Figure 2.2.11 20 ns simulation structures of **A:** *Cr*LOV1-F41Y/C57S, **B:** *Cr*LOV1-F41Y/C57A and **C:** *Cr*LOV1-F41Y/C57G. Possible hydrogen bonds are indicated by dashed yellow lines. **D and E:** Distance distribution plots of F41Y mutants between Tyr41-OH and FMN-N5 and O4, respectively.

maxima from 18° (F41Y C57S) to 22.5° (F41Y). CrLOV1 F41Y C57A additionally has a second minor peak. The dihedral angle distribution indicate a considerable flexibility between Tyr41 and FMN possibly leading to different geometry-dependent reaction pathways. The structural differences of the particular CrLOV1-F41Y are accompanied by varying accessibilities for solvent molecules into the binding pocket. In *Cr*LOV1-F41Y, a slow water exchange was observed, with always one water molecule being present in the binding pocket. A very fast water exchange occurs in *Cr*LOV1-F41Y/C57G with constantly three to four water molecules present. *Cr*LOV1-F41Y/C57A also shows fast water exchange. The water molecule is located around FMN-O4, but the pathway for the HOH entry is different. While in the other *Cr*LOV1-F41Y mutants the water enters via the phosphate backbone of FMN, in *Cr*LOV1-F41Y/C57A a new water channel opens on the polar side of FMN. Solely in *Cr*LOV1-F41Y/C57S, no water exchange was observed. During the whole simulation time one non-exchanging water molecule is present, located between Ser57 and FMN oriented towards N10.

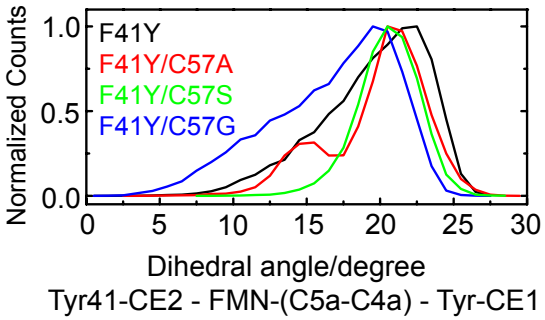

Figure 2.2.12 Dihedral angle distributions between Tyr41-CE2, FMN - (C5a-C4a) and Tyr41 - CE1 of all *Cr*LOV1 F41Y mutants.

2.3 Discussion

Adduct formation as the initial step of activation is a well known attribute of LOV domains. While the reaction mechanisms of other flavin based blue light sensors, e.g. BLUF and CRY, implicate electron transfer reactions, no other light induced photoreaction than adduct formation has been observed so far in the case of LOV domains if the reactive Cys was present. In this study, we present spectroscopic and simulation data on *Cr*LOV1 mutants, in which a Tyr was introduced as a potential electron donor in close proximity to the flavin chromophore. The substitution of Phe41 by Tyr leads to a change in the primary photoreaction of *Cr*LOV1. The naturally preferred adduct formation reaction is inhibited and instead an electron transfer can be observed.

The mutation did not significantly alter the electronic properties of FMN since the ground state absorption spectrum shows only minor changes in comparison to *Cr*LOV1 wt. Moreover, MD simulations of both, *Cr*LOV1 wt and *Cr*LOV1 F41Y, reveal that both structures are highly similar with mainly preserved hydrogen bond interactions between FMN and the surrounding amino acids. Only minor perturbations around the introduced Tyr occur.

TA measurements in the µs-time range showed that *Cr*LOV1-F41Y populates the excited FMN triplet state like observed for the wt which decays also with a similar rate constant. But instead of the characteristic flavin-cysteinyl-adduct, radical species of FMN evolved from the triplet state. Spectral fitting of the data demonstrated the presence of $FMNH^{\bullet}$, $FMN^{\bullet-}$ and $TyrO^{\bullet}$. Likewise, when additionally substituting the reactive Cys57 with Ala or Ser, the formation of flavin radical species can be observed. *Cr*LOV1-F41Y/C57A and C57S as well populate the FMN triplet state that decays with comparably short lifetimes like observed for *Cr*LOV1-F41Y and wt. However, in these cases the deactivation channel of the triplet is electron transfer. Other photo-inactive *Cr*LOV1 mutants, in which electron transfer occurs only in the presence of an external electron donor like EDTA, usually have a triplet

decay time by at least a factor of ten longer [34, 47]. Presumably, Tyr41 is the initial electron donor in the F41Y mutants although the amino acid sequence of *Cr*LOV1 wt contains four Tyr and one Trp as natural candidates. According to the crystal structure, they are located quite distant from the acceptor FMN, with Tyr47 being closest with a distance of 11.0 Å between Tyr47-OH and FMN-O4. Tyr41 on the other hand, is located very close with an average distance of 2.75 Å to FMN-O4 in each F41Y mutant providing a favored initial situation since electron transfer reactions are strongly distance dependent processes. Furthermore, the described electron transfer reactions are only observed, when Tyr41 is present.

On the other hand, our findings on the excited singlet state deactivation, including a reduced fluorescence quantum yield and a biexponential fluorescence decay, lead to the hypothesis that a second pathway for electron transfer via the excited singlet state exists in the *Cr*LOV1-F41Y mutants. This is supported by the fact that the radical species are already formed immediately after the exciting laser pulse (ca 10 ns) in the TA measurements. A reasonable explanation for the two reaction pathways would be the existence of more than one conformation of each F41Y mutant most likely regarding Tyr41. It has been reported recently, that already subtle conformational changes of the terminal electron donor Trp in the *A. thaliana* cryptochrome triade can inhibit the electron transfer to the next Trp due to a drastic change in the electronic coupling between donor and acceptor [78]. And in fact, the dihedral angle distribution including FMN and Tyr41 is rather broad for all F41Y mutants indicating a variation in the donor to acceptor orientation.

Since *Cr*LOV1-F41Y, F41Y/C57S and F41Y/C57A feature the same photo-chemical characteristics upon blue-light excitation we propose that these mutants follow the same mechanism, meaning that the reactive Cys in *Cr*LOV1-F41Y apparently becomes unreactive. Although the orientation and distance of Cys57 and FMN seem to be favorable for adduct formation according to our MD simulations, we do not observe any matching signals in our spectroscopic data. The triplet decay time of *Cr*LOV1-F41Y is 1.3 µs and therefore in the same timerange as in the wt. Consequently, the first step leading to the radical pair in the mutants containing Tyr41 is about as fast as the first step leading to the adduct in the wt. In the F41Y mutants this first step should be electron transfer from Tyr to ^{3}FMN, for the wt the first step most likely is also electron transfer, this time from Cys57 to ^{3}FMN. Accordingly, in F41Y we should expect both, adduct and FMN radicals, with similar yield.

In a previous study of the *Cr*LOV1 wt photocycle we could not detect any intermediate between the FMN triplet state and the adduct [47]. We concluded that the reaction is either concerted or it occurs as a sequence of electron transfer, proton transfer and radical recombination, with electron transfer being the rate limiting step. If adduct formation is a concerted reaction, it should compete with electron transfer from Tyr in the F41Y mutant, and both products should be observed. If however, the reaction occurs in several steps, competition between the two reactions might occur only in the second step, meaning after electron transfer from Cys the formed cysteine radical cation reacts faster with the Tyr than with the FMN radical

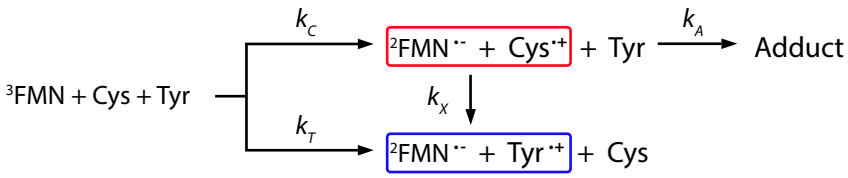

Figure 2.3.1 Scheme of the proposed triplet state reaction mechanism of *Cr*LOV1-F41Y.

anion. This is schematically shown in Figure 2.3.1. Here, k_C and k_T denote the rate constants for electron transfer from Cys and Tyr, respectively, which are both of similar magnitude of ca. 10^6 s^{-1}. In the wt, adduct formation occurs then with a rate constant $k_A \gg k_C$. If we assume that in the F41Y mutant the cysteine radical cation oxidizes the Tyr with a rate constant $k_X \gg k_A$, no adduct should be formed. Oxidation of Tyr is always associated with proton transfer since the pK_a value of tyrosine drops from 10.1 to -2 leading to inevitable deprotonation of $TyrOH^{\bullet+}$ to avoid high-energy pathways [79, 80]. If this deprotonation is faster than k_C and k_T, $TyrOH^{\bullet+}$ can not be observed, and the products are the same as in the mutants lacking the reactive Cys.

*Cr*LOV1-F41Y/C57G is the only mutant investigated which did not show a radical contribution in the µs timerange. The excited triplet state is populated in this mutant but deactivates non-radiatively to the ground state with a biphasic decay by a factor of ten to 100 slower compared to the other F41Y mutants. Therefore it behaves like *Cr*LOV1-C57G, the F41Y mutation does not influence the triplet state reaction in *Cr*LOV1-F41Y/C57G [47]. A similar behavior has been reported for a LOV based reporter protein in which a two-conformer model with different degrees of oxygen accessibility and therefore oxygen quenching has been suggested as an explanation [71]. This in turn indicates a very exposed flavin which would be accessible not only for oxygen but also for solvent molecules. And in fact, in *Cr*LOV1-F41Y/C57G we observed a very fast water exchange in the binding pocket by MD.

Nevertheless, strong quenching of the singlet state, i.e. reduced fluorescence quantum yield and lifetime, can be observed which we consider to be a consequence of electron transfer in the excited singlet state. It is known from cryptochromes that protonation of FMN N5 by a nearby Asp supports the formation of a stabilized radical pair in flavoproteins. E.g., in the case of *A. thaliana* cryptochrome, proton transfer from D396 to FAD was reported resulting in the very stable radical pair $FAD^{\bullet-}$+$W(H)^{\bullet+}$ [81, 82]. But according to our MD simulations the distance between Tyr41 and FMN is too large for direct protonation on very fast timescales and no alternative proton donor is located nearby FMN N5 in *Cr*LOV1-F41Y/C57G. Therefore, we propose that radicals formed in F41Y-C57G in the excited singlet state are not stabilized and recombine on a sub-µs timescale. The fact that two different reaction pathways are supported in *Cr*LOV1-F41Y/C57G leads to the conclusion that the FMN reactivity in this mutant is as well geometry-dependent.

The behavior of *Cr*LOV1-F41Y/C57G indicates that protonation of FMN N5 is significant for the stabilization of the radical pair $FMNH^{\bullet}$ $^{\bullet}OTyr$. Following the hypothesis of a PCET reaction from Tyr41 towards FMN, the electron as well as the proton donor is Tyr41 in *Cr*LOV1-F41Y, *Cr*LOV1-F41Y/C57S, and C57A. This is further supported by our TA measurements at basic pH values. The protonated $FMNH^{\bullet}$ could still be observed even at strongly basic pH of the solvent. This proves that protonation of the flavin radical can not be accomplished by water molecules in the binding pocket and that the proton donor must have a pK_a value higher than 11. With a calculated pKa value of > 12.00 in *Cr*LOV1-F41Y, F41Y/C57A and 11.45 in F41Y/C57S, Tyr41 is an appropriate candidate for the required pH range. Moreover, structures of the mutants derived from MD simulations reveal that Tyr41 is the only proton donor present in the binding pocket besides Cys57, which is only present in *Cr*LOV1-F41Y. The MD data further provide information about the accessibility of bulk water molecules into the binding pocket of the particular F41Y mutants. In any case, only one water molecule is located near the FMN at a given time in every particular mutant. If, however, this would be sufficient to deprotonate FMN N5 of the formed $FMNH^{\bullet}$, which we consider highly unlikely, the pK_a value of this flavin neutral radical must also be comparably high. The pK_a of $FMNH^{\bullet}$ in solution is 7.5, but can change drastically when incorporated in a protein [83].

2.4 Conclusions

We have designed a LOV domain which efficiently performs an electron transfer reaction instead of adduct formation as the initial step of the photo-reaction. This was achieved by substitution of a conserved Phe by Tyr in the LOV core, the reactive Cys still being in place. With additional mutation of this Cys to Ala or Ser, we were able to tune the yield and protonation state of the formed flavin radicals. The electron transfer in the LOV mutants comes along with a proton transfer, both provided by the introduced Tyr, and occurs either in the excited singlet or triplet state, depending on the geometry of donor and acceptor. Moreover, MD simulations on the LOV mutants allowed us to identify structural key parameters which are important for the electron transfer reaction to occur. A deeper understanding of the factors that control the reactivity of flavin in a protein environment could contribute substantially to the rational design of photoreceptor-based tools and sensors.

3 Reengineering the flavin photochemistry in iLOV

3.1 Introduction

Fluorescent proteins (FP) have become an important tool for *in vivo* imaging of protein dynamics over the last decades [84, 85]. The most prominent representative of this group is the green fluorescent protein (GFP) discovered in 1962 by Shimomura *et al.* [86]. Myriads of mutants of GFP have been made since then covering nearly the entire visible spectrum with their excitation and emission wavelengths [84]. Although being used extensively as fluorescent probes, GFP and its derivatives have some limitations: i) they are restricted to aerobic systems since their chromophore synthesis is oxygen-dependent [84], ii) their size is relatively large ($\sim 25\,\mathrm{kDa}$) and iii) GFP fluorescence is unstable at pH < 5 [87]. To overcome these limitations, LOV-based fluorescent proteins have been developed as an alternative to GFP [88–90]. One of them is the so-called iLOV protein [89]. iLOV is derived from the LOV2 domain of *Arabidopsis thaliana* Phot2. The reactive Cys426 was replaced by Ala to inhibit adduct formation and several rounds of DNA shuffling were applied to improve the fluorescent properties and the photostability [89].

The biological function of LOV domains is ultimately linked to the primary photoreaction of their FMN chromophore upon light excitation: the formation of a flavin-cysteinyl adduct. But recently, Yee *et al.* [61] showed that some LOV variants lacking the reactive Cys necessary for adduct formation, e.g. VVD and YF1, still show biological function. They revealed that photoreduction of FMN to $\mathrm{FMNH}^{\bullet}$ is sufficient for signal transduction within the protein, suggesting that the key parameter for signal transduction and hence the biological activity of LOV domains is the protonation of FMN-N5. The underlying mechanism of electron and proton transfer, however, remains unclear, in particular because the majority of LOV domains can only be photoreduced under anaerobic conditions and/or in the presence of external electron donors such as EDTA [60, 67, 69].

In this chapter, the iLOV protein was used as a model system to reengineer the flavin photochemistry towards efficient photoreduction under aerobic conditions. In the first section of this chapter the rational protein design resulting in the mutant iLOV-Q489D is described. This is followed by the experimental characterization of this mutant. The chapter closes with a discussion of the results in the context of a general applicability to LOV domains.

This research project was performed in collaboration with several groups. The results have been described in an article and submitted for publication. The protein design, production and purification, as well as the steady-state UV/Vis measurements and their analysis were done at the Institute of Molecular Enzyme Technology of the Heinrich-Heine University at the research center Jülich (Benita Kopka, Katrin Röllen, Ulrich Krauss and Karl-Erich Jäger). The EPR measurements and their analysis were conducted at the Max Planck Institute for Chemical Energy Conversion in Mühlheim/Ruhr (Anton Savitsky). The MD Simulations were performed and analyzed at the University of Aachen/DWI-Leibniz Institute for Interactive Materials Aachen (Mehdi D. Davari, Marco Bocola and Ulrich Schwaneberg). I have performed and analyzed the transient absorption measurements, analyzed several steady-state UV/Vis spectra and wrote parts of the manuscript. The main part of the manuscript was written by Ulrich Krauss. The following chapter presents the results, discussion and conclusions of this article. The experimental methods not performed by myself are not described here.

3.2 Results

3.2.1 Target protein selection and design rationale

LOV proteins in which the photo-active cysteine has been substituted for alanine cannot undergo adduct formation and thus show an intense cyan-green fluorescence resulting from excitation of the bound flavin chromophore [88, 89, 91]. Those LOV-based fluorescent proteins (LOV-FP), also called flavin-binding fluorescent proteins (FbFPs), represent a promising alternative to reporter proteins of the green fluorescent protein (GFP) family [88, 89]. Compared to GFP and related proteins, LOV-FPs often show reduced photostability [92, 93]. One potential cause for photobleaching is the photoreduction of FMN to the neutral semiquinone radical $FMNH^{\bullet}$. Thus a photostable LOV-FP should principally show little or no photoreduction in the presence of oxygen. One representative of FbFPs is the fluorescent protein iLOV derived from *A. thaliana* Phot2 [89]. iLOV has been structurally improved for increased photostability and is naturally non-photoreducible under aerobic conditions. This property makes iLOV a good engineering target to investigate whether efficient photoreduction of the flavin chromophore can be achieved by the introduction of a proton donating functional group in the LOV core. Next to a proton donor also an electron donating functional group needs to be present in the protein. While the electron has to be transferred from a protein residue, the proton can come from either a protein side chain or the aqueous solvent. We therefore reasoned that, to achieve efficient photoreduction, the introduction of a proton donating functional group is of paramount importance. Hence, we introduced an aspartate residue as potential proton donor in close vicinity of the flavin chromophore. Apart from the photo-active cysteine, or in case of LOV-FPs such as iLOV the introduced alanine,

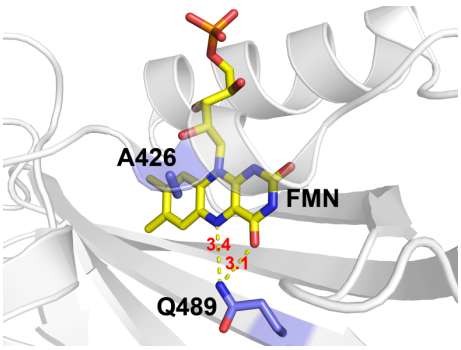

Figure 3.2.1 Close - up view of the FMN binding pocket of iLOV (PDB: 4EES) in cartoon representation. The FMN molecule, the Q489 side chain and A426, replacing the reactive Cys in iLOV, are shown in stick representation. Nitrogen, oxygen and phosphorous atoms are shown in blue, red and orange, respectively. Carbon atoms are shown in blue (Q489, A426) or yellow (FMN). Dashed lines highlight relevant interatomic distances (labeled in red) between Q489-NE2 - FMN-O4 and FMN-N5, respectively.

only a highly conserved glutamine residue (Q489 in iLOV), which according to the X-ray structure and previous MD simulations [91] forms a hydrogen bond with the FMN-O4 atom and is in close proximity of the FMN-N5 atom, is in a suitable position to enable proton transfer (Figure 3.2.1). We investigated the iLOV mutant Q489D in regard to electron and proton transfer reactions and compared the results to iLOV, hereafter referred to as parental iLOV.

3.2.2 Illumination of iLOV-Q489D results in effective formation of the neutral FMN semiquinone radical under aerobic conditions.

Steady-state UV/Vis spectrophotometric measurements of parental iLOV and iLOV-Q489D were carried out at $25 \pm 2\,^{\circ}\mathrm{C}$ under dim-red safety light. The samples were illuminated with a blue light-emitting high-power LED ($0.13\,\mathrm{mW/cm^2}$) in a pulsed fashion (5 s illumination per pulse). As expected for a photostable LOV-FP, the parental iLOV protein does not show any detectable photoreduction under aerobic or anaerobic conditions. The addition of excess amounts of the sacrificial electron donor EDTA under anaerobic conditions is necessary to photoreduce FMN to $\mathrm{FMNH^{\bullet}}$ (data not shown). In contrast, iLOV-Q489D is readily photoreduced under aerobic conditions (Figure 3.2.2A). Hereby, the illumination of dark-adapted iLOV-Q489D results in the loss of the absorbance band at around 450 nm, which corresponds to fully-oxidized FMNox (solid black line). Concomitantly, a new species with broad red-shifted absorbance with maxima at around 576 nm and 615 nm (dashed blue line) is formed, corresponding to $\mathrm{FMNH^{\bullet}}$ [60]. Photoreduction is complete within 150 s and proceeds with a lifetime of $\tau_{\mathrm{Sq}} = 25.7 \pm 0.2\,\mathrm{s}$ under the applied conditions (Figure 3.2.2A, inset). To rule out that the observed photoreduction of iLOV-Q489D is caused by reduced oxygen access to the active site compared to parental iLOV, we determined the efficiency of the reoxidation process

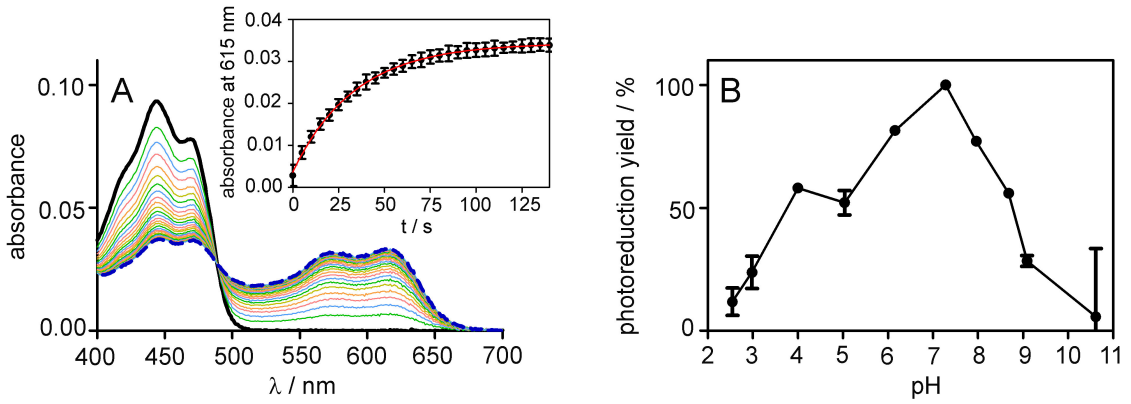

Figure 3.2.2 A: Spectral changes associated with photoreduction of iLOV-Q489D at pH 7.2. The dark-adapted sample (solid black line) was illuminated in 5 seconds time increments with a blue light-emitting LED (0.13 mW/cm^2) and sequential spectra were recorded (rainbow coloring) until no further spectral changes did occur (dashed blue line). The last spectrum corresponds to an illumination time of 150 seconds. The inset depicts the time trace of iLOV-Q489D photoreduction derived from the rise in absorbance at 615 nm. Experimental data were fit using a single-exponential decay function (red line) and proceeds with a photoreduction lifetime of $\tau_{\mathrm{Sq}} = 25.7 \pm 0.2$ s. **B:** pH dependence of iLOV-Q489D photoreduction yield. iLOV-Q489D photoreduction, at a given pH, was quantified from UV/Vis spectra by determining the rise in absorbance at 615 nm after 150 seconds illumination. Photoreduction yields are expressed relative to the maximum value (100 %) at pH 7.2. Error bars correspond to the standard deviation of the mean derived from three independent measurements.

after photoreduction for both, iLOV-Q489D and parental iLOV. Hereby, reoxidation apparently proceeds similarly fast in iLOV-Q489D ($\tau_{\mathrm{FMNox}} = 1502 \pm 27$ s) and parental iLOV ($\tau_{\mathrm{FMNox}} = 1376 \pm 520$ s) suggesting that reduced oxygen access is not the cause for the observed efficient photoreduction of iLOV-Q489D. To evaluate the pH dependence of the iLOV-Q489D photoreduction process, we carried out identical measurements in a pH range between pH 2.6 and 10.6. The spectral changes associated with illumination of iLOV-Q489D at pH 2.6 to pH 10.6 are summarized in Figure 3.2.3. Using these data, the photoreduction yield at a given pH was quantified from UV/Vis spectra by determining the blue light-induced rise in absorbance at 615 nm over the background at 700 nm (Figure 3.2.2B). The photoreduction yield is low at both acidic ($<$ pH 3) and basic ($>$ pH 9) pH values and shows a maximum at pH 7.2.

One possible explanation for low photoreduction yields at low acidic and high basic pH values could be a pH-dependent unfolding of iLOV-Q489D during the photoreduction measurement, which would result in the release of the flavin chromophore from the protein, hence abolishing the possibility of photoreduction by the protein. At a pH < 4, the corresponding UV/Vis spectra (Figure 3.2.3A, B and Figure 3.2.4A, B) show evidence for unfolding of iLOV-Q489D during the photoreduction measurement, i.e. the vibronic fine structure with a maximum at around 470 nm is lost during the photoreduction measurement and the whole spectra are broadened which results in a specific rise in absorbance at 495 nm (see Figure 3.2.4A and B).

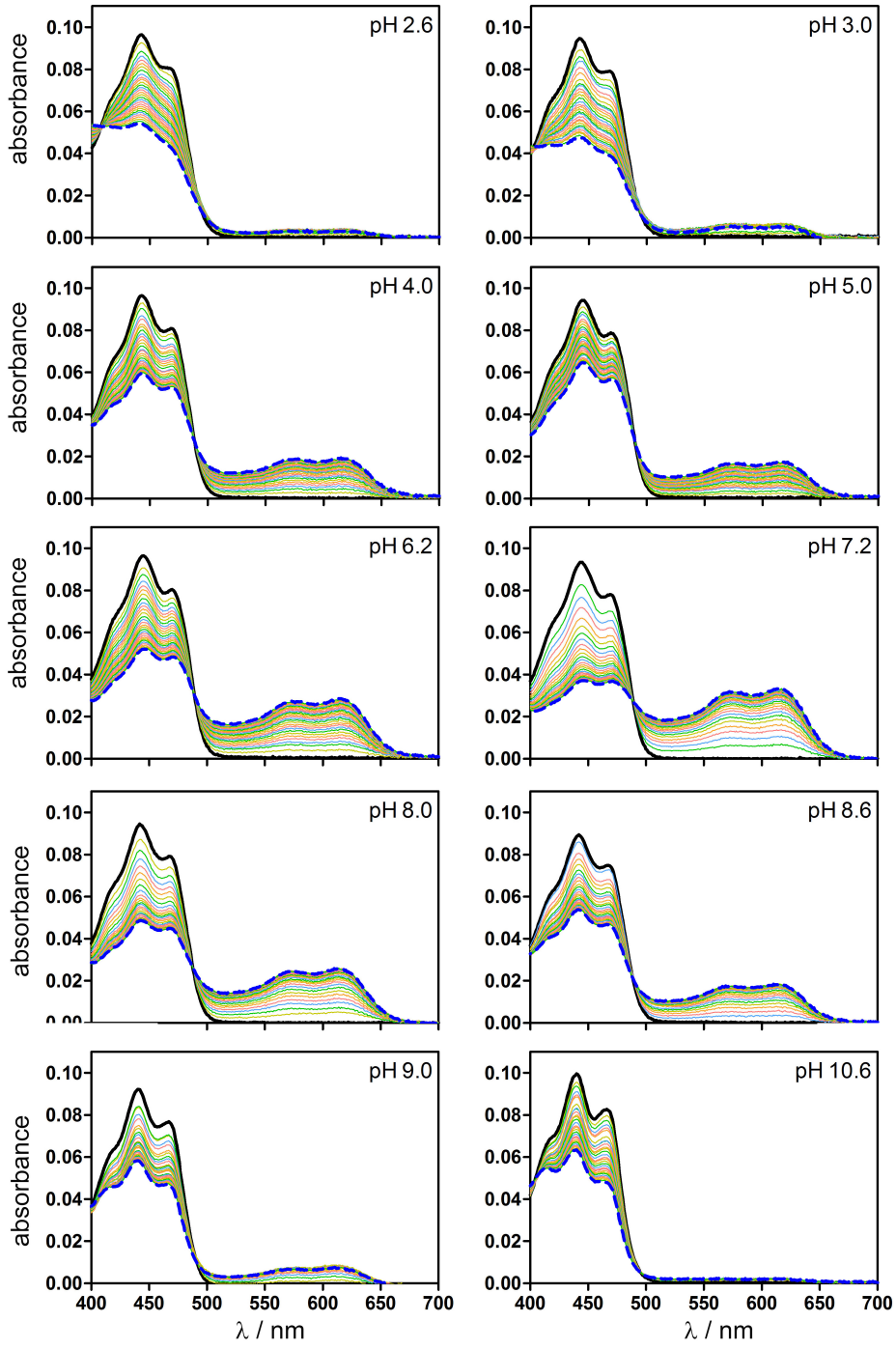

Figure 3.2.3 Spectral changes associated with illumination of iLOV-Q489D at pH 2.6 to pH 10.6. For clarity only one exemplary measurement out of three independent experiments per pH value is shown.

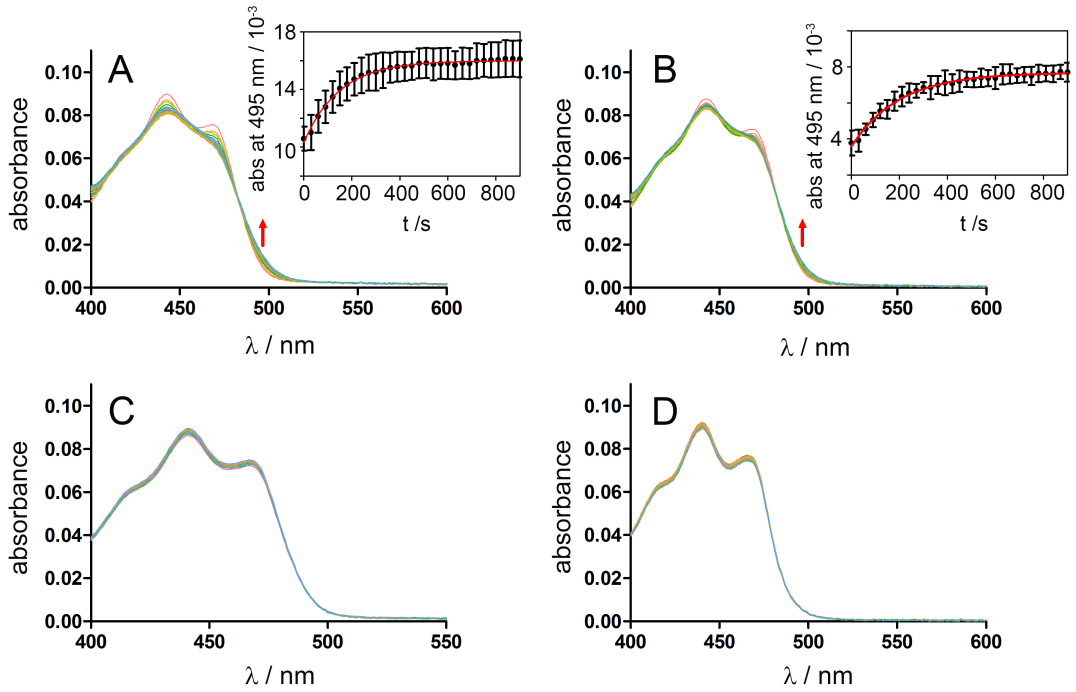

Figure 3.2.4 pH stability of iLOV-Q489D at **A:** pH 2.6, **B:** pH 3.0, **C:** pH 9.0 and **D:** pH 10.6. iLOV-Q489D was diluted to an $OD_{450\,nm}$ of approx. 0.1 in either 200 mM phosphate/citrate buffer (pH 2.6 and pH 3.0) supplemented with 10 mM NaCl or in 200 mM glycine/NaOH buffer (pH 9.0 and pH 10.6) supplemented with 10 mM NaCl. The samples were placed in a 1 cm quartz cuvette and incubated at 25 °C in the spectrophotometer for up to 15 minutes. Sequential UV/Vis spectra were recorded at a time interval of 30 s (shown in rainbow coloring). At **A:** pH 2.6 and **B:** pH 3.0 the UV/Vis spectra are indicative of unfolding and release of the flavin chromophore of iLOV-Q489D, which was followed over time by plotting the rise in absorbance at 495 nm (red arrow) against the incubation time (inset). The resulting data could be fit using a single-exponential decay function. The unfolding proceeds with a lifetime of $\tau_{pH} = 148 \pm 9$ s at pH 2.6 and $\tau_{pH} = 191 \pm 11$ s at pH 3.0. The lifetimes correspond to an illumination time of the corresponding samples of about 25 and 32 s at pH 2.6 and pH 3.0, respectively. At **C:** pH 9.0 and **D:** pH 10.6 no spectral changes are observed, which suggests that at those pH values iLOV-Q489D is stable during the incubation time. Error bars correspond to the standard deviation of the mean derived from three independent measurements.

At all other pH values no evidence for unfolding of iLOV-Q489D during the measurement is observed (see Figure 3.2.3C-J). To quantify the pH-dependent unfolding of iLOV-Q489D at the two lowest pH values (pH 2.6 and pH 3.0), we measured sequential UV/Vis spectra under identical conditions as used in the photoreduction experiment but did not illuminate the sample (Figure 3.2.4A and B). As control, the pH stability of iLOV-Q489D at the two highest pH values (pH 9.0 and 10.6) was measured (see Figure 3.2.4C and D). At pH 2.6 (Figure 3.2.4A) and pH 3.0 (Figure 3.2.4B) the UV/Vis spectra are indicative of unfolding and release of the flavin chromophore of iLOV-Q489D. The unfolding and flavin release proceeds with a lifetime of $\tau_{\mathrm{pH}} = 148 \pm 9\,\mathrm{s}$ (pH 2.6) and $\tau_{\mathrm{pH}} = 191 \pm 11\,\mathrm{s}$ (pH 3.0) which corresponds to an illumination time of the samples of about 25 and 32 seconds, respectively.

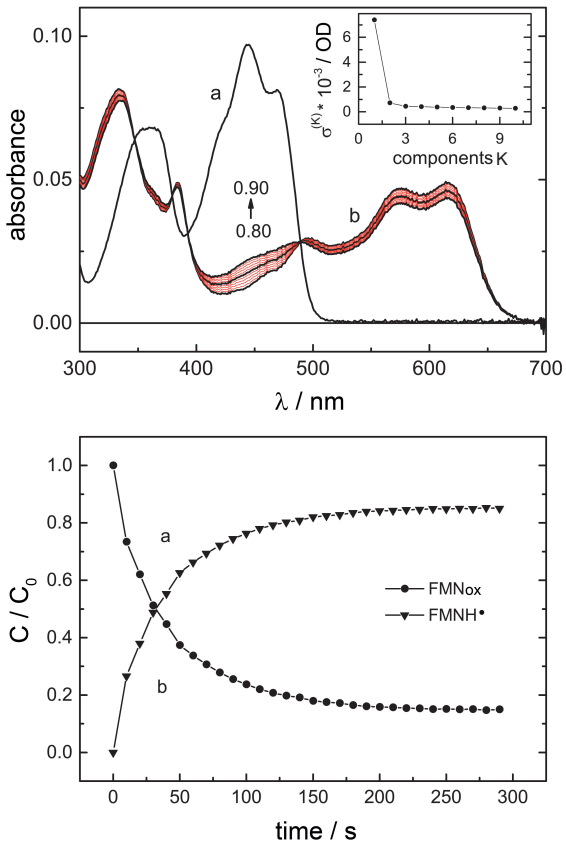

Figure 3.2.5 SVD analysis of the photoreduction data of iLOV-Q489D at pH 7.2 (data from Figure 3.2.3). **A:** The reconstructed spectra of FMNox (a) and FMNH$^\bullet$ (b) in the range $0.8 < \alpha < 0.9$. The inset shows σ(K) as a function of the components, K, indicating that two significant components are present. **B:** Concentration time profiles for $\alpha = 0.85$ of FMNox (a) and FMNH$^\bullet$ (b).

At pH 7.2 the respective spectra (Figure 3.2.3) provide clear evidence for the formation of $FMNH^{\bullet}$, with the process being fully reversible in the dark. We performed singular value decomposition (SVD) of this data set (Figure 3.2.5). The plot of the deviation σ(K) vs the components K indicates that only two components contribute significantly to the spectra at pH 7.2. We considered the absorption in the range 250 - 700 nm, and up to 290 s. For the reconstruction of the spectrum of the photo-product we used a two-component model that depends on an adjustable parameter α. The procedure is explained in detail in the Appendix. The analysis yields reasonable, reconstructed spectra in the range $0.8 < \alpha < 0.9$ (Figure 3.2.5A). The concentration-time profiles for $\alpha = 0.85$ of FMNox and the product $FMNH^{\bullet}$ are shown in Figure 3.2.5B. Note that this reconstruction conserves the isosbestic points in the two spectra.
At pH 2.8 and pH 9.8 we observe an initial rapid formation of minor amounts of $FMNH^{\bullet}$, as evidenced by an initial increase of the $FMNH^{\bullet}$ absorbance band at 615 nm, which does not increase above a certain value (Figure 3.2.3). Interestingly, the band corresponding to FMNox at 450 nm does decrease further after prolonged illumination. This is accompanied with the formation of a new maximum at around 390 nm. Hereby the initially formed $FMNH^{\bullet}$ is slowly further interconverted, as evidenced by the loss of absorbance at 615 nm during prolonged illumination. In both cases the process appears irreversible in the dark.
To address this issue we repeated the experiment and subsequently extracted the protein-bound flavins from the protein solution and analyzed the flavin composition by Ultra-High-Performance-Liquid-Chromatography (UPLC) (Figure 3.2.6). Native (pH 7.2) iLOV-Q489D binds predominately FMN with minor amounts of lumichrome present in the sample (Figure 3.2.6B). Since lumichrome is a photodegradation product of flavins [94] it seems likely that during sample preparation, which was carried out under daylight conditions, a certain amount of lumichrome accumulated. Samples illuminated at pH 2.6 and 9.8 exclusively contain lumichrome after prolonged illumination (Figure 3.2.6C and D). Thus the observed decrease of the FMNox absorbance band during prolonged illumination appears to be related to photodamage of the flavin chromophore.
In conclusion, when the pH stability of iLOV-Q489D is taken into account, the observed pH dependence of the iLOV-Q489D photoreduction appears to be linked to a proton transfer process which is most efficient at neutral pH values. This observation and the complete lack of photoreduction of parental iLOV under identical experimental conditions renders the newly introduced Asp side chain the most likely proton donor.

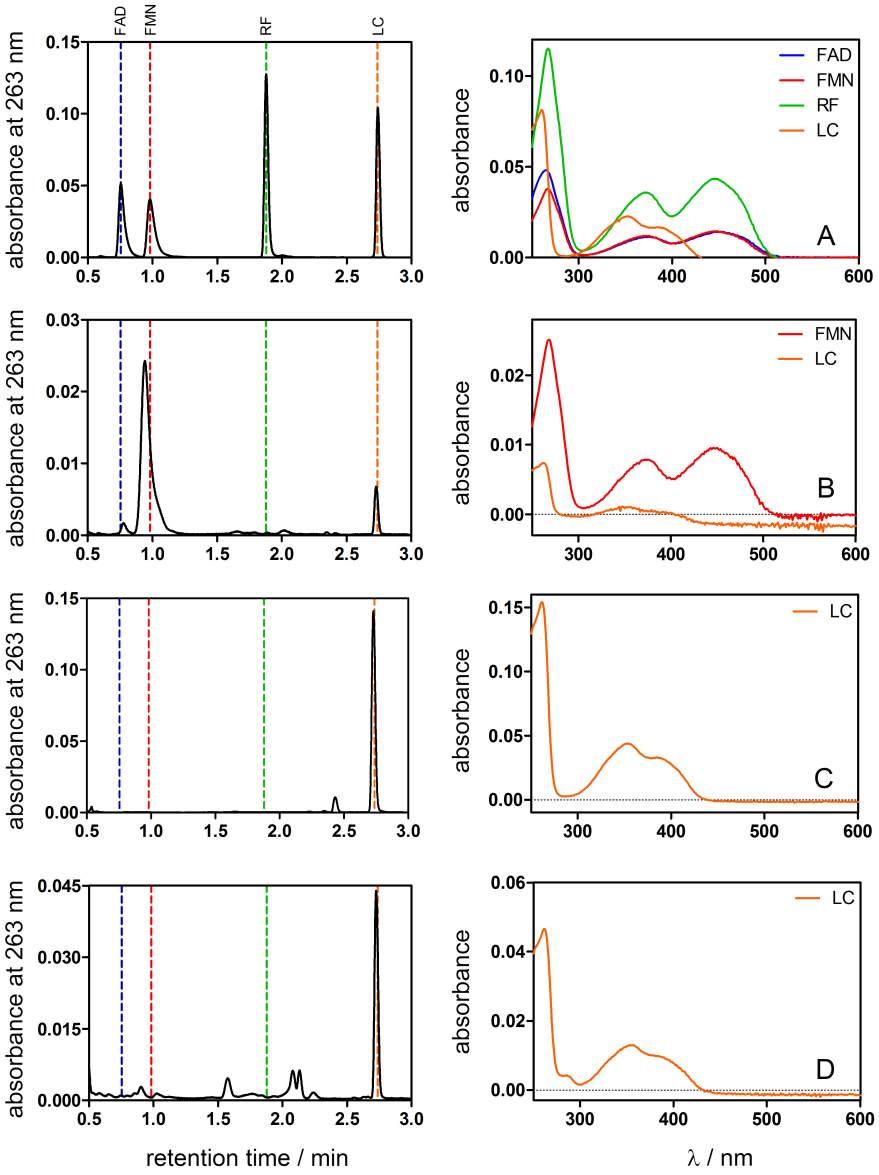

Figure 3.2.6 UPLC analysis of iLOV-Q489D at pH 7.2 and after photoreduction at pH 2.6 and 9.8. Authenic flavin adenine dinucleotide (FAD), flavin mononucleotide (FMN), riboflavin (RF) and lumichrome (LC) were used as standards. **A:** The corresponding UPLC chromatogram is shown along with the UV/Vis spectrum of the respective elution peak. FAD, FMN, RF and LC elute at 0.75 min, 0.97 min, 1.87 min and 2.73 min, respectively (marked by dashed lines). **B:** The native chromophore content of iLOV-Q489D was determined by extracting the flavins from a dark-adapted sample adjusted to pH 7.2. At pH 2.6 and pH 9.8 the samples were illuminated until no further spectral changes occurred (60 min) and protein bound flavins were extracted. Subsequently, the extracted flavins were analysed by UPLC. The corresponding chromatograms and elution peak spectra are shown in panel **C** (pH 9.8) and **D** (pH 2.6), respectively. Please note, that at pH 2.6 the overall signal intensity was 3-fold lower than for the pH 9.8 sample, although similar amounts of protein were denatured to release the protein bound flavins.

3.2.3 UV / Vis spectra of iLOV-Q489D along with computational prediction suggest that the newly introduced Asp is protonated at neutral pH values

The above presented pH dependence of the photoreduction process in iLOV-Q489D suggests that the introduced Asp acts as a proton donor for the photoreduction process. Therefore, the side chain of Q489D must be protonated at neutral pH values to account for the observed pH dependence. Hence, compared to free aspartate (pK_a = 3.9), the pK_a value of D489 must be substantially shifted towards more neutral pH values which could be caused by the protein environment [95–97]. To account for this possibility we computationally introduced the Q489D mutation in the parental iLOV structure (PDB ID: 4EES) and predicted the pK_a of the introduced Asp by using the PROPKA 3.1 program [98]. In line with the experimental data, PROPKA predicts a pK_a of 6.28 for the newly introduced Asp in iLOV-Q489D. Alteration of the H-bonding network around the FMN-N5 atom in iLOV, e.g. by substitution of Q489 for Asp or by the presence of either a protonated or unprotonated (and hence charged) Asp side chain in iLOV-Q489D at different pH values, is expected to influence the flavin absorbance band in the violet/blue region of the spectrum [91]. To address this issue we compared UV/Vis spectra of parental iLOV and iLOV-Q489D at pH 7.2, pH 2.8 and pH 9.8 (Figure 3.2.7A).

Parental iLOV (Figure 3.2.7A, black dashed line) shows an absorbance maximum at around 447 nm corresponding to the S_0-S_1 transition. At pH 7.2 (red solid line) and pH 2.8 (green solid line) the absorbance maximum of iLOV-Q489D is slightly blue-shifted by 4 or 5 nm, respectively. In contrast, at pH 9.8 the absorbance maximum of iLOV-Q489D is clearly blue-shifted by 7 nm to about 440 nm. To study how the Q489D substitution influences the structure of iLOV, the iLOV-Q489D variant was constructed *in silico* using the crystal structure of parental iLOV as a starting structure. A rotamer search was conducted with FoldX [99, 100] exploring alternative conformations of the surrounding side chains. To investigate possible conformational changes associated with the Q489D mutation, we performed three independent 50 ns MD simulations of the iLOV-Q489D variant starting from the most stable FoldX predicted structure in both protonated and deprotonated states of D489. Analysis of the D489 side chain highlights the structural changes surrounding the residue D489 near to the FMN chromophore during the MD simulations (Figure 3.2.7B and C). Figure 3.2.7C shows the analysis of the interatomic distances for the D489-FMN interaction along MD trajectories, indicating that protonated D489 preserves an H-bond with the FMN-O4 atom. Independent H-bond analysis of the trajectories shows that in approx. 70% of the trajectories protonated D489 forms an H-bond with FMN-O4. In contrast, in the simulation containing deprotonated D489 the D489 side chain samples multiple conformations along the trajectories but does at no time form an H-bond with the FMN chromophore. Inspection of the simulation reveals that D489 flips away from the FMN chromophore followed by the entrance of some water molecules to the FMN binding pocket (Figure 3.2.7B and C). The 7 nm

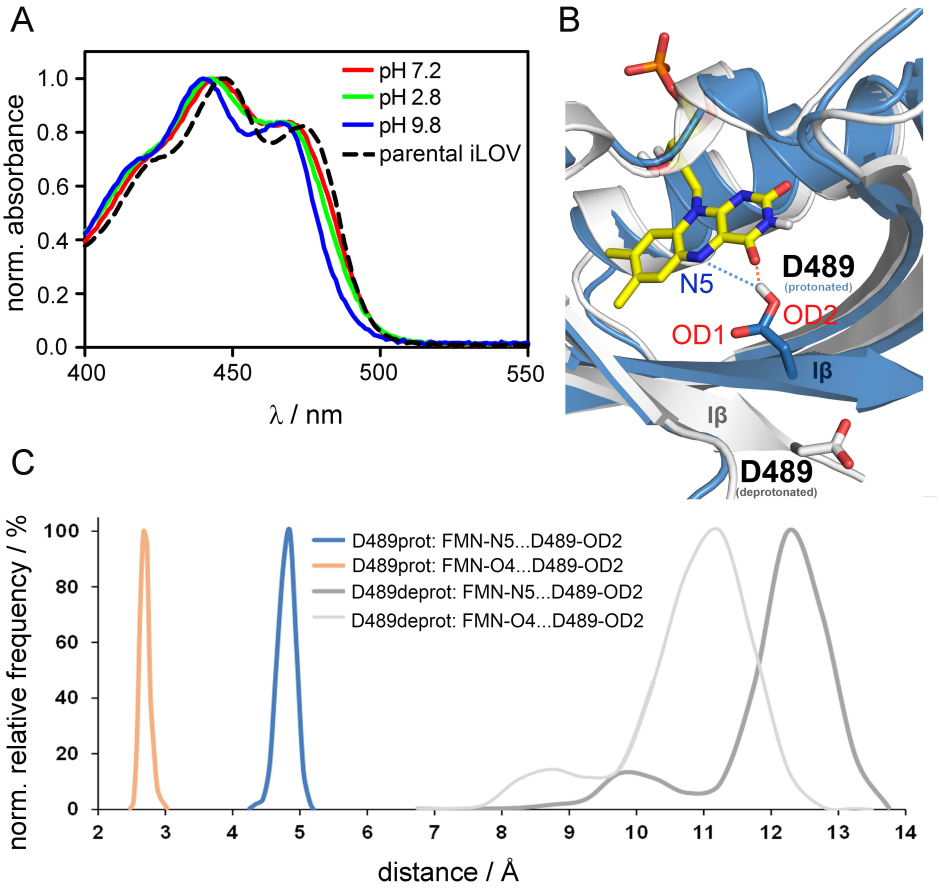

Figure 3.2.7 A: UV/Vis spectra of parental iLOV (black dashed line), iLOV-Q489D at pH 7.2 (red solid line), pH 2.8 (green solid line) and pH 9.8 (blue solid line). **B:** Close-up view of the FMN binding pocket of iLOV-Q489D in cartoon representation. Representative structure of the FMN chromophore binding pocket of iLOV with protonated D489 and deprotonated D489 taken from the MD trajectories. The snapshot was selected based on cluster analysis of the MD trajectories. The N5 and O4 atoms of FMN are labeled for reasons of clarity, as well as the OD1 and OD2 atom of D489. The atom numbering is according to the PDB file. **C:** Average distance distribution curve of the interatomic distances for the indicated residues (in Å) calculated over three independent MD trajectories of iLOV-Q489D with protonated and deprotonated D489. H-bond analysis (with geometric cutoff for hydrogen-bond distance and angle values of 3.2 Å and $150\,^{\circ}$, respectively) shows that protonated D489-OD2 preserves a hydrogen bond with FMN-O4 ∼70 % of the time in the simulations.

blue-shift observed for iLOV-Q489D at pH 9.8 can readily be explained based on our MD simulation of iLOV-Q489D with deprotonated D489, where the side chain of D489 flips away from the chromophore (Figure 3.2.7B and C), with the loss of H-bonding between D489 and FMN resulting in a blue-shifted absorption maximum similar to the recently characterized iLOV-Q489K variant [91]. Likewise, the small 4–5 nm blue-shift observed at pH 7.2 and pH 2.8, respectively, can be explained by altered protein-FMN interactions compared to parental iLOV. In parental iLOV the NE2 atom of Q489 (atom labeling according to the PDB file) is in close proximity to the FMN-N5 atom (< 3.5 Å) [91] and forms an H-bond with the FMN-O4 atom. While the H-bond to FMN-O4 is retained in our MD simulations of iLOV-Q489D with protonated D489, the average distance between the OD2 atom of D489 and FMN-N5 is increased (> 4.5 Å) (Figure 3.2.7C), which may result in a blue-shifted absorbance maximum.

3.2.4 Transient absorption spectroscopy hints at the formation of a stable FMN:protein radical pair in iLOV-Q489D

In order to gain insight into the mechanistic details upon blue light excitation, TA spectroscopy was performed with iLOV-Q489D and parental iLOV. Figure 3.2.8A and B show difference absorption spectra of iLOV-Q489D and parental iLOV extracted from the 2-dimensional TA data measured on a 200 µs time window. In a first step, the evolution of the spectrum over time of iLOV-Q489D will be discussed. The negative absorption band in the range of 410 nm–490 nm, which is not recovering within the 200 µs time window, corresponds to the ground-state bleach of FMNox. Furthermore, a positive fine-structured absorption band above 650 nm can be observed, which decays within 100 µs completely. The positive peak between 360 nm and 410 nm is decreasing simultaneously within this time range. After 100 µs the transient absorption signal stays constant within the measured time window, with a significant positive contribution between 490 nm and 650 nm and a minor absorption band around 385 nm. In contrast, a different behavior is observed for parental iLOV. In this case, the ground-state bleach of FMNox is almost fully reverted after 200 µs. Besides this, a positive absorption band between 495 nm and 750 nm and between 417 nm and 350 nm occurs, which decreases within the measured time window. After 182 µs almost no transient absorption signals can be detected.

To gain further insight into the underlying processes, global lifetime analysis was performed resulting in the DADS of iLOV-Q489D (Figure 3.2.8C) and parental iLOV (Figure 3.2.8D). In both cases two contributing species were sufficient to fit the data. The first DADS is decaying with a rate constant of 28.0 µs (iLOV-Q489D) and 21.6 µs (parental iLOV), respectively. Next to the negative absorption signal of the ground state bleach of FMNox in the range of 420 nm to 495 nm, the D_1 exhibit positive bands between 350 nm and above 495 nm. By comparison with published flavin spectra [65], these DADS can be associated with the triplet state absorption

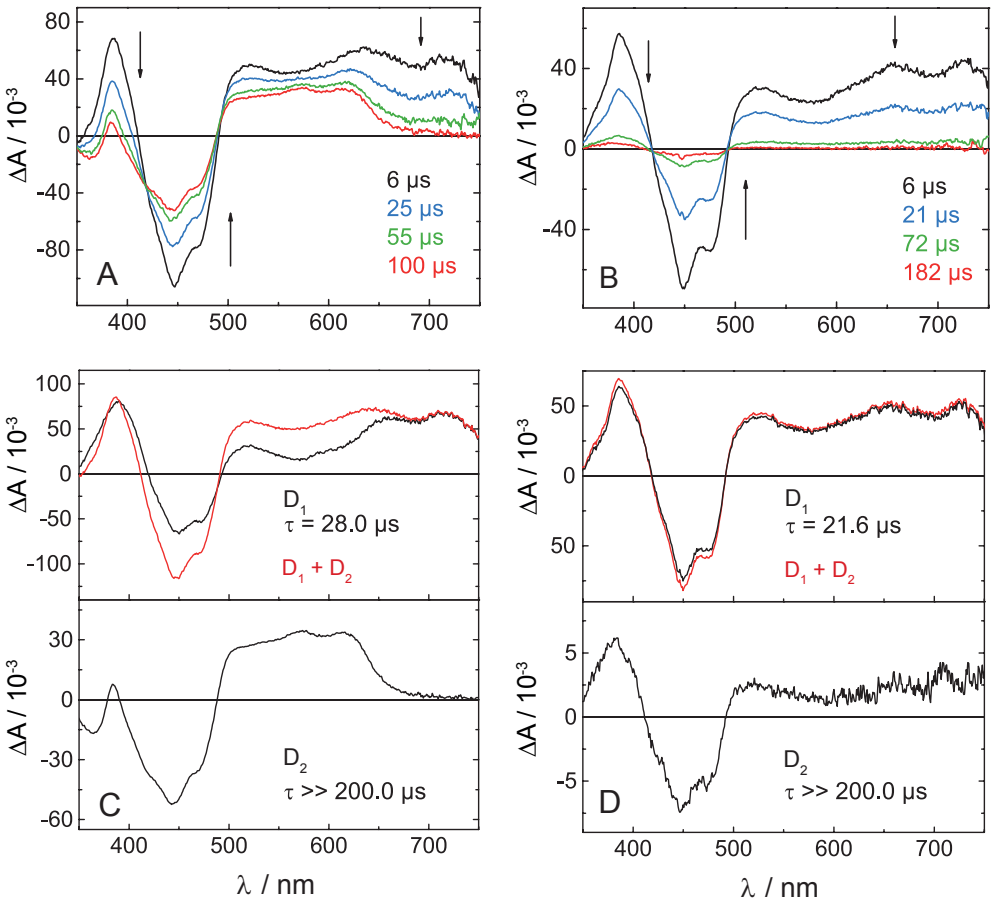

Figure 3.2.8 Difference absorption spectra of **A:** iLOV-Q489D and **B:** parental iLOV extracted from TA datasets at indicated times. TA was measured on a 200 µs time window. DADS of **C:** iLOV-Q489D and Figure 3.2.7 parental iLOV resulting from global lifetime analysis. D_1 decays with a time constant of 28.0 µs in the case of iLOV-Q489D and 21.6 µs for parental iLOV. The D_2 are non-decaying within the measured time window in both samples. The sum of both DADS (red lines in C and D) represents the initial situation of the systems before any decay processes.

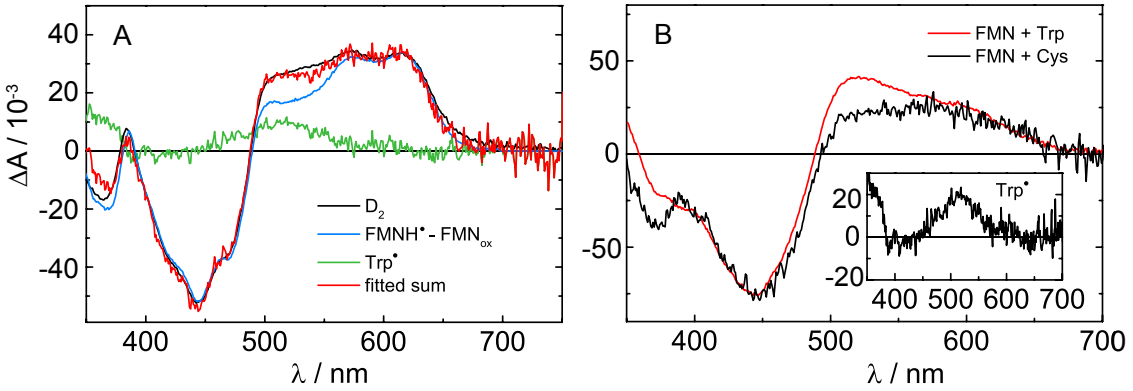

Figure 3.2.9 A: D_2 of iLOV-Q489D (black line and Figure 3.2.8C) shows typical spectral features of the FMN neutral semiquinone radical with a band around 390 nm and a fine-structured, broad absorption band between 490 nm and 670 nm. For direct comparison, the difference spectrum of $FMNH^{\bullet}$ minus FMNox obtained in the steady-state UV/Vis spectra is shown (blue line). To account for the differences in the range of 490 nm to 550 nm, the contribution of $Trp^{\bullet}$ (green line) is necessary for spectral fitting of D_2. **B:** Comparison of the difference absorption spectra of FMN+Trp (red line) and FMN+Cys (black line) in the absence of apoprotein. Blue-light excitation of FMN in the presence of Trp leads to the formation of $FMNH^{\bullet}$ and $Trp^{\bullet}$. When exciting FMN in the presence of Cys, only the neutral flavin semiquinone radical $FMNH^{\bullet}$ absorbs in the visible range of the spectrum. The difference of the two transient spectra scaled to the same minimum at 450 nm yields the difference absorption spectrum of $Trp^{\bullet}$ (inset).

of FMN. The D_2 of iLOV-Q489D and parental iLOV are both non-decaying within the measured time window and the spectra are strongly divergent. D_2 of parental iLOV is very weak and looks highly similar to the triplet decay spectrum represented by D_1, indicating a biphasic triplet decay. The slower decaying component in D_2 has approx. 10 % of the amplitude of D_1. This indicates that a second quenching channel exists in parental iLOV. A possible reason for this could be that parental iLOV adopts a minor second conformation, in which the quenching channel is not active. D_2 of iLOV-Q489D on the other hand, exhibits a strongly positive, fine-structured absorption band between 490 nm and 650 nm and a smaller peak around 385 nm, as well as the negative absorption band of the ground-state bleach of FMNox between 390 nm and 490 nm. The broad, vibronically fine-structured absorption band above 500 nm is a characteristic feature of the neutral semiquinone radical $FMNH^{\bullet}$ [65, 101]. For direct comparison, the difference spectrum of $FMNH^{\bullet}$ minus FMNox, derived from the steady-state UV/Vis spectra of iLOV-Q489D, is shown together with D_2 in Figure 3.2.9A. The two spectra diverge significantly in the range of 492 nm to 560 nm.

Therefore, an additional component is necessary to fit D_2. The efficient formation of $FMNH^{\bullet}$ in iLOV-Q489D originates from an electron transfer reaction, suggesting that the third component in D_2 refers to the radical species produced by the electron donor, most likely one of the amino acids of iLOV-Q489D. Natural candidates are Trp and Tyr. The neutral tyrosyl radical, $TyrO^{\bullet}$, is known to have solely a narrow absorption peak around 405 nm in the visible range [102, 103], while the

corresponding $Trp^{\bullet}$ has a distinct absorption between 440 nm and 580 nm [104, 105], indicating that $Trp^{\bullet}$ is more likely the counter-radical of $FMNH^{\bullet}$. $TrpH^{\bullet+}$ absorbs as well in the visible range with a broad absorption band between 450 and 650 nm exhibiting a maximum at 560 nm and additionally at 335 nm [104], but since the neutral semiquinone radical of FMN is formed, the corresponding radical species of the electron donor is considered to be also present in its neutral state. As further support for the contribution of $Trp^{\bullet}$ to D_2 of iLOV-Q489D, we generated a reference spectrum of the tryptophanyl radical in solution at pH 8.0. We excited FMN in the absence of apoprotein at 447 nm in the presence of Trp and measured TA on a 20 µs time window. The resulting difference spectrum is shown in Figure 3.2.9B (red line). The spectrum remained unchanged from 9–20 µs and was averaged. The spectral signature exhibits similarity to the D_2 of iLOV-Q489D and the contributing species can be assigned to $FMNH^{\bullet}$ and $Trp^{\bullet}$ [106]. An identical measurement was performed with FMN and Cys, also resulting in the formation of $FMNH^{\bullet}$ and the concomitant $CysS^{\bullet}$ (Figure 3.2.9B, black line). Since the cysteinyl radical does not absorb in the visible range [107], the difference between FMN+Trp and FMN+Cys yields the spectrum of $Trp^{\bullet}$ (see Figure 3.2.9B, inset). It should be noted that the reference spectra generated with FMN do not exhibit a fine structure of the absorption bands at 430, 460, 580 and 610 nm as observed for iLOV-Q489D. The vibrational fine structure of the absorption bands in the iLOV spectra are an additional proof for the incorporation of the FMN in the protein core. Including this reference spectrum of $Trp^{\bullet}$ to the fit procedure reproduces the D_2 of iLOV-Q489D adequately (see Figure 3.2.9A, red line). This clearly suggests that the electron donor responsible for the efficient formation of $FMNH^{\bullet}$ in iLOV-Q489D is W467, the only Trp of the protein.

3.2.5 $FMNH^{\bullet}$ formation occurs from the excited triplet state in iLOV-Q489D

TA measurements of parental iLOV and iLOV-Q489D reveal different processes upon blue light excitation in both iLOV proteins. While the difference absorption spectra of iLOV-Q489D show the formation of a species, which is non-decaying on the measured time window, parental iLOV exhibits almost no transient signals after 200 µs. Global lifetime analysis provides evidence for the formation of the triplet state in both iLOV variants. It is noteworthy that the spectral shape of the D_1 in Figure 3.2.8C and D differs significantly between 525 nm and 650 nm. However, DADS represent the spectra of evolving species (educts) minus the spectra of the species the educts will decay to (products) and are associated with a specific rate constant. In the case of D_1 of iLOV-Q489D, the educt is the excited triplet state of FMN and the products are the FMN ground state, FMNox, and, under the assumption that the observed flavin radical is formed via the triplet state, $FMNH^{\bullet}$ accounting for the spectral differences described above. As support for the hypothesis of an electron transfer reaction via the excited triplet state of flavin in iLOV-Q489D, the

sum of all DADS of parental iLOV and iLOV-Q489D are shown for comparison in Figure 3.2.8C and D (red lines). The sum of D_1 and D_2 represents the initial situation of the iLOV proteins before any decay processes on the µs - timescale occur (namely the t_0 spectra). The spectra are identical for parental iLOV and iLOV-Q489D (direct comparison not shown). Since no radical species could be observed in the case of parental iLOV, the t_0 spectrum represents the pure triplet spectrum of FMN in both iLOV variants, proving that the observed $FMNH^\bullet$ was not yet formed at t_0 in iLOV-Q489D. This essentially rules out $FMNH^\bullet$ formation from the excited singlet state. Further support for this triplet reaction model is given by the fact that we determined the fluorescence decay time from the S_1 state of iLOV-Q489D to be $\tau_{fl} = 5.0\,ns$. The same value has been reported for parental iLOV [108]. The observed fluorescence lifetime suggests that the S_1 state of iLOV-Q489D is not quenched as would be expected for an electron transfer occurring from the excited singlet state.

3.2.6 Electron paramagnetic resonance (EPR) spectroscopy reveals the presence of a stable radical pair in iLOV-Q489D

Figure 3.2.10A shows X-band continuous wave (cw) EPR spectra of parental iLOV (black trace) and iLOV-Q489D (blue trace) illuminated with a pulsed laser at 450 nm for 20 min at 120 K. More prolonged illumination does not lead to significant changes in the EPR spectra. The EPR spectrum of parental iLOV is composed of a symmetrical line positioned around $g = 2.0034$ with a partially resolved hyperfine structure. This spectrum is virtually identical to that of the neutral semiquinone FAD radical in *Escherichia coli* DNA photolyase reported previously [109]. In contrast, the EPR spectrum of iLOV-Q489D spreads over a larger frequency range (approx. 15 mT). It is thus much broader than the EPR spectra of individual radicals expected in the system, i.e. $FMNH^\bullet$ [109], tyrosine [110] or tryptophan [110–113] radicals. The nature of this signal was revealed using the electron spin echo nutation experiment. Here, a preparation microwave pulse of variable duration is inserted in the pulse sequence before the Hahn echo detection block, and the oscillation (nutation) of the echo signal is monitored as a function of the preparation pulse length (t_p). The frequency of the EPR signal oscillation with increasing preparation pulse length (nutation frequency, ν_{nut}) is related to the spin quantum numbers (S, m_s) of the excited EPR transition according to the equation [114, 115]:

$$\nu_{nut} = \alpha \cdot \omega_1/2\pi,\ \alpha = \sqrt{S(S+1) - m_s(m_s \pm 1)} \tag{3.1}$$

where ν_{nut} is the nutation linear frequency, ω_1 is the microwave field strength in angular frequency units, and the α factors describe the transitions in $S = 1/2$ and $S = 1$ spin manifolds are $\alpha = 1$ and $\alpha = \sqrt{2}$, respectively. The nutation curves recorded at two magnetic field positions for iLOV-Q489D are shown in Figure 3.2.10B. Their

Fourier transforms are depicted in Figure 3.2.10C. At the low field position, the nutation spectrum is composed of a single peak, whereas in the center two well resolved peaks with a frequency ratio of 1.4 can be observed (see Figure 3.2.10C). Thus, the broad spectral contribution is assigned to triplet T ($S=1$) state species. The spectral intensity in the center stems as expected from a doublet D ($S=1/2$) radical species. Simulation of the EPR spectrum using an overall inhomogeneous spectral line width of Gaussian shape of 3 mT yields the fine structure parameter of $|\mathrm{D}|=4\pm1$ mT and $|\mathrm{E}|=0$. The parameter D is directly connected to the distance r between two spins: $D=\frac{2.79}{r^3}T\cdot\text{Å}^3$ assuming g-values of radical pairs to be equal to the free electron g_e. Thus, the estimated D value corresponds to 9 ± 1 Å electron-electron distance in point-dipole approximation, i.e. neglecting spin distribution over the radical structures. We note, however, that this estimate gives the shortest possible distance, because neither the real spectral shapes of individual radicals nor the spin density distribution can be taken into account in the analysis. In order to obtain additional information about possible electron transfer pathways, annealing experiments were performed. The EPR spectrum of iLOV-Q489D was continuously monitored while the sample temperature was increased from 120 K. Up to 200 K (about the glass transition temperature of the water/glycerol solution) no changes were observed. Above 200 K the spectrum changes and the broad contribution continuously disappears to the favor of a narrow line at $g=2.0034$. The resulting spectrum recorded at 120 K after sample equilibration at 240 K for 10 min is shown in Figure 3.2.10A (green line). The spectrum mostly contains contributions of $FMNH^{\bullet}$. This spectrum is in good agreement with one recorded after room-temperature illumination and subsequent trap freezing in liquid nitrogen (data not shown).

Taken together, EPR spectroscopy performed at low temperature corroborates the presence of a flavin:protein radical pair, which was observed at room temperature in TA measurements of iLOV-Q489D. While no radical formation is observed in room temperature TA data of parental iLOV, $FMNH^{\bullet}$ is detected at low temperatures by EPR, although with a much lower amplitude.

3.2.7 Mutational analysis of the electron transfer pathway in iLOV-Q489D suggests the involvement of multiple Tyr/Trp residues

Both, transient absorption and EPR measurements, suggest that upon illumination of iLOV-Q489D a stable FMN:protein radical pair is formed, while TA measurements suggest that the sole Trp of iLOV-Q489D (W467) represents the potential counter radical (see above). Based on EPR experiments a minimum electron - electron distance of 9 ± 1 Å between the flavin radical and the protein radical can be calculated. As potential electron donors for the photoreduction process, and hence candidates for the amino acid constituting the counter protein radical, iLOV-Q489D possesses

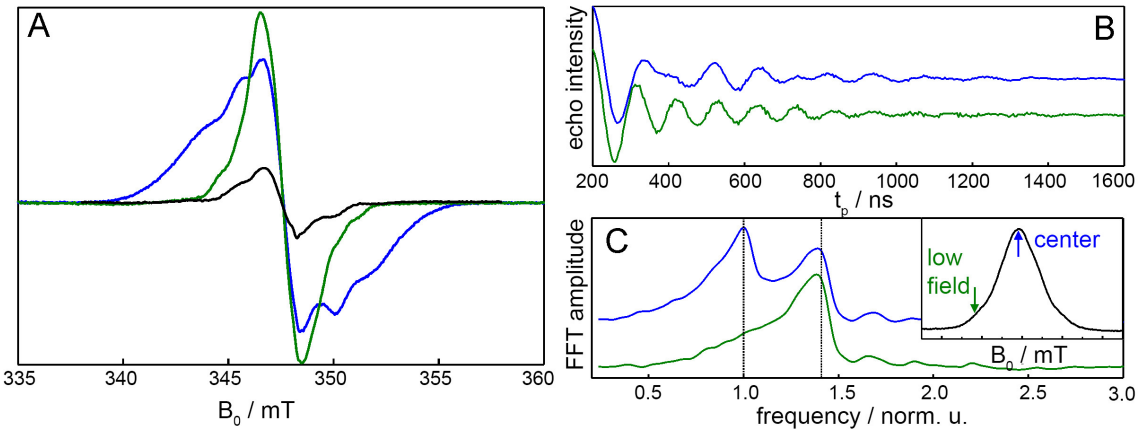

Figure 3.2.10 A: X-band continuous wave (cw) EPR spectra of parental iLOV (black trace) and iLOV-Q489D (blue trace) recorded after 20 min illumination of the dark-adapted samples. The green trace shows the EPR spectrum of illuminated iLOV-Q489D after annealing for 10 min at 240 K. All spectra were acquired at 120 K. **B:** Electron spin echo nutation time traces and **C:** their Fourier transforms for the illuminated iLOV-Q489D sample recorded at the magnetic field positions marked by arrows in the inset panel C which shows field-swept echo-detected EPR spectrum at 120 K. The dashed lines in C mark the frequency positions of FFT amplitude maxima. The frequency axis is normalized to the frequency of the low frequency peak in the upper trace.

three tyrosines (Y416, Y459 and Y484) as well as the above mentioned tryptophan (W467). In the X-ray structure of parental iLOV (PDB 4EES) they are located at a distance of 11.9 Å (Y416), 12.8 Å (Y459), 15.9 Å (Y484) and 14.1 Å (W467) from the FMN molecule. Similar distances are observed in MD simulations of iLOV-Q489D. Out of the four residues, only W467 samples multiple conformations and thus appears very flexible.

In order to infer if W467, which is observed as counter radical in TA measurements, despite its larger distance from the FMN chromophore, represents the sole electron donor in iLOV-Q489D, we generated variants of iLOV-Q489D in which the respective residues were substituted for phenylalanine. The corresponding double mutants were expressed and purified in an identical manner like parental iLOV and iLOV-Q489D. With the exception of iLOV-Q489D/Y459F, which did not express well and showed a reduced flavin load (data not shown), all proteins could readily be obtained. Subsequently, the purified proteins were used in photoreduction measurements in an identical manner as described for iLOV-Q489D. Surprisingly, all double mutants showed photoreduction in the presence of oxygen. The detailed analysis of the photoreduction yield and efficacy is given in Table 3.1.

Among the double mutants, only iLOV-Q489D/W467F showed a significantly reduced photoreduction yield ($89 \pm 0.5\,\%$) relative to iLOV-Q489D. All other double mutants showed photoreduction yields that are, within the error of the measurement, identical to the one observed for iLOV-Q489D. In contrast, in terms of efficiency, iLOV-Q489D/Y416F, iLOVQ489D/Y459F, iLOV-Q489D/Y484F and iLOV-Q489D/W467F showed significantly faster $FMNH^{\bullet}$ formation, quantified by

Table 3.1 Photoreduction and reoxidation yields and efficiencies of iLOV-Q489D, iLOV-Q489D/Y416F, iLOV-Q489D/Y459F, iLOV-Q489D/Y484F and iLOV-Q489D/W467F.

Protein	Photoreduction yield / % [a,b]	τ_{Sq} / s [b]	τ_{FMNox} / s [b]
iLOV-Q489D	100 ± 6	25.7 ± 0.2	1502 ± 27
iLOV-Q489D/Y416F	101 ± 1 (NS)	13.2 ± 0.8 (***)	1621 ± 25 (NS)
iLOV-Q489D/Y459F	103 ± 2 (NS)	5.6 ± 0.1 (***)	1622 ± 66 (NS)
iLOV-Q489D/Y484F	101 ± 2 (NS)	20.8 ± 0.6 (***)	1525 ± 41 (NS)
iLOV-Q489D/W467F	89 ± 0.5 (NS)	11.5 ± 0.4 (***)	1329 ± 29 (NS)

[a]Photoreduction yield relative to the yield of iLOV-Q489D (100 %). [b]Values represent the mean and standard deviation of the mean derived from three independent measurements. Statistical significance (in brackets) of the observed differences was tested by One - Way ANOVA and Dunnett's Post Test ($P < 0.01$) for comparison against iLOV-Q489D. NS: Not Significant.

deriving τ_{Sq} for the photoreduction process (Table 3.1). To address if introduction of the mutations resulted in altered oxygen accessibility we determined the reoxidation lifetime τ_{FMNox} for FMN reoxidation in the dark after photoreduction by following the reoxidation of FMN at 450 nm. Hereby, one would expect that a slower reoxidation would result in a faster $FMNH^{\bullet}$ formation. However, among the tested double mutants only iLOV-Q489D/W467F showed significantly faster, but not slower, FMN reoxidation, essentially ruling out an influence of oxygen access on the observed processes.

Since iLOV-Q489D/W467F shows efficient photoreduction although the electron donor Trp, identified by TA, has been substituted for Phe, we additionally performed TA measurements of this variant. Global lifetime analysis of the 2D TA data of iLOV-Q489D/W467F results in two DADS (Figure 3.2.11) similar to the spectra we observed in the case of iLOV-Q489D: D_1 can be associated with the excited triplet state of FMN and decays with $\tau = 108$ µs. This is by a factor of four slower compared to iLOV-Q489D. D_2 of iLOV-Q489D/W467, on the other hand, is characterized by the typical absorbance of $FMNH^{\bullet}$, which is formed via the excited triplet state as indicated by the t_0 spectrum. Since iLOV-Q489D/W467 is lacking the Trp, which we identified to serve as the counter-radical of $FMNH^{\bullet}$ in the TA data of iLOV-Q489D, the D_2 of both iLOV variants are compared in Figure 3.2.12. Both D_2 are scaled to the same value at 620 nm. At this wavelength only $FMNH^{\bullet}$ absorbs in iLOV-Q489D and iLOV-Q489D/W467F. When comparing both spectra, it can be clearly seen that the D_2 of iLOV-Q489D (black line) has more positive absorption in

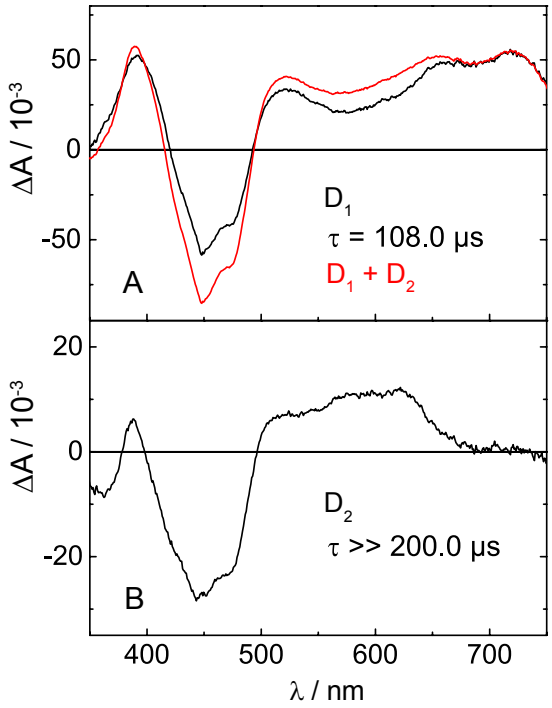

Figure 3.2.11 A: DADS of iLOV-Q489D/W467F (black line) obtained via global analysis of a 200 µs TA data set. D_1 associated with the excited triplet state of FMN decays with $\tau = 108.0$ µs. The sum of both DADS (red line) representing the pure triplet spectrum of FMN incorporated in iLOV is displayed for comparison. **B:** D_2 is non-decaying on the measured streak window and shows typical contributions of $FMNH^{\bullet}$.

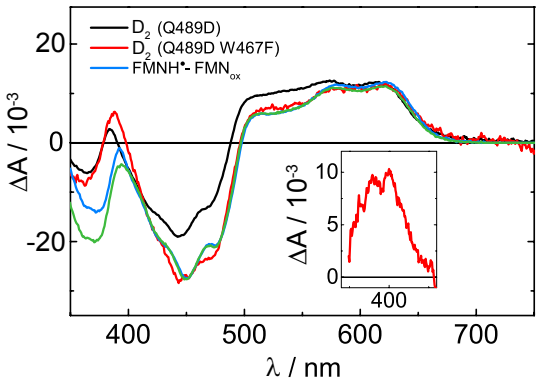

Figure 3.2.12 Comparison of the D_2 of iLOV-Q489D (black line) and iLOV-Q489D/W467F (red line) derived from global analysis of TA data. The spectra are scaled to the same value at 620 nm. The reference spectrum of $FMNH^{\bullet}$ minus FMNox (blue line) is in good agreement with the D_2 of iLOV-Q489D/W467F above 420 nm. **Inset:** Spectrum obtained by subtraction of the reference spectrum $FMNH^{\bullet}$ minus FMNox from the D_2 of iLOV-Q489D/W467F corresponding to $TyrO^{\bullet}$.

the range of $Trp^{\bullet}$ absorption from 490 nm to 575 nm than D_2 of iLOV-Q489D/W467 (red line).

However, it should be noted that the amplitude of the ground-state bleach differs between the two iLOV spectra. This is due to positive absorption of $Trp^{\bullet}$ until 440 nm (see Figure 3.2.9) and a certain fraction of irreversible photodamage of iLOV-Q489D/W467 during the TA measurement. When comparing D_2 of iLOV-Q489D/W467 with the difference absorption spectra of $FMNH^{\bullet}$, obtained by linear combination of the steady-state spectra of $FMNH^{\bullet}$ and FMNox, both spectra are in good agreement above 420 nm. Subtraction of the difference absorption spectrum of $FMNH^{\bullet}$ from D_2 of iLOV-Q489D/W467 yields the spectrum shown in the inset in Figure 3.2.12. The typical narrow absorption band at 400 nm with a shoulder at 380 nm can be assigned to the neutral radical of tyrosine, $TyrO^{\bullet}$, blue-shifted by 10 nm compared to previously reported spectra [102, 103]. The observation of $TyrO^{\bullet}$ demonstrates that one of the tyrosines of iLOV-Q489D/W467 substitutes W467 to act as the counter-radical of $FMNH^{\bullet}$.

3.3 Discussion

A recurrent theme observed in various flavin-binding photoreceptors is the light-driven photoreduction of oxidized flavin via electron transfer (eT) and subsequent proton transfer (pT) reactions to yield the neutral semiquinone radical $FMNH^{\bullet}$ [45]. Very recently, it was shown for different LOV photoreceptors, that $FMNH^{\bullet}$ formation (photoreduction) in LOV variants lacking the photo-active cysteine residue, suffices to elicit a functional response of the photoreceptor [61]. Hereby, the propensity for FMN photoreduction seems to vary widely between different photoreceptors and

most importantly, the residues involved in eT and pT reactions remain elusive. To address this issue, we set out to reengineer the photochemistry of the flavin chromophore in the photostable LOV-based fluorescent protein iLOV, which lacks the photo-active cysteine. The photostability of the protein hereby suggests that iLOV is not prone to photoreduction in the presence of oxygen. iLOV therefore represents an ideal target protein to reengineer efficient eT and pT reactions by the introduction of rational amino acid substitutions.

3.3.1 Efficient proton transfer is essential for stabilizing $FMNH^{\bullet}$ in parental iLOV

Given the conserved nature of the flavin-binding pocket in LOV proteins, we reasoned that the most important step for stabilizing $FMNH^{\bullet}$ in iLOV would be the introduction of a suitable proton donor. We therefore introduced an Asp residue at the position of a highly conserved Gln (Q489) which in parental iLOV is forming H-bonds to the FMN chromophore. The presented results show that, while parental iLOV cannot be photoreduced in the presence or absence of oxygen, iLOV-Q489D is efficiently photoreduced in the presence of oxygen rapidly accumulating $FMNH^{\bullet}$ during illumination. The observed pH dependence of the photoreduction process as well as modelling studies suggest that the newly introduced Asp is (at least partially) protonated at neutral pH values and hence can serve as proton donor. At the same time, this observation suggests that eT pathway(s) should be naturally present in iLOV. This observation is corroborated by the presented EPR measurements, as at low temperatures flavin radical formation is observed in parental iLOV, although with a much lower amplitude as in iLOV-Q489D. Additionally, EPR studies provide evidence for the formation of a stable protein:FMN radical pair with a minimum electron-electron distance of 9 ± 1 Åat low temperatures, which is also observed by room-temperature TA spectroscopy. The latter approach hinted at W467 as potential counter protein radical. As we do not observe $FMN^{\bullet-}$ or $TrpH^{\bullet+}$, protonation in iLOV-Q489D is apparently faster than the time resolution of the streak camera, meaning 1.5 µs for a 200 µs time window. Electron transfer from a Trp residue to FMN and subsequent protonation via an aspartic acid nearby the FMN-N5 is known from plant cryptochromes (CRY) [116, 117]. There, the electron transfer occurs via a Trp cascade in the ps time-range, while the protonation step varies between ns and µs [81, 118]. In *A. thaliana* CRY the Trp triad is constituted by W400, W377 and W324 [81, 119] located at a distance of 9.0, 13.4 and 19.6 Å from the FAD chromophore, with the closest Trp (W400) representing the intial electron donor for FAD photoreduction [81]. Likewise, photoreceptors of the BLUF family were suggested to undergo related photochemical reactions. While still under debate [45], the BLUF photocycle may involve the fast (ps) formation of $FMNH^{\bullet}$ as part of a radical-pair intermediate between the flavin and a conserved Tyr [50]. In iLOV-Q489D, the larger distance of W467 (14.1 Å) compared to W400 in AtCRY (9.0 Å) or Y8 of the Slr1694 BLUF protein (8.2 Å), could account for the eT reaction occurring in the

µs - time range via the triplet state of FMN, compared to eT on the ps timescale from the singlet state in CRY [81, 118].

One possible explanation for the observed differences in photoreduction yield and efficiency of the double mutants, which contained a Phe instead of Tyr or Trp, compared to iLOV-Q489D, is that more than one of the mutated residues can contribute to the photoreduction process. Hereby, Y416, Y459 and W467 could form a multistep electron transfer pathway, similar to the Trp triad in cryptochromes [81, 119], in which each of the amino acids can independently donate an electron to the FMN molecule. Our results, however, indicate that the direct electron transfer from W467 to FMN represents the most efficient and fast pathway for photoreduction in iLOV Q489D. An electron transfer pathway from W467 via Y459 and/or Y416 might be possible, but the fact that the tyrosyl radical could not be observed as an intermediate in the iLOV Q489D TA data contradicts a multistep electron transfer process. When substituting W467 with phenylalanine, on the other hand, Y459 and/or Y416 replace W467 as electron donor. In this case, the tyrosyl radical can be observed in the TA data and the triplet lifetime of iLOV Q489D/W467F is increased almost 4-fold, indicating that this electron transfer pathway is slower and hence less efficient than the direct transfer from W467 to FMN. As a further support for this hypothesis, the photoreducion yield of iLOV Q489D/W467F, measured in steady-state experiments, is significantly reduced relative to iLOV Q489D.

3.3.2 The electron transfer pathway present in iLOV is conserved in all LOV proteins

Recently, a comprehensive LOV protein sequence dataset was provided by Glantz and co-workers [46]. To address the issue of conservation of the respective eT and pT reactions observed in iLOV-Q489D, we analyzed this dataset for conservation of the respective amino acid positions. Figure 3.3.1 depicts the sequence logo obtained from the multiple sequence alignment of 1975 LOV domain sequences extracted from [46] as well as a superposition of various LOV domain structures highlighting the structural conservation of the respective residues. The conservation analysis suggests that the residues constituting the eT pathway in iLOV-Q489D are highly conserved among LOV domains (Figure 3.3.1B marked by blue asterisk). Likewise, Q489 is highly conserved (Figure 3.3.1B, red asterisk), i.e. no potential proton donating residues are found at the respective positions, suggesting that evolution eventually has favored a Cys-adduct-dependent LOV photochemistry over FMN photoreduction.

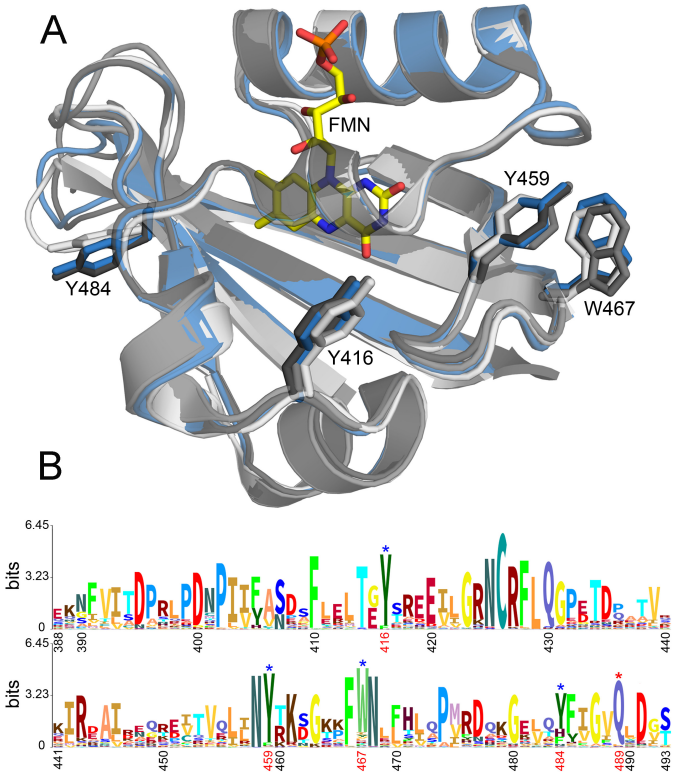

Figure 3.3.1 A: Superposition of representative LOV domain structures and **B:** sequence logo generated to visualize the sequence conservation within the LOV domain family. The structure of the parental iLOV protein is shown as blue cartoon (PDB: 4EES). Additional LOV domain structures are shown in different shades of grey (from light to dark grey: LOV domain of YF1 (PDB: 4GCZ), *Chlamydomonas rheinhardtii* phototropin LOV1 (PDB: 1N9L), LOV2 domain of *Avena sativa* phototropin 2 (PDB: 2V0U). The residues corresponding to Y416, Y459, Y484 and W467 of parental iLOV are shown in stick representation in the corresponding color. The sequence logo shown in panel **B** was generated using the Skylign tool [120] using a multiple sequence alignment containing 1975 LOV domain sequences taken from [46]. Sequence positions are numbered according to iLOV numbering. Amino acids relevant for the discussion are marked by blue (potential electron donating residues) and red (conserved glutamine Q489) asterisks and numbered in red.

3.4 Conclusions

In the present study, efficient FMN photoreduction could readily be engineered into the iLOV protein, which in its "native" form did not possess any propensity for photoreduction in the presence of oxygen. Hereby, introduction of a potentially proton donating Asp residue close to the FMN chromophore appears to be of primary importance as the small size of the LOV domain apparently provides ample possibilities for eT from redox active amino acids. Sequence analyses suggested that the eT pathway involving a Trp and - when removing the Trp also Tyr residues - is conserved among LOV proteins. This suggests that the propensity for photoreduction is evolutionary imprinted in all LOV domains, while the efficiency of $FMNH^{\bullet}$ formation, which varies widely in the corresponding cysteine to alanine mutants of different LOV domains, is determined by the possibility for an efficient pT either from an amino acid residue in the proximity of FMN chromophore (as in iLOV-Q489D) or from a water molecule to stabilize $FMNH^{\bullet}$. In the latter case, a subtle balance would be needed between rigid anchoring of the FMN chromophore (for efficient eT) and the access of water to enable pT. The apparent easy adaptability of the LOV photochemistry to follow a route with intriguing similarity to other flavin-binding photoreceptors such as CRY and BLUF provides a rational basis for the evolutionary success of the flavin cofactor to act as light absorbing chromophore in various structurally and evolutionary unrelated blue light photoreceptors, and highlights the possibility that todays' adduct forming LOV photoreceptors evolutionary derive from ancestral redox-active flavoproteins.

4 Investigation of the intermolecular interactions of LOV domains

4.1 Intermolecular interactions and biological function of LOV domains

LOV domains act as photosensory units in various procaryotic and eucaryotic organisms. They can be found in multidomain proteins or as stand-alone domains accompanied by N- and/or C-terminal flanking regions. A recent study unraveled 119 different primary effectors so far identified [46], emphasizing the high modularity of LOV proteins. As a subset of the PER-ARNT-SIM (PAS) superfamily, LOV domains preserved their typical, globular α/β fold with a central β-scaffold flanked by N- and C-terminal extensions, as well as their tendency to dimerize [22–25].

LOV proteins' activation and signaling is very complex and not fully understood, yet. This is partly because of the high modularity and complexity of LOV proteins, but also due to a lack of available full-length constructs. The initial trigger of signaling, however, is light-induced adduct formation which in turn induces conformational changes in the LOV core. A conserved Gln flips due to protonation of FMN-N5 and propagates the conformational changes to the β-sheet [38–40, 42]. The subsequent steps of signal propagation can, in general, be categorized into: i) Release of effector helices or domains suppressing the inhibitory interactions with the LOV β-sheets [23, 121, 122]. ii) Reorganization of C- or N-terminal flanking regions to allow for LOV-LOV dimer formation [123, 124]. iii) Reorientation of dark-state β-sheet mediated dimers [125].

Besides the so-called LOV/LOV proteins and neochromes [126, 127], Phototropins (Phot) are the only LOV proteins with two LOV domains [10]. Although both LOV domains, LOV1 and LOV2, undergo flavin-cysteinyl adduct formation upon blue light, it has been shown that they have distinct physiological roles [128]. LOV2 is responsible for the activation of the effector domain of Phot, a Ser/Thr-kinase (STK) [129–131]. Upon blue light absorption detachment of the Jα linker occurs which connects the LOV2 domain and the STK [23]. This liberates the STK and stimulates autophosphorylation of Phot [132]. In contrast, the role of LOV1 is not completely resolved yet. It has been shown that LOV1 is not essential for STK activation although it might play a regulatory role on LOV2 signaling [130, 133, 134]. Based on the observation of blue light-induced oligomeric state changes it has been

proposed that LOV1 domains act as dimerization sites of full-length Phot. Although light-induced dimerization has been observed for isolated Phot-LOV1 domains *in vitro* [135–137], it requires further examination to which extend this has an impact on full-length Phot *in vivo*. *In vivo* light-induced dimerization of Phot1 of *Arabidopsis thaliana* e.g. is necessary for the intermolecular autophosphorylation of the protein [128], but Phot1-LOV1 is presumably not essential for the dimerization although it is dimeric *in vitro* [135].

The dynamics and functional role of the oligomeric state of LOV proteins have been subject to many studies in the literature. Over the last years, data obtained on different LOV systems more and more suggest that blue-light induced oligomeric state changes, often involving the N- and C-terminal extensions, determine the physiological function of LOV proteins. Furthermore, there are indications that dimerization is a highly dynamic process in solution.
A very well investigated example is VVD-LOV from the fungi *Neurospora crassa*. VVD-LOV is a so-called short LOV domain since it is not coupled to an effector domain. The protein is monomeric in the dark state [123]. Upon light excitation, VVD-LOV forms the flavin-cysteinyl adduct and conformational changes at the Ncap (the N-terminal extension of the LOV core) occur, which shift VVD-LOV to a highly dynamic monomer-dimer equilibrium in the light state [123]. The dimeric form constitutes the active, signaling state which interacts with the White Collar Complex (WCC) in *N. crassa* [123, 138].
Another example of light-induced oligomeric state changes represents the LOV domain of Aureochrome 1a from the stramenophile alga *Phaeodactylum tricornutum* (PtAureo1a). Aureochromes exhibit an inverted domain architecture with a LOV-domain coupled to a N-terminal bZIP (basic region leucine zipper) domain as effector [139]. In the active state, this bZIP domain binds its target DNA sequence TGACGT [139]. The LOV domain is flanked by an A'α helix at the N-terminus and a Jα helix at the C-terminus. The PtAureo1a LOV-module with its flanking helices has been shown to be monomeric in the dark state and to undergo light-induced dimerization, whereas unfolding of both, Jα and A'α, is required [28, 124]. Recently, it has been shown that the LOV module of PtAureo1a docks against bZIP of the full-length PtAureo1a dimer in the dark [140]. Upon blue light illumination, the LOV domain dissociates from bZIP and subsequently dimerizes. This in turn increases the structural dynamics of bZIP and enhances the affinity of PtAureo1a for its target DNA sequence [140]. The same behavior has been already described for another aureochrome, Aureochrome-1 from the stramenophile alga *Vaucheria frigida* (VfAureo1). VfAureo1 also shows blue light-induced dimerization of its LOV domain which subsequently increases the affinity of this transcription factor for its target DNA [141]. Recently, multiple LOV-bZIP constructs of VfAureo1 have been engineered and investigated by dynamic light scattering, size exclusion chromatography and emission spectroscopy, in order to use them as natural optogenetic modules for controlling DNA binding in a light-dependent manner [142].

On the other hand, the short LOV domain of *Rhodobacter sphaeroides* (RsLOV) was found to exist as dimers in the dark, which dissociate upon light excitation [143]. RsLOV is flanked by a short C-terminal aα helix and an unusual C-terminal HTH-motif, which also constitutes the dimerization surface in the dark state. Dissociation of the dimers in the light-adapted state hints to a correlation between the oligomeric state and the so far unknown biological function of RsLOV. These examples support the hypothesis that the oligomeric state of a LOV domain is linked to its physiological function. Detailed investigations of LOV-LOV interactions could therefore further contribute to the elucidation of the complex LOV protein signaling.

Addressing this issue, we investigated the intermolecular interactions two different LOV domain systems. The most common techniques used in the literature for this purpose are size exclusion chromatography (SEC), small angle X-ray scattering (SAXS), light scattering or sometimes the transient grating method. We decided to monitor potential LOV interactions spectroscopically using Förster Resonance Energy Transfer (FRET). In contrast to the aforementioned methods, fluorescence spectroscopy in combination with FRET is a very sensitive method and allows to investigate LOV-LOV interactions even at very low concentrations. The following chapter starts with a short introduction into the basic concepts of FRET. Following this, the experimental setup to conduct the FRET emission measurements is described. In order to follow the LOV-LOV interactions via FRET the proteins needed to be labeled with a fluorescent donor-acceptor pair. Due to the small size of LOV domains ($\sim$ 15 kDa) fluorescent biomolecules e.g. of the GFP family ($\sim$ 25 kDa) were not suitable as labels. Thus labeling with the commercially available organic dyes Cy3 and Cy5 was achieved. Their labeling chemistry is also described in this chapter. The main part of this chapter deals with a FRET study on the short LOV domain of *Rhodobacter sphaeroides* (RsLOV) and the LOV1 domain of *Chlamydomonas reinhardtii* Phot (CrLOV1). The oligomeric behavior of RsLOV in the dark state and after light illumination has been published in the literature [143]. RsLOV exists as dimers in the dark state, which dissociate upon blue light. This made RsLOV a good model system to validate our setup and analysis method. Secondly, intermolecular interactions of CrLOV1 were investigated. It has been proposed that the LOV1 domains of Phot act as dimerization sites of the full-length proteins. The question whether this applies to CrLOV1 is being discussed controversially in the literature [144, 145]. The results are presented and discussed in the context of literature.

4.2 Förster Resonance Energy Transfer (FRET)

4.2.1 Principles of FRET

Dynamic protein-protein interactions play a key role in the biological function of proteins. As described above, LOV domain interactions regulate essential processes in many proteins in nature. A promising method to elucidate such interactions is the Förster resonance energy transfer (FRET). Even though the phenomenon of resonance energy transfer has been observed before [146], Theodor Förster was the first who proposed a theory describing FRET in 1948 [147]. FRET can be defined as the photophysical process in which energy is transferred non-radiatively from an excited chromophore (the donor, D) to another chromophore in the ground state (the acceptor, A) based on dipole-dipole interactions. The principle is schematically presented in Figure 4.2.1. The equations given in the following two sections give a basic overview over the principle of FRET according to [148–152]. For further details and derivations of the equations see [147, 153–155] and references therein. The rate of Förster dipole-dipole energy, k_t, is given by the equation:

$$k_t = \frac{1}{\tau_D}\left(\frac{\mathrm{R}_0}{r}\right)^6 \;,\; \mathrm{R}_0^6 = \frac{9\,(\ln 10)}{128\pi^5\,\mathrm{N_A}}\,\frac{\kappa^2\,\Phi_D}{n^4}\,J \tag{4.1}$$

where τ_D is the donor lifetime in the absence of acceptor, r is the donor-acceptor distance and R_0 is the Förster or critical transfer distance at which the energy transfer rate is equal to the decay rate. The efficiency of FRET is 50 % at $r = \mathrm{R}_0$. Minor changes of the donor-acceptor distance around R_0 lead to a major change in FRET efficiency (see Figure 4.2.2A). R_0 is determined by the orientation factor κ^2 between donor and acceptor and the quantum yield of the donor in the absence of acceptor, Φ_D. $\mathrm{N_A}$ refers to the Avogadro constant. The refractive index, n, is generally taken to be 1.4 in aqueous solution. J is the spectral overlap integral between the donor and the acceptor. In this work J is defined in the wavelength scale *(J^λ)*:

$$J^\lambda = \int \mathrm{F_D^*}(\lambda)\,\epsilon_A(\lambda)\,\lambda^4\,d\lambda\,;\int \mathrm{F_D^*}(\lambda)d\lambda\;=\;1 \tag{4.2}$$

where $\mathrm{F_D^*}$ refers to the fluorescence spectrum of the donor normalized to an area of one. ϵ_A is the molar absorption coefficient of the acceptor in units of $\mathrm{M^{-1}\ cm^{-1}}$. In this thesis, the unit of *(J^λ)* is expressed as [$\mathrm{nm^4\ M^{-1}\ cm^{-1}}$], which can also be written as [$\mathrm{L\ nm^4\ mol^{-1}\ cm^{-1}}$] or [$\mathrm{dm^3\ nm^4\ mol^{-1}\ cm^{-1}}$]. Together with the unit of the Avogadro constant [$\mathrm{mol^{-1}}$], R_0 in Equation 4.1 can be expressed as:

$$\mathrm{R}_0^6 = 8.785\cdot 10^{-5}\,\frac{\kappa^2\,\Phi_D}{n^4}\,J \text{ in } [\mathrm{\AA}^6] \tag{4.3}$$

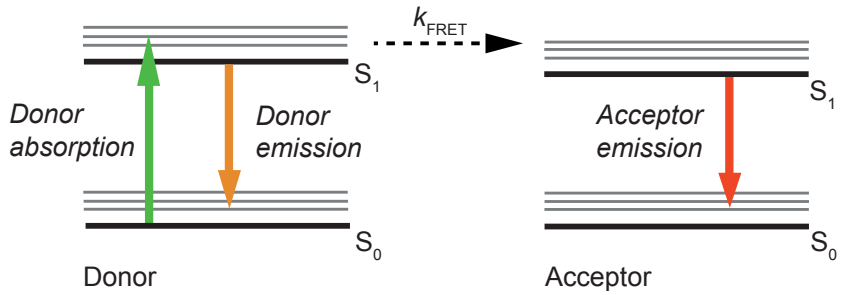

Figure 4.2.1 Schematic Jablonski diagram to illustrate FRET between a donor and an acceptor molecule. The donor absorbs a photon, which can either be emitted via fluorescence of the donor or be transferred non-radiatively to the acceptor. The acceptor can then emit a photon red-shifted compared to the donor. Other non-radiative deactivation processes than FRET and donor/acceptor emission are not included in this scheme.

In this expression, the fraction is dimensionless. The R_0 values given in this work are calculated according to Equation 4.3. Hence, the J values are also given without the unit [$nm^4\ M^{-1}\ cm^{-1}$]. A schematic illustration of the spectral overlap between donor and acceptor spectra required for FRET is shown in Figure 4.2.2B.

The orientation factor κ^2 represents the angle between the two chromophore dipoles and can adopt values between 0 and 4. A parallel orientation results in a higher FRET efficiency than a perpendicular one. Usually, κ^2 is assumed to be 2/3 which corresponds to the dynamically averaged value. This approximation is good as long as both chromophores have a certain degree of rapid rotational freedom, which in general is the case for chromophores attached to biomolecules in solution. Further details on the orientation factor κ^2 can be found in reference [156]. The parameters κ^2, Φ_D and J affect R_0 only by the sixth power. Most FRET pairs have R_0 values of around 5 nm [148].

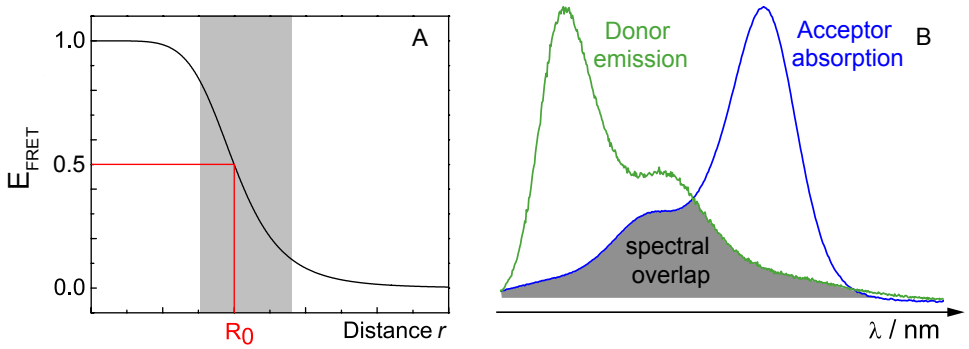

Figure 4.2.2 A: Distance dependency of the FRET efficiency. At the Förster radius, R_0, 50 % efficiency is achieved. The gray area indicates the radius range, which is sensitive to changes of the donor-acceptor distance. **B:** Scheme of the spectral overlap between donor emission (green line) and acceptor absorption (blue line) required for FRET.

4.2.2 Determination of the FRET efficiency

The FRET efficiency, E_{FRET}, is a quantitative measure of the energy transferred from the donor to the acceptor [149]. It can be associated with the quantum yield of FRET and is defined by:

$$E_{FRET} = \frac{\text{the number of quanta transferred from D to A}}{\text{the number of quanta absorbed by D}} \tag{4.4}$$

with D referring to the donor and A referring to the acceptor, respectively. E_{FRET} is experimentally accessible via the determination of the fluorescence lifetime of the donor in the absence and presence of the acceptor, τ_D and τ_{DA}, which can be expressed as:

$$\tau_D = \frac{1}{k_f + k_{nr}} \tag{4.5}$$

and

$$\tau_{DA} = \frac{1}{k_f + k_{nr} + k_t}\,. \tag{4.6}$$

k_f, k_{nr} and k_t are the rates of fluorescence, non-radiative decay and energy transfer. Thus, the FRET efficiency can also be written as:

$$E_{FRET} = \frac{k_t}{k_t + \tau_D^{-1}} = 1 - \frac{\tau_{DA}}{\tau_D}. \tag{4.7}$$

or according to Equation 4.1 as:

$$E_{FRET} = \frac{R_0^6}{R_0^6 + r^6}\,. \tag{4.8}$$

Alternatively, E_{FRET} can also be calculated via the fluorescence intensity of the donor in the presence and absence of acceptor, F_D and F_{DA}. The total fluorescence intensity F_x corresponds to the integral of the fluorescence decay curve:

$$F_x = \int_0^\infty F_x^0 \exp\left(-t/\tau\right) \cdot dt = F_x^0\,\tau \tag{4.9}$$

and is hence proportional to the fluorescence lifetime τ and the amplitude F_x^0. Equation 4.7 can be rewritten as:

$$E_{FRET} = 1 - \frac{F_{DA} \,/\, F_{DA}^0}{F_D \,/\, F_D^0} \tag{4.10}$$

Under the assumption that F^0_{DA} and F^0_D stay constant during the measurement Equation 4.10 can be written as:

$$E_{FRET} = 1 - \frac{F_{DA}}{F_D}, \tag{4.11}$$

with F_{DA} and F_D referring to the fluorescence intensities of the donor in the presence and absence of acceptor.

4.2.3 FRET measurement setup

The FRET experiments in this chapter were performed in solution as ensemble measurements. Figure 4.2.3 schematically presents the setup designed to measure emission spectra of the FRET samples. The sample can be excited with either a blue LED ($\lambda_{max} = 470\,nm$) and/or a green LED ($\lambda_{max} = 530\,nm$), both equipped with a bandpass filter to allow for a narrow excitation spectrum. Photodamage of the samples is significantly reduced compared to laser excitation due to the low power of the LEDs. The emitted light of the sample is focused onto the entrance slit of an imaging spectrograph coupled to a CCD camera as detection unit. This allows for detection over a broad spectral range either as steady-state spectra or with a time-resolution down to 100 ms. For further technical details see chapter 5, subsection 5.5.5.

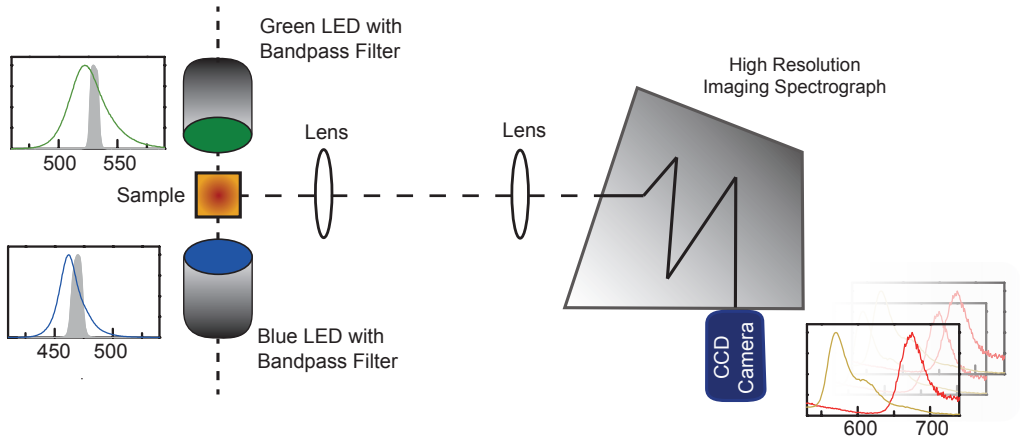

Figure 4.2.3 Schematic of the setup used for FRET emission measurements. The sample is excited by a green and/or blue LED and the emitted light is focused onto the entrance slit of an imaging spectrograph coupled to a CCD camera as detection unit.

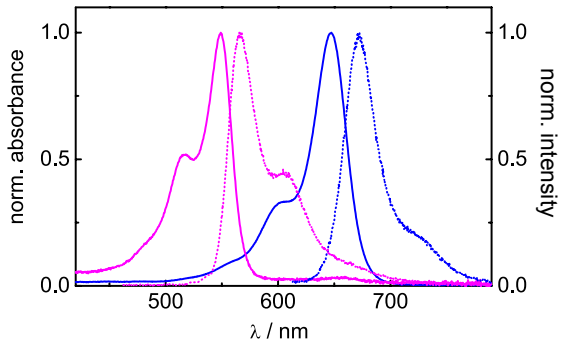

Figure 4.2.4 Normalized absorption (solid lines) and emission (dotted lines) spectra of Cy3 (magenta) and Cy5 (blue) dye in sodium phosphate buffer.

4.2.4 Labeling with Cy3 and Cy5

All proteins in the following chapter were labeled with the sulfoindocyanine dyes Cy3 and Cy5 mono-functionalized with either N-hydroxysuccinimide (NHS) ester or maleimide ester for the coupling reaction. These dyes were originally described by Waggoner and co-workers [157, 158] and have proven their utility in a wide range of applications due to their brightness and photostability.

Dyes with NHS ester modification bind to terminal amino groups of proteins, most probably of Lys residues. Lys is rather abundant in most proteins and therefore the amino-reactive Cy dyes come in handy when attaching several dye molecules to one protein. Site-specific labeling, on the other hand, can be achieved via conjugation to Cys, since this amino acid is less abundant [159]. Figure 4.2.5 displays the structures of Cy3 and Cy5 with both, NHS and maleimide ester modification, as well as the labeling reaction for each case. Table 4.1 lists some important intrinsic properties of Cy3 and Cy5 in sodium phosphate buffer (PB). The values of the fluorescence quantum yields refer to the dyes attached to a protein. The values of the absorption and emission maxima in PB were determined spectroscopically, the other values are according to the manufacturer. The absorption and emission spectra of free Cy3 and Cy5 dye in PB are shown in Figure 4.2.4.

Table 4.1 Cy3 and Cy5 properties according to the manufacturer, except the absorption and emission maxima, which were determined in PB.

	λ_{max}^{Abs} / nm	λ_{max}^{Em} / nm	ϵ_A / M^{-1} cm^{-1}	Φ_F	τ_F / ns
Cy3	549	567	150 000	$> 0.15^a$	< 0.3
Cy5	647	672	250 000	$> 0.28^a$	1.0

[a] for labeled proteins with a dye:protein ratio of 2 according to the manufacturer.

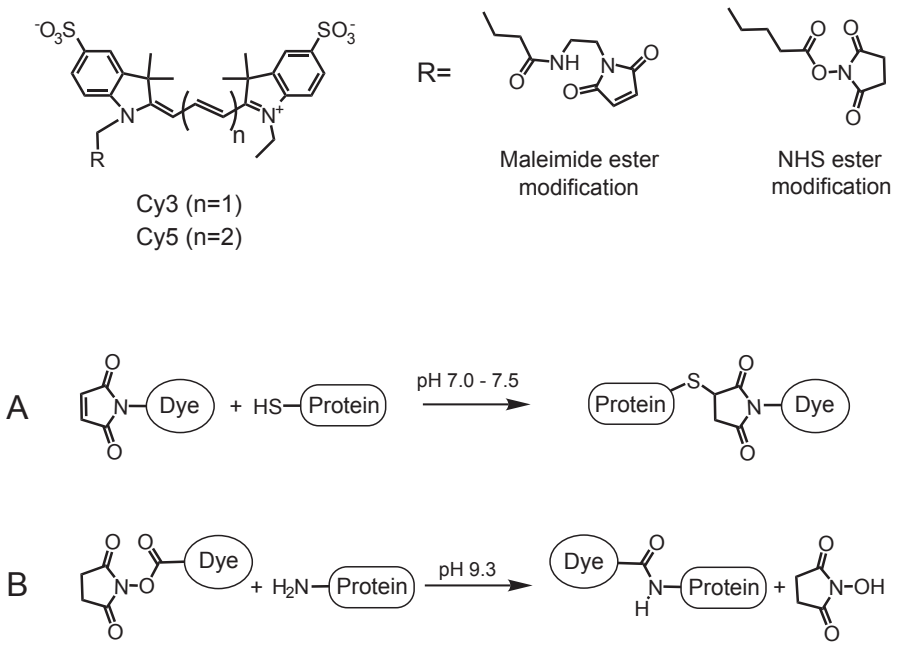

Figure 4.2.5 Structures of Cy3 and Cy5 maleimide and NHS esters. **A:** Reaction scheme of a maleimide-modified dye with the sulfur group of Cys and **B:** a NHS-modified dye with the primary amino group of e.g. Lys.

4.3 *Rhodobacter sphaeroides* LOV

4.3.1 RsLOV wt

RsLOV is a short LOV domain of the purple, photosynthetic, Gram-negative bacterium *Rhodobacter sphaeroides* [160, 161]. It non-covalently binds FMN as a chromophore. In contrast to most other known LOV domains, RsLOV is lacking an effector domain and its physiological role is still under discussion, including the implication in photosynthetic gene expression, carbohydrate metabolism, chemotaxis and cellular response to photooxidative stress [162]. The crystal structure of RsLOV has been determined by X-ray (PDB 4HIA) [143]. Next to the LOV core exhibiting the typical α/β PAS fold, RsLOV has both, a short C-terminal extension consisting of the aα helix and a N-terminal extension forming an unique HTH (helix-turn-helix) motif composed of the Jα and the Kα helix. Both extensions could potentially interact with an effector domain or partner protein, yet to be defined. The dark state crystal structure of RsLOV is shown in Figure 4.3.1. A combined crystallographic and biochemical study revealed oligomeric changes of RsLOV upon light activation [143]. RsLOV exists as dimers in the dark state where

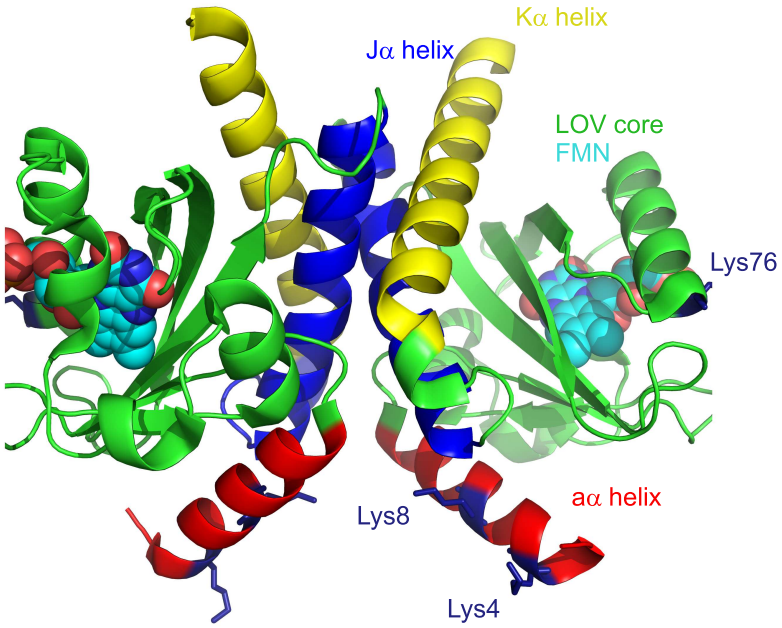

Figure 4.3.1 Crystal structure of the RsLOV dark state dimer (PDB 4HIA). The LOV core is colored in green, non-covalently binding the FMN chromophore (cyan, sphere representation). The Jα and the Kα helices, forming the HTH motif, are colored in blue and yellow. The aα helix is shown in red. The three potential labeling sites, Lys4, Lys8 and Lys76, are shown in stick representation.

the HTH motif constitutes the dimer surface. Upon blue light excitation the dimers dissociate. The dissociation is reversible in the dark. This behavior makes RsLOV a good model system to perform FRET measurements on labeled LOV domains and validate our setup.

The gene encoding RsLOV (*R. sphaeroides* 17025) was cloned into the expression vector pET-28a and expressed in *E.coli*. RsLOV was obtained as a soluble, green protein in solution. The N-terminal His-tag was cleaved off to not interfere with dimerization. As a first step, we determined the solution state parameters including the oligomeric state and adduct formation and recovery described in reference [143] to verify the functionality of our RsLOV. Following this, RsLOV was labeled with Cy3 and Cy5 dye and the emission properties of the labeled proteins were determined via fluorescence spectroscopy in solution. Experiments on mixed solutions of RsLOV-Cy3/Cy5 were conducted in order to follow the light-induced changes of the oligomeric state spectroscopically.

4.3.1.1 Size exclusion chromatography (SEC)

The oligomeric state of RsLOV in the dark and in the light state was determined via SEC (Figure 4.3.2). The dark state runs were performed under dim red safelight conditions. During the light state run, the column was continuously illuminated with two blue LEDs to prevent dark state recovery of the sample. The RsLOV samples were injected with a concentration of 7 µM onto the SEC column. The dark state of RsLOV elutes at 233 mL corresponding to a molecular weight of 31 kDa. Upon conversion to the adduct state, RsLOV elutes much later at 245 mL corresponding to a molecular weight of 21 kDa, which is consistent with the monomeric mass of RsLOV. The calculated molecular weights of RsLOV monomers and dimers are 20.1 kDa and 40.2 kDa, respectively, meaning that the dark state mass is smaller than predicted for a dimer. These findings are consistent with the results of Conrad *et al.* [143]. The authors explain the intermediate mass of the RsLOV dark state with a monomer-dimer equilibrium exchanging on the timescale of SEC. This is supported by the fact that the dark-state SEC peak exhibits an asymmetric profile: the advancing edge is much sharper than the tailing counterpart. This can be observed in SEC in the case of associating systems with a rapid exchange occuring on a timescale faster than SEC. This results in a single peak with a polydisperse molecular weight distribution [163, 164].

The adduct lifetime of RsLOV was reported to be 2357 s [143]. Measurements with our setup yielded a very similar lifetime of 2340 s. An unlabeled RsLOV sample with a concentration of 33 µM was excited with two high power LEDs at 450 nm for 500 ms and subsequently UV/Vis spectra were taken every 30 s for the next four hours. Time traces at 450 nm and 310 nm were analyzed assuming a monoexponential behavior. The recovery lifetime was averaged from three independent measurements.

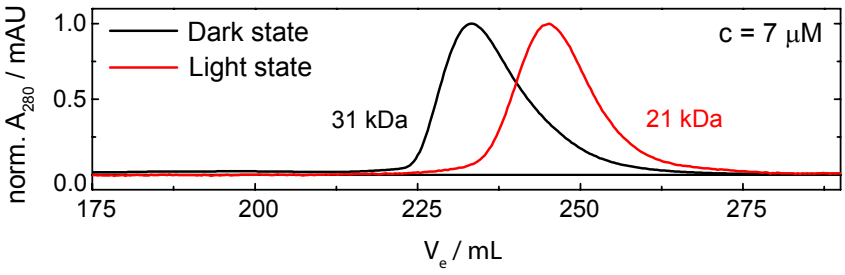

Figure 4.3.2 SEC of RsLOV without His-tag at a concentration of 7 µM in the dark state (black line) and under continuous blue light illumination (red line).

4.3.2 RsLOV-Cy3 and RsLOV-Cy5

The amino acid sequence of RsLOV includes three Lys, but only one Cys, which represents the reactive Cys participating in adduct formation buried deep inside the LOV core. The three Lys, Lys76 and Lys4 and Lys8, are exposed to the solvent according to the crystal structure (pdb 4HIA) [143] and should be accessible for labeling. The positions of the Lys are highlighted in Figure 4.3.1. Hence, RsLOV was labeled with amino-reactive Cy3 and Cy5 NHS ester, respectively. The corresponding steady-state UV/Vis spectra are shown in Figure 4.3.3. The absorption maximum of RsLOV-Cy3 is at 552 nm with a shoulder at 515 nm. The dye:protein ratio is calculated to be 1.7:1 for this sample using the extinction coefficients for flavin (12 500 mol L^{-1} cm^{-1} at 450 nm [165]), Cy3 (150 000 mol L^{-1} cm^{-1} at 550 nm) and Cy5 (250 000 mol L^{-1} cm^{-1} at 650 nm) [166]. The absorption maximum of RsLOV-Cy5 is located at 605 nm with a second minor peak at 649 nm. The intensity of the two peaks are inverted compared to free Cy5 indicating that Cy5 is firmly attached to RsLOV. The labeling ratio of RsLOV-Cy5 is calculated to be 1.4 dye molecules per 1 molecule FMN. The absorption spectrum of RsLOV-Cy5 additionally exhibits the typical fine-structured absorption band of FMN around 450 nm. In the case of RsLOV-Cy5, the flavin absorption bands overlaps with the dye absorption. In order to check whether labeled RsLOV is still photo-active, the samples were irradiated with blue light for 200 s. The absorbance of RsLOV-Cy3 decreases by 30 % in the range of FMN absorption between 400 and 500 nm and in the case of RsLOV-Cy5 a decrease of 60 % can be observed. The absorption bands of the dyes are not affected by the change of flavin absorbance. The spectral changes are reversible in the dark. We therefore assign the observed decrease in the UV/Vis spectra to the adduct formation of the LOV domain.

4.3.2.1 Emission measurements of labeled RsLOV

Prior to performing FRET measurements of mixed Cy3/Cy5-labeled RsLOV samples, the emission properties of RsLOV-Cy3 and RsLOV-Cy5 were determined individually. Figure 4.3.4A and B show the emission spectra of labeled RsLOV when exciting the donor Cy3 at $\lambda_{exc} = 530$ nm or exciting the FMN chromophore

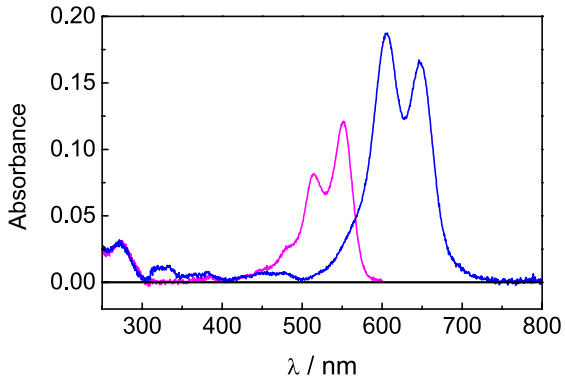

Figure 4.3.3 UV/Vis spectra of RsLOV-Cy3 (magenta line) and RsLOV-Cy5 (blue line).

at $\lambda_{exc} = 470\,nm$. It is noted that at $\lambda_{exc} = 530\,nm$ also Cy5 is excited directly to some extend and $\lambda_{exc} = 470\,nm$ also leads to excitation of Cy3 and to a small extend of Cy5. The concentration of FMN is 0.5 µM in each sample, Cy3 and Cy5 concentration 0.8 µM and 0.7 µM, respectively. The samples were irradiated continuously with either a blue or a green LED for 200 s. With green light excitation (Figure 4.3.4A) the emission of both labeled RsLOV samples stays constant over time with an emission maximum of 575 nm for RsLOV-Cy3 and 668 nm for RsLOV-Cy5. Although RsLOV-Cy5 only absorbs to a minor extend at 530 nm, the emission signal when exciting at this wavelength is not negligible. In contrast, direct excitation of FMN at $\lambda_{exc} = 470\,nm$ results in a decrease of Cy3 and Cy5 emission (Figure 4.3.4B). The intensity of the Cy3 emission in RsLOV-Cy3 is quenched by 25 % and no FMN emission can be observed. On the contrary, the FMN fluorescence is clearly visible between 495 nm and 620 nm when exciting RsLOV-Cy5 under the same conditions. During the 200 s irradiation, FMN as well as Cy5 emission decrease by approx. the same value of 40 - 50 %. The emission of RsLOV-Cy3 and RsLOV-Cy5 fully recovers in the dark on the timescale of adduct recovery. The behavior upon blue-light excitation is reproducible within the same samples for several excitation cycles. Furthermore, the emission decrease can be tuned by variation of the excitation duration and intensity.
These findings at $\lambda_{exc} = 470\,nm$ indicate that FRET occurs between the FMN chromophore of RsLOV and the attached Cy3 and Cy5 dye. The donor FMN can only transfer the energy to the acceptor as long as RsLOV is not in the adduct state. With ongoing blue light illumination adduct formation increases, the FMN chromophore becomes non-fluorescent and the energy transfer is interrupted which in turn causes the decrease of the Cy emission.

To further investigate a possible FRET between the FMN and the Cy dyes, the fluorescence decay times of labeled and unlabeled RsLOV were determined via TCSPC. The samples were excited at 378 nm. At this wavelength mainly the FMN is excited but to a smaller extend also Cy3. The fluorescence was detected either at 500 nm corresponding to FMN fluorescence or at 570 nm and 670 nm corresponding

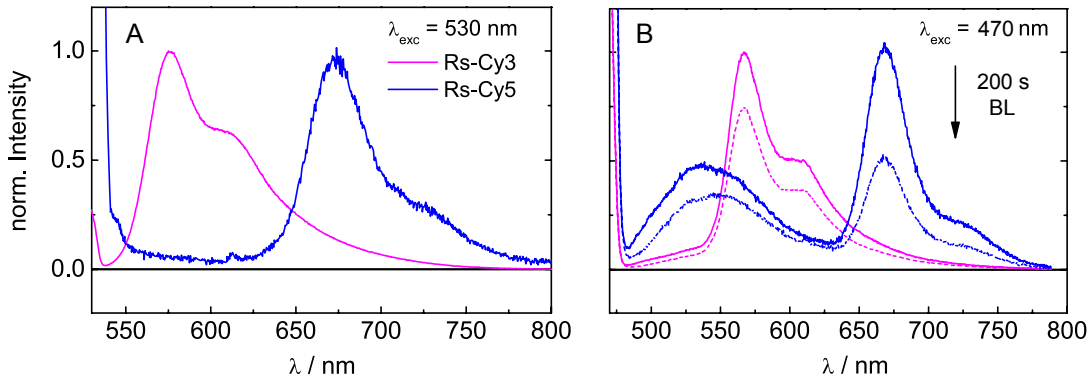

Figure 4.3.4 Normalized emission spectra of RsLOV-Cy3 (magenta) and RsLOV-Cy5 (blue) with **A:** $\lambda_{exc} = 530\,nm$ and **B:** $\lambda_{exc} = 470\,nm$. The samples were irradiated continuously during the measurement for 200 s.

to Cy3 and Cy5 fluorescence. The values are given in Table 4.2. The fluorescence decay of unlabeled RsLOV was determined to be monoexponential with $\tau_F = 2.3\,ns$, which is in good agreement with the values reported for other LOV domains, e.g. CrLOV1 or iLOV (see chapter 2 and chapter 3). In contrast, a biexponential fluorescence decay of FMN could be observed for RsLOV-Cy3 and RsLOV-Cy5. Thereby, one decay time is strongly quenched compared to unlabeled RsLOV with $\tau_1 = 0.3\,ns$ (RsLOV-Cy3) and $\tau_1 = 0.5\,ns$ (RsLOV-Cy5), while the second lifetime is in the range of unlabeled RsLOV. This longer component most likely refers to the fraction of unlabeled LOV domains in the labeled RsLOV samples. Since the contributions of the longer components are small, the accuracy of the lifetime analysis is reduced. As a consequence, the lifetimes of the longer components deviate from the lifetime of RsLOV (2.3 ns). The fluorescence lifetimes of the Cy3 and Cy5 dye attached to the LOV core are identical to the values obtained for the free dyes in solution with $\tau_F = 0.1\,ns$ (Cy3 emission) and $\tau_F = 1.1\,ns$ (Cy5 emission). But in both cases, a rise time of the fluorescence could be detected. These findings demonstrate that FRET occurs between the FMN and the Cy dyes upon blue light excitation. According to Equation 4.7, the FRET efficiency between FMN and the Cy dyes can be calculated:

$$\begin{aligned} E_{FRET}\,(RsLOV - Cy3) &= 1 - \frac{\tau_{DA}}{\tau_D} = 1 - \frac{0.3\,ns}{2.3\,ns} = 0.85 \\ E_{FRET}\,(RsLOV - Cy5) &= 1 - \frac{\tau_{DA}}{\tau_D} = 1 - \frac{0.5\,ns}{2.3\,ns} = 0.78 \end{aligned} \tag{4.12}$$

The high FRET efficiencies are not surprising, considering the good spectral overlap between the emission spectrum of FMN and the absorption spectra of Cy3 and Cy5. The Förster radii of the donor-acceptor pairs FMN-Cy3 and FMN-Cy5 can be calculated according to Equation 4.3:

$$\begin{aligned} \mathrm{R_0\,(FMN-Cy3)} &= 45.9\,\text{Å} \\ \mathrm{R_0\,(FMN-Cy5)} &= 46.9\,\text{Å} \end{aligned} \tag{4.13}$$

The fluorescence quantum yield of the donor FMN incorporated in RsLOV was determined to be $\Phi_D = 0.13 \pm 0.05$. The refractive index, n, was assumed to be 1.4 for aqueous solutions. For κ^2 the average value of 2/3 was used. The spectral overlap integral, J, between donor FMN and acceptor Cy3 or Cy5 were calculated with the a|e-UV-Vis-IR Spectral Analysis Software v2.2 [167]. The calculated values for J (FMN-Cy3) and J (FMN-Cy5) are $4.740 \cdot 10^{15}$ and $5.357 \cdot 10^{15}$, respectively. With the calculated FRET efficiencies in Equation 4.12, the average distance between the FMN chromophore and the Cy dyes is calculated to be 36.5 Å in RsLOV. According to the crystal structure RsLOV is therefore most probably labeled at Lys4 or Lys8.

Table 4.2 Fluorescence decay times, τ_F, of RsLOV, RsLOV-Cy3 and RsLOV-Cy5 determined via TCSPC. The samples were excited at $\lambda = 378$ nm and the fluorescence was detected at 500 nm for FMN fluorescence or at 570 nm and 670 nm for Cy3 and Cy5 emission, respectively. The integral weighted fractions of the biexponential decays are given in brackets.

sample	τ_F / ns at 500 nm	τ_F / ns at 570 nm	τ_F / ns at 670 nm
RsLOV	2.3	-	-
RsLOV-Cy3	0.3 (∼ 95 %)	0.1	-
	1.5 (∼ 5 %)	-	-
RsLOV-Cy5	0.5 (∼ 90 %)	-	1.1
	4.0 (∼ 10 %)	-	-

Next to the FRET between FMN and Cy5, the emission spectra of RsLOV-Cy3 with $\lambda_{\mathrm{exc}} = 530$ nm exhibit another photophysical effect. They are not identical before and after 200 s of blue light irradiation. As can be seen in Figure 4.3.5, the Cy3 emission intensity is increased by 10 % after 200 s blue light irradiation of RsLOV-Cy3. It reverts back to the initial value over night in the dark and therefore on a much longer timescale than adduct recovery. After recovery, the effect is reproducible within the same sample. This indicates that blue light irradiation induces a change within the RsLOV-Cy3 system which is presumably correlated with the light-induced dissociation of RsLOV dark-state dimers. In contrast, the emission increase after blue light irradiation cannot be observed in RsLOV-Cy5 under the same conditions. But the emission properties of the Cy3 and Cy5 dyes are rather divergent. Therefore, the increase in Figure 4.3.5 can likely be originating from an intrinsic property of

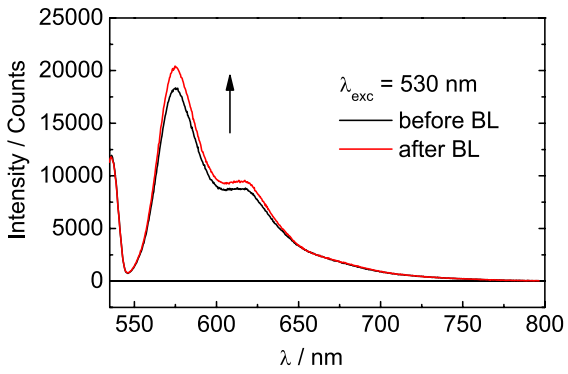

Figure 4.3.5 Comparison of the emission spectrum of RsLOV-Cy3 with $\lambda_{exc} = 530\,nm$ before (black line) and after (red line) 200 s of continuous blue light irradiation. The intensity of the Cy3 emission increases by around 10 %.

Cy3. This will be discussed within the picture of dimer dissociation at a later part of this section.

4.3.2.2 RsLOV-Cy3/Cy5 mix

After determination of the emission properties of RsLOV-Cy3 and RsLOV-Cy5 individually, measurements of mixed RsLOV-Cy3/Cy5 samples were performed. The labeled samples were mixed at a 1:1 ratio with the same concentrations already used for the experiments with RsLOV-Cy3 and RsLOV-Cy5 alone. The following experiment was conducted to monitor the blue light-induced dissociation and dark-adapted association of RsLOV: Emission spectra of the 1:1 RsLOV-Cy3/Cy5 mixture was recorded with $\lambda_{exc} = 530\,nm$ and a time resolution of 1 s prior to blue light irradiation. In this case, no adduct formation of RsLOV occurs and the spectra represent the initial dark state situation of Cy3 - and Cy5-labeled homodimers. Following this, the sample was irradiated with blue light for 200 s. Adduct formation occurs in RsLOV accompanied by dimer dissociation. Single labeled RsLOV-Cy3 showed that this already has an impact on the emission intensity of Cy3. Subsequent incubation of RsLOV-Cy3/Cy5 in the dark brings the system back into the dark state. At this point, heterodimers consisting of Cy3- and Cy5-labeled subunits should be formed and show a considerable FRET compared to the initial spectrum with $\lambda_{exc} = 530\,nm$. In a 1:1 mixture of RsLOV-Cy3 and RsLOV-Cy5 with similar labeling ratios, a maximum FRET efficiency of 50 % due to heterodimer formation can be expected assuming that all molecules participate in the reaction and that hetero- and homodimers are formed with the same probability. Figure 4.3.6 shows the emission spectra of RsLOV-Cy3 / Cy5 corresponding to the described experiment. The initial dark state spectrum is shown in Figure 4.3.6B (green line), the first and the last spectrum of the 200 s blue light irradiation are shown in Figure 4.3.6A and the spectrum after blue light irradiation (blue line) and subsequent incubation of the sample in the dark (black and red lines) are shown in Figure 4.3.6B.

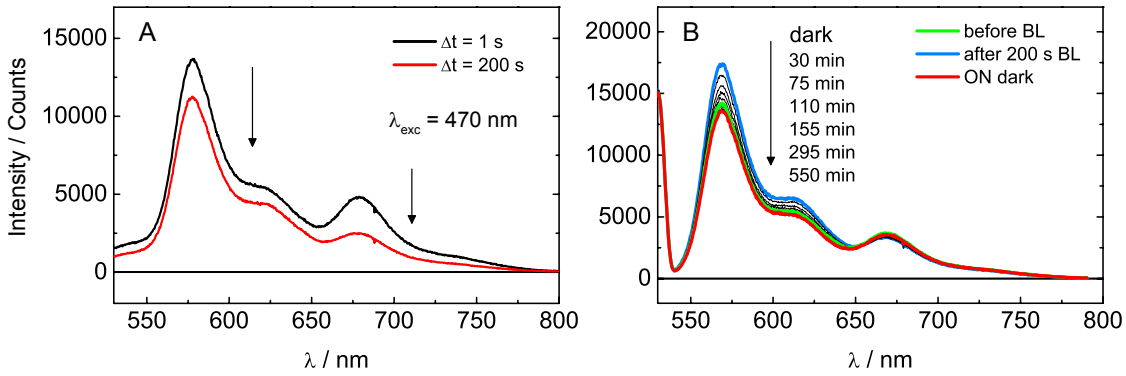

Figure 4.3.6 Emission spectra of a 1:1 mixture of RsLOV-Cy3 and RsLOV-Cy5. **A:** The sample was excited at $\lambda_{exc} = 470$ nm for 200 s. **B:** Emission spectra with $\lambda_{exc} = 530$ nm before (green line) and after (red line) 200 s blue-light excitation. Subsequently, the sample was incubated in the dark and spectra were taken at indicated times (ON:over night).

During blue light excitation (Figure 4.3.6A) the Cy3 and Cy5 intensities decrease like already observed for the unmixed samples. Likewise, the emission spectra of RsLOV-Cy3/Cy5 at $\lambda_{exc} = 530$ nm are not identical before and after blue-light excitation (Figure 4.3.6B). But the Cy3 emission is increased by 20 % and therefore 10 % more than RsLOV-Cy3 under the same conditions. In contrast, the Cy5 emission is decreased by 10 %. Both, Cy3 and Cy5 emission, return to their initial value in the dark. No FRET can be observed due to mixing of the differently labeled RsLOV subunits after redimerization. But the increase of the donor emission and decrease of the acceptor emission of RsLOV-Cy3/Cy5 in Figure 4.3.6B due to blue-light excitation can be explained be an "inverse" FRET effect due to dissociation of RsLOV dimers. These observations in turn indicate that RsLOV-Cy3/Cy5 dimers did not just mix after light-induced dissociation, but that the dimers already exchange their subunits directly after mixing of RsLOV-Cy3 and RsLOV-Cy5 in the dark. Accordingly, the mixing experiment was repeated without blue light irradiation and a higher time resolution of 100 ms to pursue this indication. The RsLOV-Cy3 sample was prepared with the same concentration like before in a volume of 396 µL. The measurement was started and during the measurement 4 µL RsLOV-Cy5 was added. In this way, the RsLOV-Cy3/Cy5 mixture is identical to the measurement with 1 s time resolution but the volume of the sample does not change significantly upon addition of RsLOV-Cy5. During addition of RsLOV-Cy5 and mixing of the solutions, the beam path is blocked by the pipette tip and the spectra taken during the mixing phase cannot be taken into account for the analysis of the spectra. This results in a "blind" window of 4 s. Most of the spectral changes during the experiment occurred during this mixing phase.
To slow down the kinetics of the mixing, the experiment was repeated once more with 30 % (v/v) glycerol added to the sample solution in order to increase the viscosity of the solvent. The corresponding spectra are shown in Figure 4.3.7A. Prior to addition of RsLOV-Cy5, only the emission of RsLOV-Cy3 is visible with a emis-

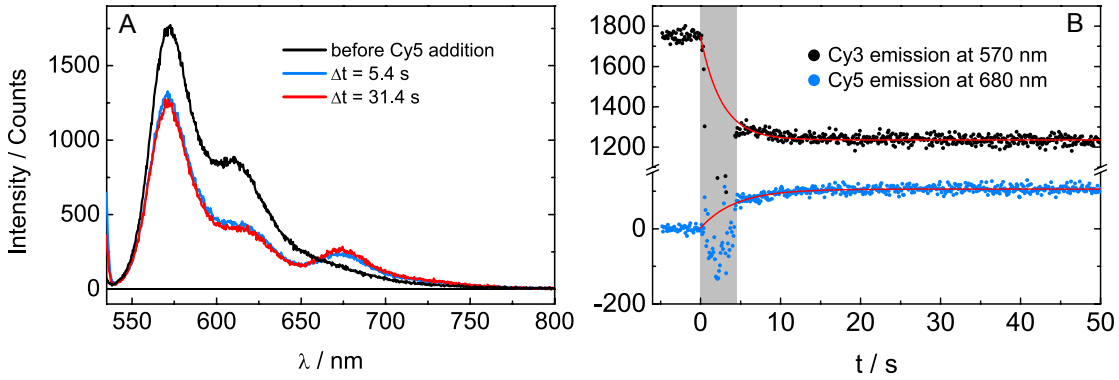

Figure 4.3.7 A: Emission spectra of the RsLOV-Cy3/Cy5 mixing experiment with a 100 ms time resolution in the presence of 30 % (v/v) glycerol. The spectra before (black line), 5.4 s (blue line) and 31.4 s (red line) after RsLOV-Cy5 addition are compared. **B:** Corresponding time traces of the Cy3 (black dots) and Cy5 (blue dots) emission taken at the peak maximum over time. The addition of RsLOV-Cy5 is defined as t = 0. The gray rectangle illustrates the mixing phase. Red lines illustrate monoexponential fits to the data, interpolated in the mixing time window.

sion maximum at 573 nm (black line). Upon addition of RsLOV-Cy5 and mixing of the solution ("blind" window of 5.4 s in this case), the emission of RsLOV-Cy5 becomes visible with a maximum at 674 nm. The Cy3 emission decreases by 30 % upon addition of RsLOV-Cy5 proving an immediate FRET between Cy3 and Cy5. In the following seconds, only small spectral changes of RsLOV-Cy3/Cy5 occur and after approximately 30 s the emission spectrum stays constant. The FRET efficiency between Cy3 and Cy5 can be calculated to be 0.28 using Equation 4.11.
Figure 4.3.7B illustrates the development of the Cy3 and Cy5 emission over the time of the experiment. The value at 680 nm was corrected for Cy3 emission. The spectral profiles of Cy3 and Cy5 emission clearly show that most of the changes still occur during the mixing window. But with knowing the initial values of the emission bands and the spectral changes 30 s after mixing, a monoexponential fit to the data with interpolation of the data points during the mixing window could be performed. This analysis results in time constants of $\tau = 1.8$ s in the case of Cy3 and $\tau = 2.9$ s for Cy5. Analogue analysis of the measurement without glycerol yields even faster time constants of $\tau = 1.4$ s (Cy3 emission) and $\tau = 1.5$ s (Cy5 emission). The time constants of RsLOV-Cy3 and RsLOV-Cy5 mixing suggest very fast exchange of the RsLOV subunits in the dark state dimers.

In order to determine an accurate value of the subunit exchange in RsLOV, additionally stopped-flow measurements with a time resolution of 7 ms were performed. RsLOV-Cy3 and RsLOV-Cy5 were mixed at a 1:1 ratio to a total volume of 400 µL in the mixing chamber. The concentrations of the samples were the same like used in the experiments described before (0.5 µM FMN and 0.8 µM Cy3 or 0.7 µM Cy5). The samples were excited at 540 nm, Cy3 emission was detected at 595 nm and Cy5 emission at 690 nm. The great advantage of the stopped-flow setup is that there is no dead-time between mixing and detection. Figure 4.3.8 shows the development

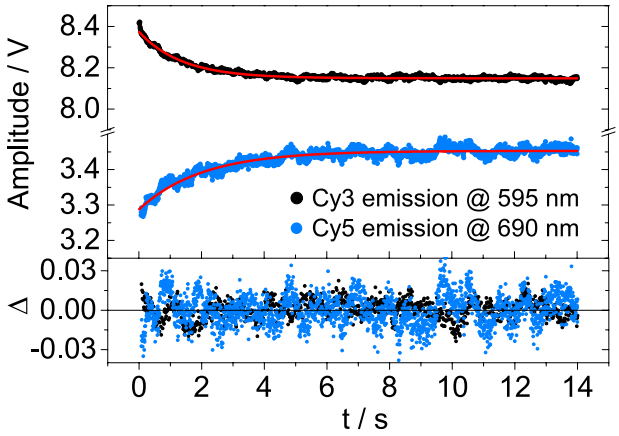

Figure 4.3.8 Stopped-flow plot of RsLOV-Cy3/Cy5 at a concentration of 1 µM. Cy3 emission (black dots) was detected at 595 nm, Cy5 emission (blue dots) at 690 nm. The data were fit with monoexponential decay functions. The residuals of the fit are presented in black for Cy3 and in blue for Cy5.

of Cy3 and Cy5 emission upon mixing of RsLOV-Cy3 and RsLOV-Cy5 over 15 s. The curves represent the average of five individual measurements. The data were analyzed assuming a monoexponential decay. Using a biexponential decay function did not improve the fit significantly. The residuals of the fit are also shown in Figure 4.3.8. The rates for the subunit exchange in the dark state can be calculated for the Cy3 trace to be $k = 0.82\,s^{-1}$ and for the Cy5 trace to be $k = 1.05\,s^{-1}$. These rates correspond to an average exchange time under the applied conditions of $t_{av} = 1.07\,s$.

As further support for the hypothesis of exchanging dimer subunits in dark-state RsLOV, another experiment was designed. The emission measurements of RsLOV-Cy3 showed, that the emission of Cy3 is sensitive to the number of other Cy3 molecules in its environment (see Figure 4.3.5). Due to the dissociation of RsLOV-Cy3 dimers upon blue light excitation, an increase of the Cy3 emission by $\sim 10\,\%$ could be observed. Hence, addition of unlabeled RsLOV to a solution of RsLOV-Cy3 should result in an increase of Cy3 emission under the assumption that the dimer subunits exchange. This leads to dimers with only one labeled subunit per dimer which in turn emit like monomers. Figure 4.3.9A and B shows the corresponding spectra. Increasing volumes of a 18 µM solution of unlabeled RsLOV was added to a RsLOV-Cy3 solution with a concentration of 1.6 µM of Cy3 and 1.0 µM FMN. The total volume of the sample was 400 µL containing either 10 µL, 20 µL or 30 µL of unlabeled RsLOV. The UV / Vis spectra in Figure 4.3.9A show that the absorbance of the FMN band increases upon addition of RsLOV while the Cy3 absorption band stays constant. The corresponding steady-state emission spectra in Figure 4.3.9B display RsLOV-Cy3 with and without wt addition. The samples were excited at $\lambda = 530$ nm. It is evident from the data that with increasing amount of RsLOV an increase of Cy3 emission can be observed immediately after mixing of Cy3-labeled and unlabeled RsLOV. Upon addition of 30 µL RsLOV the Cy3 emission intensity

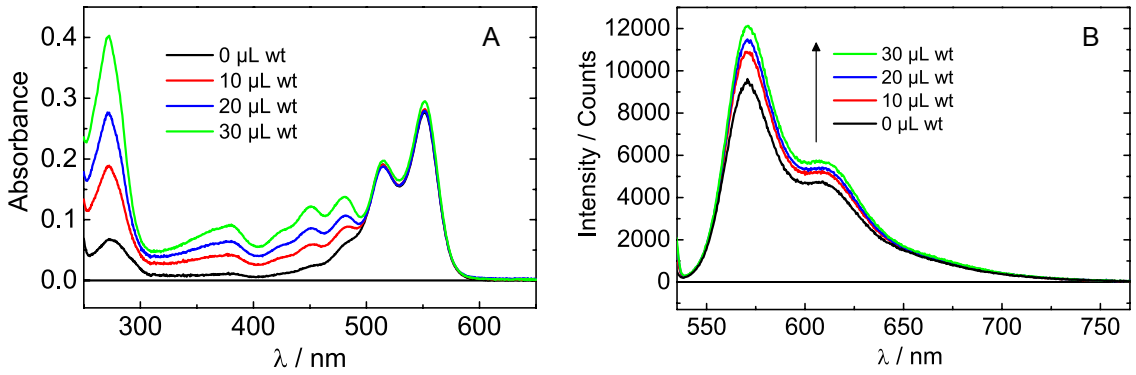

Figure 4.3.9 A: UV/Vis spectra of RsLOV-Cy3 (black line) and RsLOV-Cy3 plus 10 µL (red line), 20 µL (blue line) and 30 µL (green line) unlabeled RsLOV wt. **B:** Corresponding emission spectra of the RsLOV-Cy3 samples. The samples were excited at $\lambda = 530$ nm.

is 30 % higher compared to the sample without unlabeled RsLOV. The result of this experiment is a further proof for rapidly exchanging RsLOV dimers in the dark.

The results obtained on the subunit exchange in RsLOV dimers described so far in this section are all dependent on the conditions applied, in particular they are concentration-dependent. In order to further elucidate the monomer-dimer equilibrium of RsLOV in the dark state the dissociation constant, K_D, was determined. Therefore, the FRET efficiencies of 1:1 mixtures of RsLOV-Cy3/Cy5 were determined over a FMN concentration range from 100 nM to 10.9 µM. With decreasing concentration, the monomer-dimer equilibrium of dark-state RsLOV shifts to the monomeric side. The corresponding FRET spectra are shown in Figure 4.3.10A. The spectra were obtained by subtraction of the emission spectra of RsLOV-Cy3 and RsLOV-Cy5 from the emission spectrum of RsLOV-Cy3/Cy5 at each concentration to correct for the effects of unlabeled RsLOV and Cy3/Cy3 or Cy5/Cy5 homodimers. ΔF refers to the decrease of Cy3 fluorescence due to FRET. For each sample, the concentration of RsLOV-Cy3 and RsLOV-Cy5 was the same in the unmixed and the mixed solutions. It is evident from the spectra in Figure 4.3.10A that FRET is decreasing with decreasing FMN concentration. The FRET efficiency was calculated according to Equation 4.11 and is plotted as a function of total protein concentration c_0 in Figure 4.3.10B. K_D was estimated from fitting the data to the equation:

$$E_{FRET} = \frac{E_{FRET}max}{4}\left(\frac{K_D}{c_0} - \sqrt{\frac{K_D}{c_0}\left(\frac{K_D}{c_0} + 8\right)} + 4\right) \tag{4.14}$$

This equation refers to a equilibrium dimerization model previously described in [142]. Further details and the derivation of this model is also given in the Appendix A, section A.2. Fitting the data to Equation 4.14 without any restraints yields $K_D = 7.0 \pm 2.0$ µM and a saturation limit for the FRET efficiency , $E_{FRET}max$, of 0.67 (red line in Figure 4.3.10B. According to combinatrial statistics, the value of $E_{FRET}max$ is limited to 0.50. Fitting the data with $E_{FRET}max$ fixed to 0.50 yields

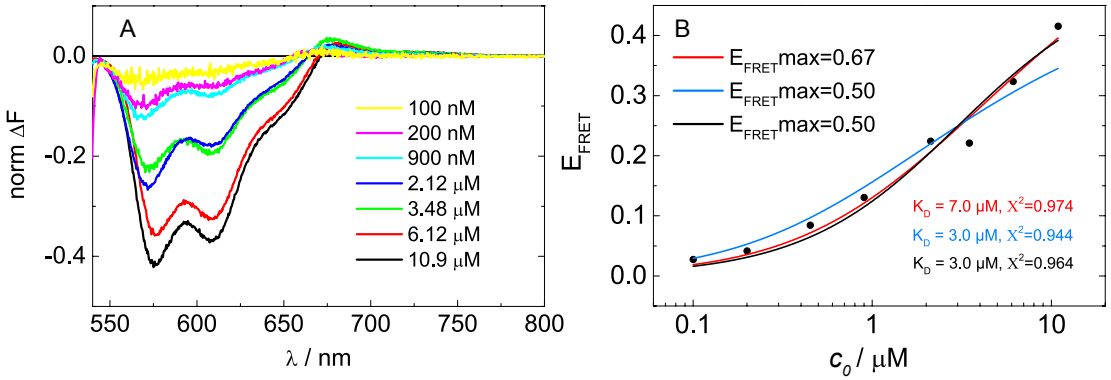

Figure 4.3.10 A: FRET spectra of RsLOV-Cy3/Cy5 over a FMN concentration range from 100 nM to 10.9 µM with $\lambda_{exc} = 530$ nm. The spectra were generated by subtraction of RsLOV-Cy3 and RsLOV-Cy5 spectra from RsLOV-Cy3/Cy5 to correct for the effects of homodimers and unlabeled RsLOV. All samples contained an equal concentration of RsLOV-Cy3 and RsLOV-Cy5, respectively. **B:** E_{FRET} calculated according to Equation 4.11 plotted versus the total FMN concentration. The date were fit either to Equation 4.14 without restraints (red line), with E_{FRET}max fixed to 0.50 (blue line) or to Equation 4.15 without any restraints (black line).

$K_D = 3.0 \pm 0.5$ µM (blue line in Figure 4.3.10B). The variance of the E_{FRET}max and hence the K_D values might be explained by the fact that the data points at low concentrations do not contain enough information for the correct estimation of E_{FRET}max. For comparison, the data were additionally fit to the merely empirical model:

$$E_{FRET} = \frac{E_{FRET}\text{max} \cdot c_0}{K_D + c_0} \tag{4.15}$$

The fit is shown as the black line in Figure 4.3.10B and yields $K_D = 3.0 \pm 0.8$ µM and $E_{FRET}\text{max} = 0.50$ when fit without any restraints which is identical to Equation 4.14 with E_{FRET}max fixed to 0.50. Anyway, the model underlying Equation 4.14 correctly describes the monomer-dimer equilibrium of RsLOV although the error of E_{FRET}max is high, while Equation 4.15 is empirical. In conclusion, although some variance of K_D exists depending on the fit procedure, we can, however, limit the magnitude of K_D to be in the µM-range.

4.3.3 Discussion

RsLOV is a member of the so-called "short" LOV domain family, which are lacking an effector domain. They carry terminal peptide extensions via which they are thought to interact with partner proteins. Such multistep signaling pathways are complex although the LOV domain architecture seems rather simple [46]. RsLOV has both, a short C-terminal extension consisting of the aα helix and a N-terminal extension forming an unique HTH (helix-turn-helix) motif composed of the Jα and the Kα

helix [143]. Both extensions could potentially interact with an effector domain, but so far no partner proteins have been identified and the function of RsLOV remains unclear. It is, however, known that RsLOV activation is intriguingly linked to an light-dependent oligomeric state change [143]. In the dark state, RsLOV forms a coiled-coil dimer via the HTH motif forming an unusual dimerization surface. Upon light excitation the RsLOV dimers dissociate [143].
Due to its light-dependent oligomeric state changes RsLOV was chosen as a model system to use FRET as a spectroscopic tool to investigate intermolecular LOV domain interactions. RsLOV was expressed in *E. coli* as a soluble, green protein with the same adduct and oligomeric state parameters like reported in the literature [143]. RsLOV was labeled successfully with Cy3 and Cy5 NHS ester with calculated dye:protein ratios of around 1.7:1 and 1.4:1. The labeled RsLOV samples are still able to undergo adduct formation upon blue light excitation although with a reduced yield compared to unlabeled RsLOV.

4.3.3.1 Labeled RsLOV shows FRET between FMN and the Cy dyes

The emission spectra of Cy3- and Cy5-labeled RsLOV indicate that very efficient FRET occurs between the FMN chromophore of the LOV domain and the attached dyes. Upon excitation of the Cy3 dye at $\lambda = 530\,\mathrm{nm}$, the emission of RsLOV-Cy3 and RsLOV-Cy5 stays constant like expected for samples with only one type of Cy label. In contrast, direct excitation of the FMN at $\lambda = 470\,\mathrm{nm}$ leads to a decrease of the Cy3 and Cy5 emission over time. In the case of RsLOV-Cy5 additionally the FMN emission could be detected, which also decreases upon blue light excitation. Assuming the occurrence of FRET between FMN and the Cy dyes, this behavior can be explained by the blue light-induced adduct formation of RsLOV. With ongoing irradiation of the sample, the adduct state accumulates in RsLOV-Cy3 and RsLOV-Cy5. Since the FMN becomes non-fluorescent in the adduct state, the energy can no longer be transferred to the acceptor Cy3 or Cy5, which in turn causes the decrease of the Cy emission. Within dark state reversion of the adduct state, the Cy emission recovers to the initial intensity.
This hypothesis is further supported by the fluorescence decay measurements. The fluorescence lifetimes of RsLOV-Cy3 and RsLOV-Cy5 are biexponential, with the major component being strongly quenchend compared to unlabeled RsLOV. According to these lifetimes, the FRET efficiencies of RsLOV-Cy3 and RsLOV-Cy5 can be calculated to be 0.85 and 0.78. These findings allow for two conclusions: firstly, the majority of RsLOV in the sample covalently or non-covalently binds a Cy dye since the short lifetime component in both labeled RsLOV samples constitutes more than 90 %. The quenching of the fluorescence lifetime requires an acceptor in close distance, which is only the case if the LOV domain is labeled. The Förster radii for RsLOV FMN-Cy3 and RsLOV FMN-Cy5 were determined to be 42.9 Å and 43.9 Å and hence the average distance between donor and acceptor was calculated to be 35.0 Å , hinting towards Lys4 or Lys8 as most probable labeling sites in RsLOV. Secondly, the fact that the FMN chromophore of RsLOV efficiently

performs FRET with the attached dyes adds an additional photophysical effect to the RsLOV-Cy systems, which needs to be taken into account when performing FRET measurements of mixed RsLOV-Cy3/Cy5 solutions.

Furthermore, another photophysical effect was observed in the case of RsLOV-Cy3. The emission intensity of the Cy3 emission at $\lambda_{exc} = 530\,nm$ increased upon blue light excitation. This behavior could not be observed for RsLOV-Cy5. A labeling study with Cy3 and IgG revealed that the brightness of the Cy3 emission is depending on the number of Cy labels per protein [166]. This means in particular that Cy3 emission is more intense in the case of single-labeled proteins than it is for double-labeled proteins. The increase observed for RsLOV-Cy3 can hence be explained by the dissociation of RsLOV dimers upon blue light. The number of Cy3 labels per RsLOV unit is reduced when switching from dimers to monomers which in turn leads to an increase in Cy3 emission. After reequilibration of RsLOV in the dark over night, the Cy3 emission intensity reverts back to the initial value. Thus, the re-dimerization of RsLOV occurs on a much longer time-scale than adduct recovery. SAXS data on RsLOV indicate that a large conformational change is possible upon activation of the LOV domain, which extends Jα and Kα away from the LOV core [143]. This may play a role in the interaction of RsLOV with a partner protein. Our data indicate that reversion of the conformational changes of RsLOV required to reconstitute the dimer interface occurs on a slower timescale than adduct recovery. This in turn means that once RsLOV is shifted to the signaling state it stays active for a longer time than the adduct state.

4.3.3.2 RsLOV is a rapidly exchanging dimer in the dark

The aforementioned FRET between FMN and the Cy dyes in RsLOV-Cy3 and RsLOV-Cy5 as well as the sensitivity of Cy3 emission to its environment did superimpose the emission measurements of the mixed RsLOV-Cy3/Cy5 samples. Taking these effects into account, no FRET could be observed due to an exchange of Cy3/Cy3 and Cy5/Cy5 homodimers into Cy3/Cy5 heterodimers after re-dimerization of blue light-induced RsLOV monomers. In contrast, an inverse FRET effect was observed upon blue light irradiation, meaning an increase of the donor intensity with a simultaneous decrease of acceptor intensity. This indicates, that the RsLOV dimers persistently exchange their subunits in the dark via a monomer-dimer equilibrium. Under this assumption, the "inverse" FRET effect in the range of 10 % can be assigned to the dissociation of RsLOV dimers which in turn interrupts the FRET interaction between Cy3 and Cy5 dye of heterodimers. Exchanging RsLOV dimers would also explain the fact, that no spectral changes of RsLOV-Cy3/Cy5 could be observed when comparing the emission spectra before blue-light excitation and after reequilibration to the dark state. Repeating the mixing experiment without blue light irradiation, with a higher time resolution and glycerol in the solution revealed a very rapid dimer exchange in RsLOV. Stopped-flow measurements of RsLOV-Cy3/Cy5 reveal an exchange time constant of approximately 1.0 s at a LOV domain concentration of 1 µM. Stepwise addition of unlabeled RsLOV wt to a solution of

RsLOV-Cy3 further confirmed the hypothesis of exchanging subunits of darks state RsLOV dimers.

Indications for a monomer-dimer equilibrium of RsLOV, which shifts to the monomeric side upon light excitation, have been proposed before. Conrad *et al.* determined the oligomeric state of RsLOV using SEC, multiangle scattering (MALS) and SEC-coupled small angle X-ray scattering (SAXS) [143]. In all cases, the light-state mass matches with the calculated mass for a RsLOV monomer, but the dark-state mass was obtained as an intermediate mass of calculated monomer and dimer mass. The authors concluded, that this can only be explained by the fact, that RsLOV exists as dimers and monomers in the dark. They could narrow down the exchange kinetics to be faster than 10 min according to the fastest experimental technique they used [143]. Likewise, our SEC data show a peak corresponding to the RsLOV monomer in the light state, but the dark-state peak eluted at a mass of 31 kDa corresponding the intermediate mass of RsLOV monomers and dimers. It is known, that associating systems can elute as a single peak on SEC if the exchange of e.g. monomers and dimers is rapid on the timescale of SEC and if the binding affinity is low [163, 164]. Furthermore, the determination of E_{FRET} over a large concentration range allowed us to calculate K_D to be in the range of 3.0–7.0 µM.

Light-induced structural changes of LOV domains probing the downstream signal propagation have been the subject of many mechanistic studies [28, 42, 125]. Within these, dimerization usually occurs upon activation of the LOV domain like observed for *Aureochrome* LOV domains or VVD LOV of the fungus *Neurospora crassa* [28, 123]. In contrast, RsLOV behaves oppositely and dissociates upon light activation. The long C-terminal HTH motif consisting of Jα and Kα helix establishes the dimerization surface in the dark state. This has not been observed previously in LOV domains [143]. Upon light activation the signal is propagated from FMN N5 to the conserved Gln 118 via the Iβ sheet to the Ncap and Jα [143]. The SAXS data in reference [143] also suggest that subsequently the Jα and Kα move away from the LOV domain. This in turn could allow for the interaction with a signaling partner, yet to be defined.
In conclusion, labeling of RsLOV with Cy3 and Cy5 dyes is associated with some experimental challenges. The FMN chromophore interacts strongly with the attached labels in competition with the intended FRET between the Cy dye pair. Additionally, the environmental influence on the emission intensity of Cy3 dye needs to be taken into account. But by determining the magnitude of these effects on the emission data of RsLOV-Cy3/Cy5, it was possible to obtain further information on the intermolecular interactions of RsLOV with our experimental setup.

4.4 The LOV1 domain of *C.reinhardtii* phototropin

4.4.1 CrLOV1 wt

In contrast to higher plants, the unicellular green alga *C. reinhardtii* has only one phototropin (CrPhot) gene [13]. CrPhot triggers blue light-dependent sexual differentiation [168], photosynthetic gene expression [169], regulation of eyespot size and phototactic behavior [170]. Phot of *C. reinhardtii* is a multidomain protein consisting of around 1000 amino acids [13]. The structure of CrPhot is shown in Figure 4.4.1. It is comprised of two N-terminal LOV domains, CrLOV1 and CrLOV2, acting as the photosensory units. They are coupled to the C-terminal effector domain, a serine/threonine kinase (STK) [17].
Light-activation of the LOV domains induces signal transduction to the kinase which in turn autophosphorylates. Adduct formation of the LOV domains thereby leads to conformational changes within the LOV core and the C-terminal and N-terminal α-helices of CrLOV2, Jα and A'α [23, 41, 121, 132, 171]. In this way the signal is propagated downstream to the STK which in turn gets activated [145, 172, 173]. The details, however, of how Phot transduces light into physiological responses is still not fully understood and remains subject to future investigations.

Although the two LOV domains exhibit similarities regarding their sequence, structure and photocycles, they have distinct roles [128]. LOV2 acts predominantly as the light-sensing domain and mediates the light-dependent autophosphorylation of Phot [129]. LOV1, on the other hand, is thought to contribute little to the activation of the kinase. It has been proposed that LOV1 rather acts as a regulator of LOV2 activation [130, 134]. Furthermore, it has been suggested that LOV1 may play a role in dimerization of full-length Phot [135, 136].

The oligomeric state of CrLOV1 has been discussed controversially. Fedorov *et al.* solved the crystal structure of CrLOV1 in 2003, in which the LOV domain is monomeric [76]. They determined the oligomeric state of CrLOV1 in solution via gel filtration to be mainly monomeric (80-90 %) and to some extent tetrameric (10-20 %). Determination of the oligomeric state of full-length CrPhot via SEC and SAXS as well indicated a monomeric form of the protein in the dark and in the light state contradicting the hypothesis that CrLOV1 acts as a dimerization site [145, 173]. In contrast to this, Kutta *et al.* reported blue light-dependent oligomeric state

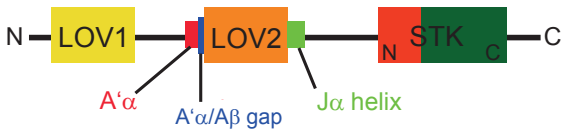

Figure 4.4.1 Structure of *C. reinhardtii* Phot consisting of the two N-terminal LOV domains and the C-terminal serine/threonine kinase (STK). CrLOV2 has two flanking helices, Jα and A'α. The figure was modified according to [134].

changes of CrLOV1 [144]. They crosslinked CrLOV1 via PEGylation (polyethylene glycol-ylation) followed by SDS-PAGE analysis and detected a monomer-dimer equilibrium in the dark state, which shifted towards dimers upon blue light irradiation. The authors concluded that CrLOV1 performs blue light-induced intermolecular interactions. It should, however, be noted that native CrLOV1 eluted as dimers and high molecular weight oligomers in this study. In conclusion, up to date the oligomeric state of CrLOV1 and its changes upon blue light are not unambiguously resolved.

We addressed this issue and labeled CrLOV1 with Cy3 and Cy5 dye in order to investigate potential interdomain interactions via FRET. Additionally, SEC measurements were performed on the unlabeled CrLOV1 samples. The results are shown in the following part of this chapter. The data obtained with CrLOV1 wt, however, did not provide clear results potentially due to unspecific labeling. Hence, we designed a CrLOV1 mutant with a single, specific labeling site, CrLOV1 A16C. This mutant was labeled with Cy3 and Cy5 at the N-terminus and investigated via FRET and SEC. At the end of this section the results of both systems are discussed.

4.4.1.1 SEC

The oligomeric state of unlabeled CrLOV1 in solution was determined using SEC. The measurements were carried out in the dark and under continuous blue light irradiation at different concentrations. Figure 4.4.2A shows the elution profiles of CrLOV1 in the dark and in the light state at a concentration of 7 µM. CrLOV1 elutes in the dark at 240 mL (29.0 kDa) and with a broad peak between 150 and 200 mL exhibiting two maxima at 163 mL and 181 mL. With a theoretical molecular weight of 14.9 kDa for the monomer, the peak at 240 mL (i.e. 29.0 kDa) corresponds to CrLOV1 dimers. The broad elution peak between 150 and 200 mL indicates that high molecular weight oligomers greater than decamers are additionally formed in the CrLOV1 sample. The elution profile of CrLOV1 does not change significantly upon blue light illumination. The small shift of the dimer peak towards a higher molecular weight can be explained by a shape change of the LOV domain due to adduct formation.
To check whether the formation of high molecular weight oligomers is concentration-dependent, the experiment was repeated at 100 µM yielding the same results. Hence, both fractions were collected separately and prepared for a second SEC run to exclude that the high molecular weight oligomers are artifacts of the protein purification. The samples are named CrLOV1 I (200 kDa) and II (29 kDa) hereafter. The elution volumes in Figure 4.4.2A cannot be compared directly with Figure 4.4.2B and C since a different SEC column was used. Fraction I mainly exists of higher aggregates eluting at 8.4 mL with a shoulder at 8.9 mL ($\sim$ 150 kDa) (Figure 4.4.2B), but also a peak at 12.4 mL (26 kDa) consistent with the dimer mass of CrLOV1 can be detected. On the other hand, fraction II elutes mainly at 12.2 mL (28 kDa) corresponding to CrLOV1 dimers (Figure 4.4.2C). Upon blue light excitation the peak corresponding to high molecular weight oligomers reoccurs. The same experiment

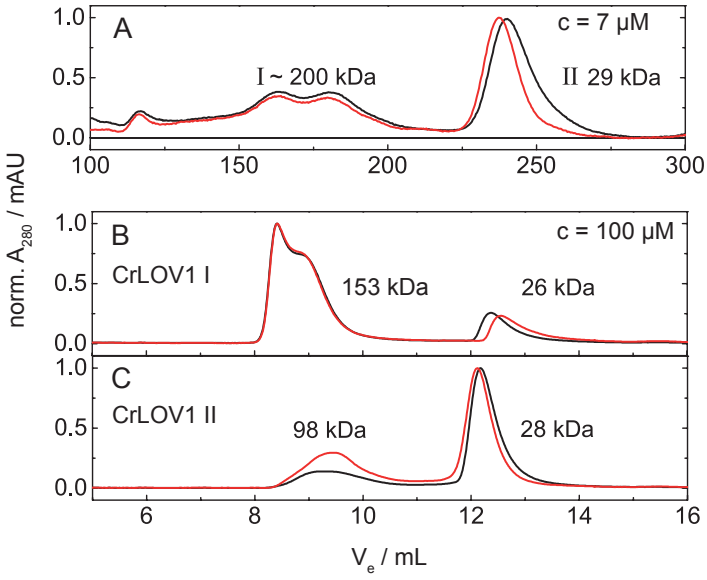

Figure 4.4.2 Size exclusion chromatography of CrLOV1 in the dark (black lines) and in the light state (red lines). **A:** CrLOV1 at 7 µM elutes with two major peaks corresponding to dimers and high molecular weight oligomers. **B** and **C:** Peak I and II were fractionated and injected separately at a concentration of 100 µM.

was repeated at a concentration of 50 µM giving an identical result. This suggests that association of CrLOV1 resulting in high molecular weight oligomers is not an artifact of the purification process and can be found in a concentration range from 7 µM up to 100 µM.

4.4.2 CrLOV1-Cy3 and CrLOV1-Cy5

The amino acid sequence of CrLOV1 includes three cysteines and nine lysines. According to the crystal structure (pdb 1N9L [76]), at least four lysines and two cysteines are located on the protein surface and are therefore potential labeling sites. Selective labeling of the two surface cysteines, Cys32 and Cys83, with maleimide ester was not successful, hence CrLOV1 was labeled with Cy3 and Cy5 NHS ester. The covalent attachment of the dyes to CrLOV1 was verified via mass spectrometry. Figure 4.4.3 shows the normalized UV/Vis spectra of CrLOV1-Cy3 (black line) and CrLOV1-Cy5 (dashed black line) in comparison with the spectra of pure Cy3 (magenta line) and Cy5 (blue line) NHS ester in PB. The absorption maximum of Cy3 is at 549 nm. When labeled to CrLOV1 the absorption maximum shifts by 5 nm to 554 nm. Analogously, the absorption maximum of CrLOV1-Cy5 (652 nm) is 5 nm red-shifted compared to Cy5 (647 nm). The labeled proteins additionally show the flavin absorption band around 450 nm. The dye to protein ratio was calculated from the UV/Vis spectra to be 1.2:1 in the case of CrLOV-Cy3 and 1.3:1 for CrLOV-Cy5.

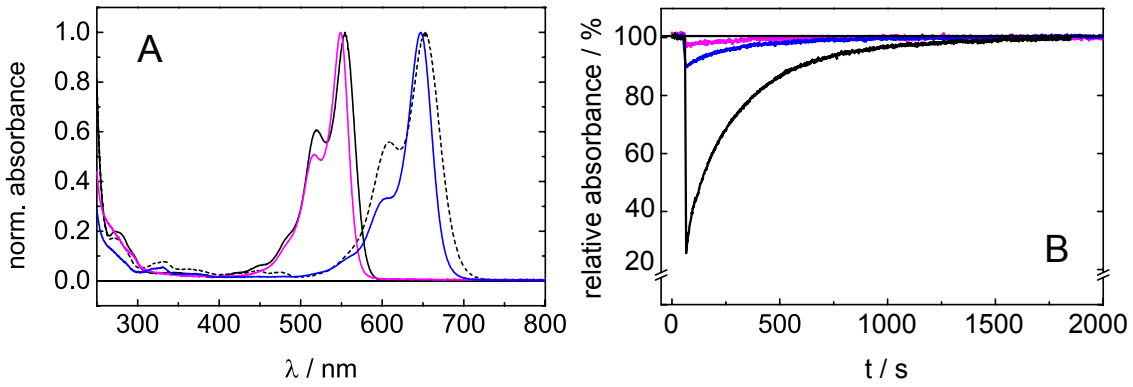

Figure 4.4.3 **A:** Normalized UV/Vis spectra of CrLOV1-Cy3 (black line), CrLOV1-Cy5 (dashed black line) and the dyes Cy3 (magenta line) and Cy5 (blue line) in PB (10 mM sodium phosphate / 10 mM NaCl, pH 8.0) in the range of 250 nm to 800 nm. **B:** Adduct recovery of unlabeled CrLOV1 (black line), CrLOV1-Cy3 (magenta line) and CrLOV1-Cy5 (blue line) after 500 ms blue light excitation.

To check whether labeled CrLOV1 is still photo-active, the adduct formation yield and recovery kinetics were determined. The Cy3- and Cy5-labeled samples were excited with two LEDs, $\lambda_{exc} = 450$ nm, for 500 ms. Subsequently the decay kinetics of the adduct state in the dark were monitored at 475 nm and compared with unlabeled CrLOV1. The absorption of the labeled proteins at 475 nm was corrected for the particular dye absorbance at this wavelength. While the unlabeled CrLOV1 forms approximately 75 % adduct upon blue light illumination under the applied conditions, the adduct formation yield in the Cy3-labeled sample is reduced to less than 10 %, in the Cy5-labeled sample to around 10 % under the same conditions.
The kinetic traces were analyzed by fitting exponential functions to the data. For unlabeled CrLOV1, a biexponential function was used yielding the time constants $\tau_1 = 63$ s (30 %) and $\tau_2 = 302$ s (70 %) with R^2=0.999. These values are in agreement with the adduct recovery time constants of CrLOV1 given in the literature ($\tau_1 = 45$ s (15 %) and $\tau_2 = 320$ s (85 %)) [133]. The decay kinetics of the labeled CrLOV1 samples result in similar values. No specific numbers are given, because the signal to noise ratio of the measurement was poor due to the small adduct formation yield. In summary, it can be stated that attachment of Cy3 and Cy5 decreases the yield of adduct formation, but does not have impact on the recovery kinetics.

4.4.2.1 Emission measurements of labeled CrLOV1

Analogously to the labeled RsLOV samples, the photophysical properties of CrLOV1-Cy3 and CrLOV1-Cy5 were determined individually. Figure 4.4.4 shows the emission spectra of CrLOV1-Cy3 and CrLOV1-Cy5 with either blue or green light excitation for 1000 s to check whether the illumination wavelength has an influence on the emission behavior. Figure 4.4.4A shows the emission spectra with $\lambda = 530$ nm. The emission maximum of CrLOV-Cy3 is at 578 nm with a shoulder at 617 nm, red-shifted by 11 nm compared to free Cy3 dye in the same buffer system. The emission

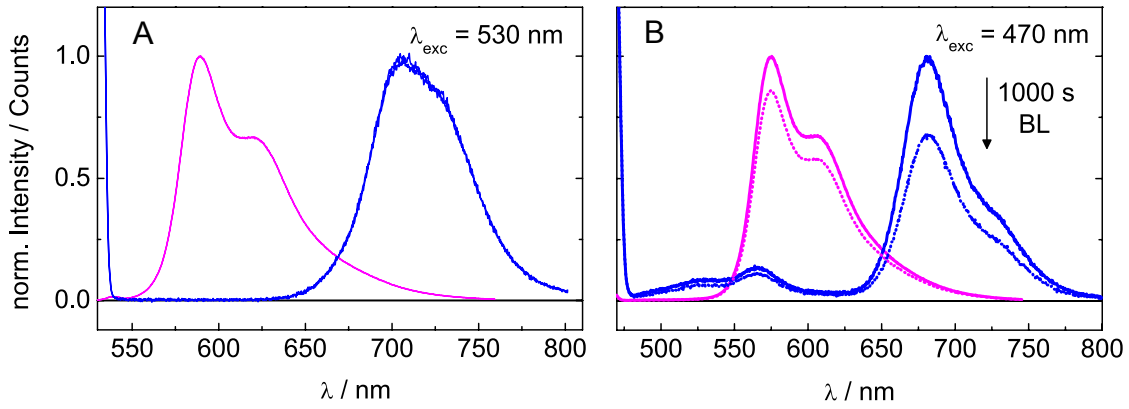

Figure 4.4.4 Normalized emission spectra of CrLOV1-Cy3 (magenta lines) and CrLOV1-Cy5 (blue lines) with λ_{exc}=530 nm **(A)** and λ_{exc}=470 nm **(B)**. The spectra were recorded over 1000 s under continuous illumination. In each case the first and the last spectrum of the measured sequence is shown.

maximum of CrLOV1-Cy5 is at 702 nm red-shifted by 30 nm compared to Cy5 dye under the same conditions. Both emission spectra stay constant during the measurement. Direct excitation of the FMN chromophore at $\lambda_{exc} = 470$ nm leads to a decrease of Cy3 and Cy5 emission like already observed for RsLOV. The emission intensity of CrLOV-Cy3 decreases by 14 %, the one of CrLOV-Cy5 by 35 %. The emission maximum of CrLOV1-Cy5 changes to 686 nm at this excitation wavelength. The spectra of CrLOV1-Cy5 additionally exhibit the FMN emission band, which decreases by the same percentage like Cy5. The emission bands completely recover in the dark within 60 min in both samples on the timescale of adduct recovery.

Like in the case of RsLOV, these results can be associated with a FRET between FMN and the Cy dyes, which is interrupted by adduct formation of the LOV domain. The adduct yield of Cy-labeled CrLOV1 obtained in the UV/Vis measurements in Figure 4.4.3 does not match with the adduct-induced Cy emission decrease observed in the spectra in Figure 4.4.4. This is due to the fact that the samples were excited with a single, 500 ms-blue light pulse to determine the adduct formation yield, while the samples were continuously irradiated with a blue LED for 1000 s in the case of the emission measurements. This allows for accumulation of the adduct state over time while adduct recovery is prevented, which results in a higher adduct yield.

As a further proof for the hypothesis of FRET between FMN and the Cy dyes in CrLOV1 additionally the photo-inactive mutant CrLOV1 C57S was labeled. CrLOV1 C57S cannot form the flavin-cysteinyl adduct due to the mutation of the reactive Cys. We labeled CrLOV1 C57S with Cy3 and Cy5 NHS ester and used it as a reference for labled CrLOV1. In this way, spectral effects induced by adduct formation of the LOV domain can be identified. Covalent binding of the dyes to CrLOV1 C57S was confirmed by mass spectrometry. Single and double labeled CrLOV1 C57S was detected in both cases next to a fraction of unlabeled LOV domain. The dye to protein ratio was calculated from the UV/Vis spectra to be 2:1

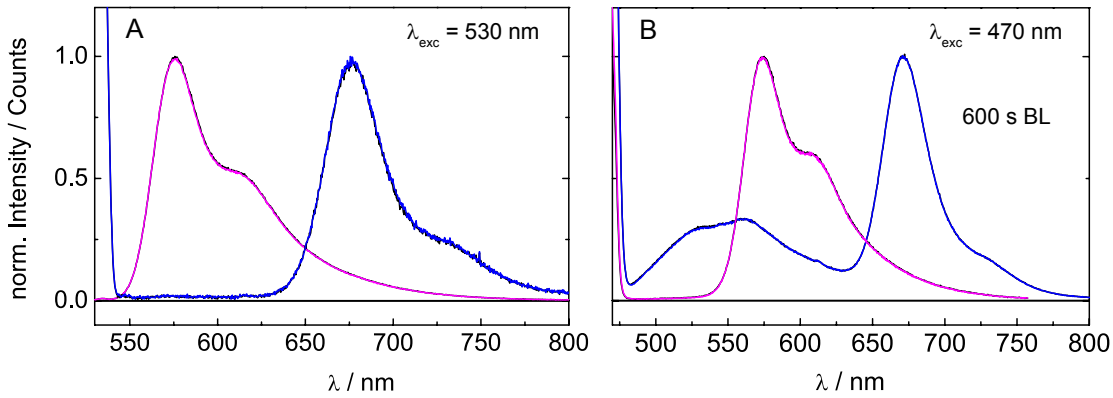

Figure 4.4.5 Normalized emission spectra of CrLOV1 C57S-Cy3 (magenta) and CrLOV1 C57S-Cy5 (blue) with **A:** green light excitation at $\lambda = 530\,\text{nm}$ and **B:** blue light excitation at $\lambda = 470\,\text{nm}$. The spectra were recorded for 600 s with continuous light irradiation. The first (black lines) and the last spectrum (colored: Cy3 in magenta, Cy5 in blue) of each sequence is compared.

(CrLOV1 C57S-Cy3) and 1.6:1 (CrLOV1 C57S-Cy5).
Emission measurements of the individually labeled CrLOV1 C57S were carried out as already described for CrLOV1-Cy3 and CrLOV1-Cy5. Figure 4.4.5 shows the emission spectra of CrLOV1 C57S-Cy3 and CrLOV1 C57S-Cy5 with excitation at $\lambda = 530\,\text{nm}$ (Figure 4.4.5A) or $\lambda = 470\,\text{nm}$ (Figure 4.4.5B), respectively. The spectra were recorded for 600 s with continuous irradiation of the samples. The emission spectra of labeled CrLOV1 C57S stay constant with green light excitation at $\lambda = 530\,\text{nm}$. However, with $\lambda_{\text{exc}} = 470\,\text{nm}$ no decrease of the FMN or Cy emission occurs like observed for CrLOV1-Cy3 and Cy5. The data on labeled CrLOV1 C57S unambiguously prove that the reversible emission quenching under blue light conditions can be associated with adduct formation in CrLOV1-Cy3 and CrLOV1-Cy5.

In order to determine the efficiency of the FRET between FMN and the Cy dyes in CrLOV1, the fluorescence decay times of labeled and unlabeled CrLOV1 were determined using TCSPC. The samples were excited at 280 nm and the fluorescence was detected either at 500 nm to measure the FMN fluorescence lifetime or at 570 nm and 670 nm, respectively, to measure the Cy3 and Cy5 lifetime. The fluorescence of the flavin chromophore of unlabeled CrLOV1 decays monoexponentially with $\tau = 2.9\,\text{ns}$ [74]. In contrast, FMN incorporated in CrLOV1-Cy3 or CrLOV1-Cy5 eshibits a biexponential fluorescence decay, with one component being strongly quenched compared to CrLOV1 with $\tau_1 = 0.3\,\text{ns}$ (CrLOV1-Cy3) and $\tau_1 = 0.5\,\text{ns}$ (CrLOV1-Cy5). The second components have a similar lifetime like CrLOV1 and can be associated with unlabeled CrLOV1.
Analogously to the labeled RsLOV samples, the FRET efficiencies can be calculated:

Table 4.3 Fluorescence decay times, τ_F, of CrLOV1, CrLOV1-Cy3 and CrLOV1-Cy5 determined via TCSPC. The samples were excited at $\lambda = 280\,\text{nm}$ and the fluorescence was detected at 500 nm for FMN fluorescence or at 570 nm and 670 nm for Cy3 and Cy5 emission, respectively. The data are the result of a maximum entropy analysis. The values in brackets correspond to the fraction of each component obtained by integrating the peaks of the distribution functions resulting from maximum entropy analysis.

sample	τ_F / ns at 500 nm	τ_F / ns at 570 nm	τ_F / ns at 670 nm
CrLOV1	2.9	-	-
CrLOV1-Cy3	0.3 (85 %)	0.2	-
	3.1 (15 %)	-	-
CrLOV1-Cy5	0.5 (90 %)	-	1.4
	3.0 (10 %)	-	-

$$\begin{aligned} \mathrm{E_{FRET}}\,(\mathrm{CrLOV1-Cy3}) &= 1 - \frac{\tau_{DA}}{\tau_D} = 1 - \frac{0.3\,\mathrm{ns}}{2.5\,\mathrm{ns}} = 0.88 \\ \mathrm{E_{FRET}}\,(\mathrm{CrLOV1-Cy5}) &= 1 - \frac{\tau_{DA}}{\tau_D} = 1 - \frac{0.5\,\mathrm{ns}}{2.9\,\mathrm{ns}} = 0.82 \end{aligned} \tag{4.16}$$

The efficiency of the energy transfer between FMN and CrLOV1-Cy3 is in the same range like observed for RsLOV. The Förster radii of the donor-acceptor pairs FMN-Cy3 and FMN-Cy5 can be calculated according to equation Equation 4.1 to be:

$$\begin{aligned} \mathrm{R_0}\,(\mathrm{FMN-Cy3}) &= 48.0\,\text{Å} \\ \mathrm{R_0}\,(\mathrm{FMN-Cy5}) &= 46.7\,\text{Å} \end{aligned} \tag{4.17}$$

with $\Phi_D = 0.16 \pm 0.05$ (determined in chapter 2). In the case of CrLOV1, the calculated values for J (FMN-Cy3) and J (FMN-Cy5) are $4.997 \cdot 10^{15}$ and $4.253 \cdot 10^{15}$, respectively. With the calculated FRET efficiencies in Equation 4.16 the average distance between the FMN chromophore and the Cy dyes can be calculated to be 35.4 Å in CrLOV1.

4.4.3 Emission measurements of CrLOV1-Cy3/Cy5

Mixed solutions of CrLOV1-Cy3 and CrLOV1-Cy5 with a ratio of 1:1 were prepared in order to investigate potential interdomain interactions of CrLOV1. At first, mixing of the two solutions without blue light irradiation was performed. The concentration of CrLOV1-Cy3/Cy5 was adjusted to be 2 µM. CrLOV1-Cy3 and

CrLOV1-Cy5 were mixed directly in the cuvette and changes of the emission spectra were monitored over a time of 400 s with a time resolution of 100 ms. The corresponding spectra are shown in Figure 4.4.6A. The first spectrum after mixing was taken at 300 ms. After 2.5 s, a decrease of the Cy3 emission was observed, while the Cy5 emission did not change. However, after 400 s also an increase of the Cy5 emission occurred. The development of the Cy3 and Cy5 emission over the time of the experiment clearly shows that donor emission decrease and acceptor emission increase occur with different kinetics (Figure 4.4.6B). The quenching of the donor is faster.

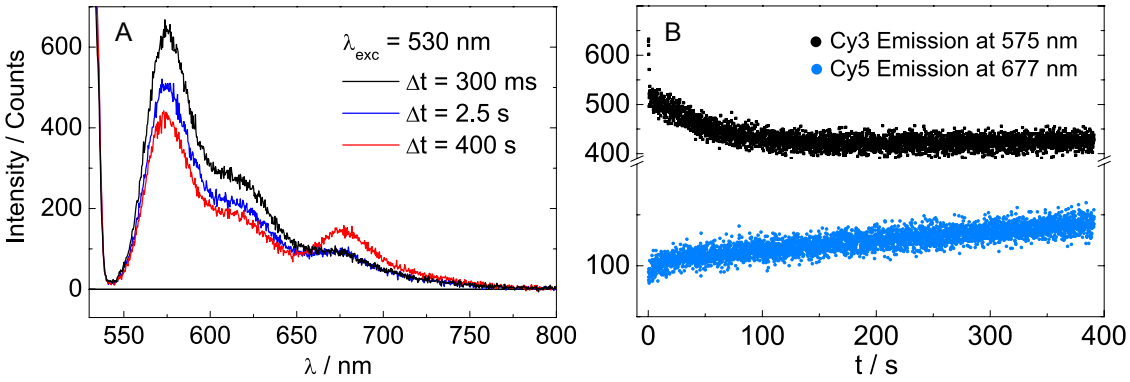

Figure 4.4.6 A: Mixing of CrLOV1-Cy3 and CrLOV1-Cy5 monitored over 400 s with λ_{exc}=530 nm and a time resolution of 100 ms. Spectra at t = 300 ms (black line), at t = 2.5 s (blue line) and at t = 400 s (red line) are compared. **B:** Development of Cy3 and Cy5 emission over the time of the experiment.

The spectral changes upon mixing of CrLOV1-Cy3 and CrLOV1-Cy5 indicate FRET. To quantify the effect, the emission spectrum of CrLOV1-Cy3/Cy5 at λ_{exc}=530 nm was compared with those of CrLOV1-Cy3 and CrLOV1-Cy5 containing equal concentrations of the particular labeled LOV domains (Figure 4.4.7). It is evident from the spectra that the CrLOV1-Cy3 donor emission is quenched in the presence of acceptor-labeled CrLOV1. Figure 4.4.7B represents the FRET spectrum and was calculated from the emission spectrum of CrLOV1-Cy3/Cy5 minus the one of CrLOV1-Cy3 and CrLOV1-Cy5 to eliminate the effect of CrLOV1-Cy3/Cy3 and CrLOV1-Cy5/Cy5 homodimers and unlabeled CrLOV1. The spectra were normalized to the emission maximum of CrLOV1-Cy3. ΔF corresponds to the emission difference of Cy3. The FRET efficiency can be calculated to be $E_{FRET} = 0.33$.

Furthermore, the influence of blue light irradiation on CrLOV1-Cy3/Cy5 was investigated. Mixed solutions of CrLOV1-Cy3 and CrLOV1-Cy5 with a ratio of 1:1 and a dye concentration of 800 nM were prepared. Figure 4.4.8 shows the corresponding emission spectra of CrLOV1-Cy3/Cy5. Upon mixing of the samples, the initial spectrum with $\lambda_{exc} = 530$ nm was recorded (Figure 4.4.8A). Subsequently, CrLOV1-Cy3/Cy5 was illuminated with blue light for 1000 s (Figure 4.4.8B). During blue light irradiation, the Cy3 emission decreases like already observed for CrLOV1-Cy3 (see Figure 4.4.4B). In contrast, the emission of Cy5 initially decreases over the first

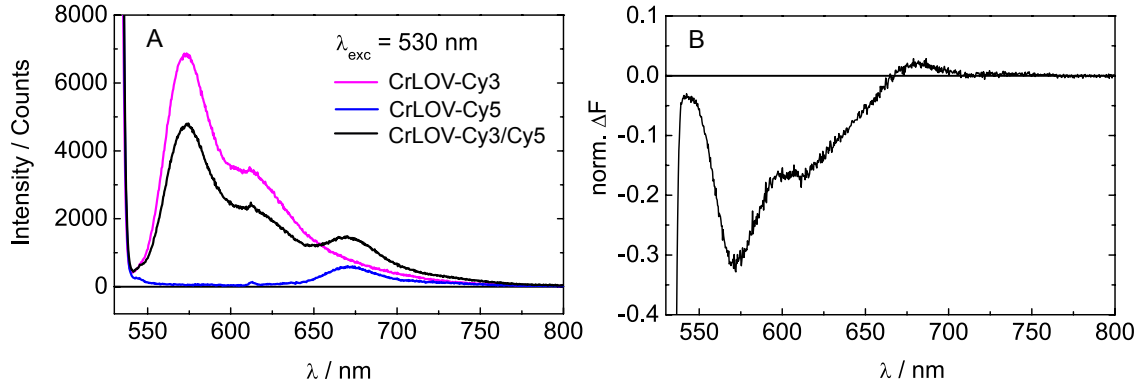

Figure 4.4.7 A: Comparison of the emission spectra of CrLOV1-Cy3 (magenta), CrLOV1-Cy5 (blue) and CrLOV1-Cy3/Cy5 (black) with λ_{exc}=530 nm. The concentrations of CrLOV1-Cy3 and CrLOV1-Cy5 were equal in mixed and unmixed samples. **B:** FRET spectrum of CrLOV1-Cy3/Cy5. The emission spectra of CrLOV1-Cy3 and CrLOV-Cy5 were subtracted from the emission spectrum of CrLOV1-Cy3/Cy5.

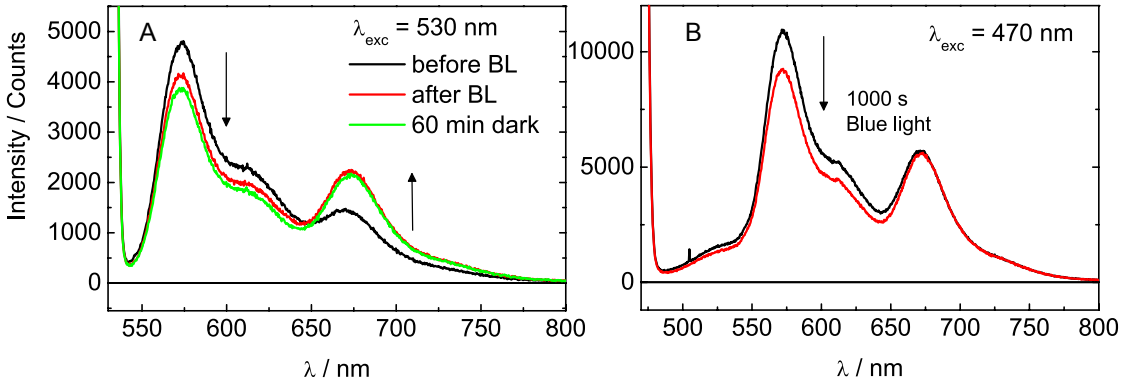

Figure 4.4.8 Emission spectra of CrLOV1 - Cy3 - Cy5 with a dye concentration of 400 nM each. **A:** CrLOV1-Cy3/Cy5 excited at λ_{exc}=530 nm before (black line) and after (red line) blue light irradiation. Additionally, the emission spectrum after 60 min recovery in the dark is shown. **B:** CrLOV1 - Cy3 - Cy5 was excited at λ_{exc}=470 nm for 1000 s. The first and the last spectrum of the sequence is shown.

100 s and then increases again resulting in a similar value like $\Delta t = 1$ s. The emission spectrum of CrLOV1-Cy3/Cy5 with $\lambda_{exc} = 530$ nm after blue light irradiation, however, changed compared to the initial spectrum (Figure 4.4.8A). The Cy3 emission is reduced by 30 %, while the Cy5 emission is increased by 60 %. This indicates that blue light-induced oligomeric changes of CrLOV1 occur, which result in FRET (Figure 4.4.8A).

Additionally, this blue light induced effect was only observed at low concentrations up to 2 µM. Mixed samples, which were incubated in the dark for several days prior to measuring do also not show any blue light-induced spectral changes. This indicates that the FRET is due to mixing of the CrLOV1-Cy3 and CrLOV1-Cy5. FRET can be observed with green light excitation only, but is accelerated upon activation of the LOV domain.

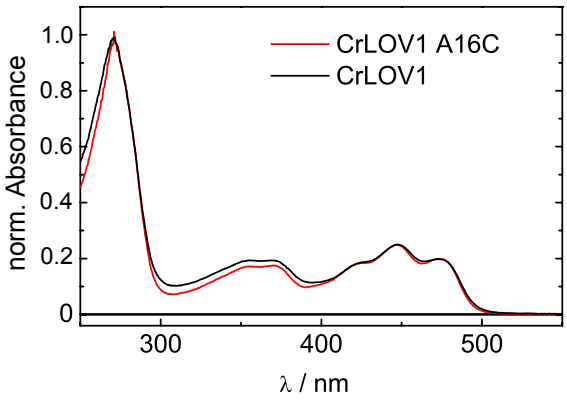

Figure 4.4.9 Comparison of the UV/Vis spectra of CrLOV1 (black line) and CrLOV1 A16C (red line) in the range of 250 nm to 550 nm.

4.4.4 CrLOV1 A16C C32S C83S

The experiments on labeled CrLOV1 did not yield a clear picture of the light-induced LOV-LOV interactions. A possible reason could be the unspecific labeling with Cy NHS esters. Therefore, we designed a CrLOV1 mutant with a single labeling site at the N-terminus for site-specific labeling. In this mutant the two surface Cys, Cys32 and Cys83, were mutated to Ser and the first amino acid of the CrLOV1 sequence, Ala16, was mutated to Cys to act as the labeling site. The cDNA of A16C C32S C83S mutant, named CrLOV1 A16C hereafter, was cloned into the expression vector pTBSG carrying a N-terminal 6 x His-tag. CrLOV1 A16C was expressed heterologously in *E.coli* and was obtained as soluble, yellow protein with a molecular mass of 15.6 kDa. The UV/Vis spectrum of CrLOV1 A16C shows the typical fine structured absorption bands with maxima at 447, 371 and 354 nm of the non-covalently bound oxidized FMN and is very similar to the absorption spectrum of CrLOV1 (Figure 4.4.9). Upon blue light illumination CrLOV1 A16C converts to the adduct state. Due to the high similarity with the wild-type, CrLOV1 A16C was used as a model system to study the behavior of CrLOV1. The N-terminal cysteine 16 was selectively labeled with either Cy3 or Cy5 maleimide ester. Mass spectrometry verified single labeled protein in both cases and showed no unlabeled protein in the samples.

The UV/Vis spectra of Cy3- and Cy5-labeled CrLOV1 A16C are shown in Figure 4.4.10A. In order to check whether labeled CrLOV1 A16C is still photo-active, the samples were irradiated with blue light for 500 ms and subsequently the absorbance at 475 nm was monitored. The same experiment was conducted with unlabeled CrLOV1 A16C to determine the adduct recovery kinetics. Figure 4.4.10B displays a comparison of the adduct recovery kinetics of unlabeled and labeled CrLOV1 A16C. While the unlabeled CrLOV1 A16C forms 100 % adduct upon blue light illumination, the adduct formation yield in the Cy3-labeled sample is reduced to approximately 10 % and in the Cy5-labeled sample to 30 % under the same condi-

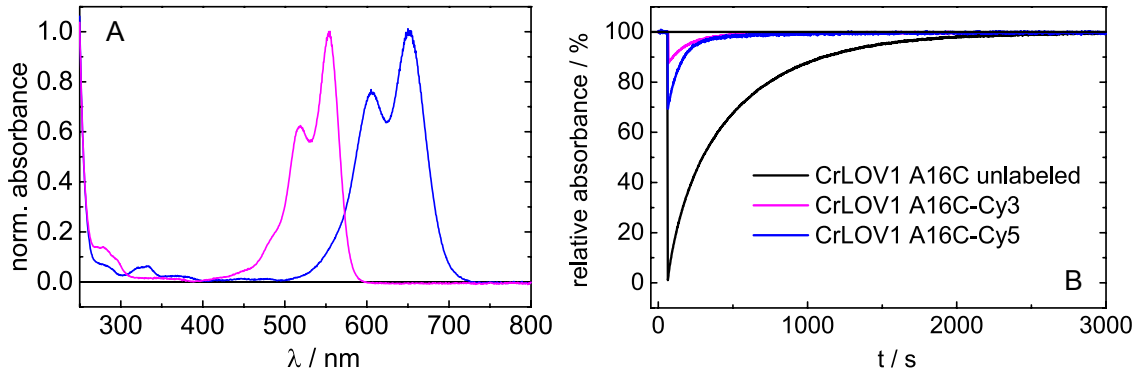

Figure 4.4.10 **A:** Normalized UV / Vis spectra of CrLOV1 A16C - Cy3 (magenta line) and CrLOV1 A16C - Cy5 (blue line) in the range of 250 nm to 800 nm. **B.** Adduct recovery kinetics of labeled and unlabeled CrLOV1 A16C recorded at 475 nm after excitation with blue light for 500 ms.

tions. The kinetic traces were analyzed by fitting exponential functions to the data. For unlabeled CrLOV1 A16C, a biexponential function was used yielding the time constants 101 s (31 %) and 510 s (69 %) with R^2=0.99993. The decay kinetics of the labeled CrLOV1 A16C samples were in a similar range. A biexponential fitting resulted in time constants of 122 s (83 %) and 393 s (17 %) for CrLOV1 A16C-Cy3 and 84 s (90 %) and 585 s (10 %) for CrLOV1 A16C-Cy5 with R=0.995 in both cases. The adduct formation yield is reduced for labeled CrLOV1 A16C like already observed for labeled CrLOV1, while the recovery kinetics are not affected significantly.

4.4.4.1 SEC measurements

SEC was applied to investigate the oligomeric state of CrLOV1 A16C at concentrations from 7 µM up to 100 µM (Figure 4.4.11). Measurements were performed in the dark and under continuous blue light irradiation. The absorbance of the eluted proteins was detected at 280 nm. Figure 4.4.11A shows the elution profiles of CrLOV1 A16C in the dark and in the light state at a concentration of 7 µM. Dark state CrLOV1 A16C eluted at 230 mL (34 kDa) and at 246 mL (19 kDa). With the theoretical mass of CrLOV1 A16C of 15.6 kDa, the first peak was assigned to be a dimer and the second peak to be a monomer. Under continuous blue light illumination only the dimer peak at 230 mL (34 kDa) appears. In contrast to CrLOV1, no high molecular weight oligomers were detected in both, the dark and the light state. To determine whether the monomer:dimer ratio in the dark state is concentration dependent SEC measurements at 100 µM and 50 µM were perfomed. Figure 4.4.11B shows the corresponding elution profiles. The elution volumes are different compared to the measurements at 7 µM, because a different column (Sephadex S75) was used for SEC. At both concentrations CrLOV1 A16C mainly elutes at 11.6 mL (36.3 kDa) which can be assigned to the dimeric mass. At 100 µM a shoulder of the main peak appears at 12.45 mL (25 kDa) and at 50 µM a second peak appears at 12.8 mL (21.1 kDa). The appearance of a second peak, which shifts to lower molec-

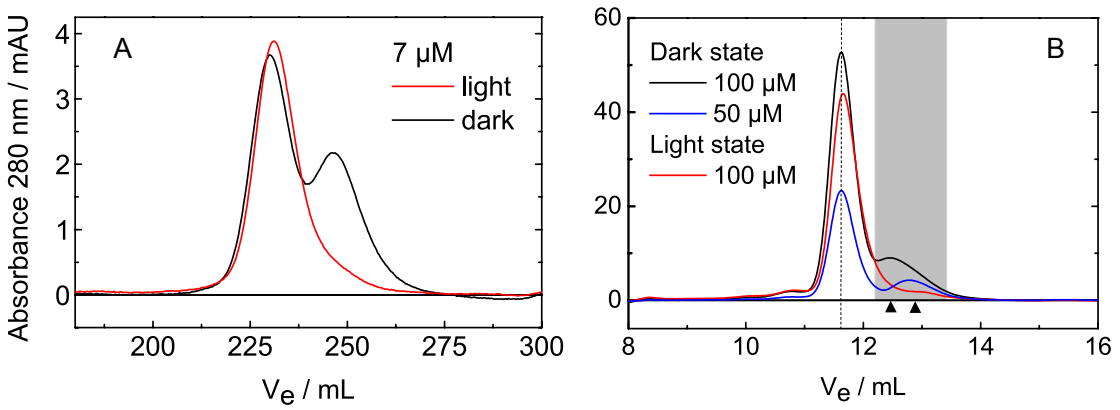

Figure 4.4.11 Size exclusion chromatography of CrLOV1 A16C at 7 µM **(A)**, 50 µM and 100 µM **(B)** in the dark state and under continuous blue light illumination. The black triangles indicate the monomer peak increasing with decreasing concentration.

ular masses, points to an increase of monomeric CrLOV1 A16C with decreasing concentration. Under continuous blue light irradiation, CrLOV1 A16C eluted with a single peak at 11.6 mL (36.3 kDa) also at a concentration of 100 µM. At 50 µM no light state run was performed.
These data suggest that the oligomeric state of dark-state CrLOV1 A16C is concentration-dependent. With decreasing concentration the fraction of monomer increases within the sample. Upon blue light illumination the monomers change their oligomeric state and only dimers are present also at low concentrations.

4.4.4.2 Emission measurements of labeled CrLOV1 A16C

Figure 4.4.12 shows emission spectra of CrLOV1 A16C-Cy3 and CrLOV1 A16C-Cy5. The samples were irradiated for 1000 s with either green or blue light. Like already observed in the case of labeled RsLOV and CrLOV1, the spectra stay constant over time with $\lambda = 530$ nm (Figure 4.4.12A) while an emission decrease occurs at $\lambda = 470$ nm (Figure 4.4.12B). Adduct formation of the LOV domains interrupts the FRET between FMN and the Cy dyes and results in an emission decrease of 16 % in the case of CrLOV1 A16C-Cy3 and 30 % in the case of CrLOV1 A16C-Cy5. FMN emission was only observed in the case of CrLOV1 A16C-Cy5 and decreased simultaneously and by the same amount like the Cy5 emission. The emission bands fully recover within 60 min in the same time range like adduct recovery. The maxima of CrLOV1 A16C-Cy3 and CrLOV1 A16C-Cy5 emission are located at 582 nm and 683 nm, respectively.

Emission measurements of mixed CrLOV1 A16C-Cy3/Cy5 were performed to further elucidate the FRET effects observed in CrLOV1-Cy3/Cy5. Therefore, 1:1 mixtures of the individually labeled protein samples at a concentration of 2 µM were prepared. The samples were mixed in the dark just before starting the measurements. Figure 4.4.13A shows the emission spectra of CrLOV1 A16C-Cy3/Cy5 with

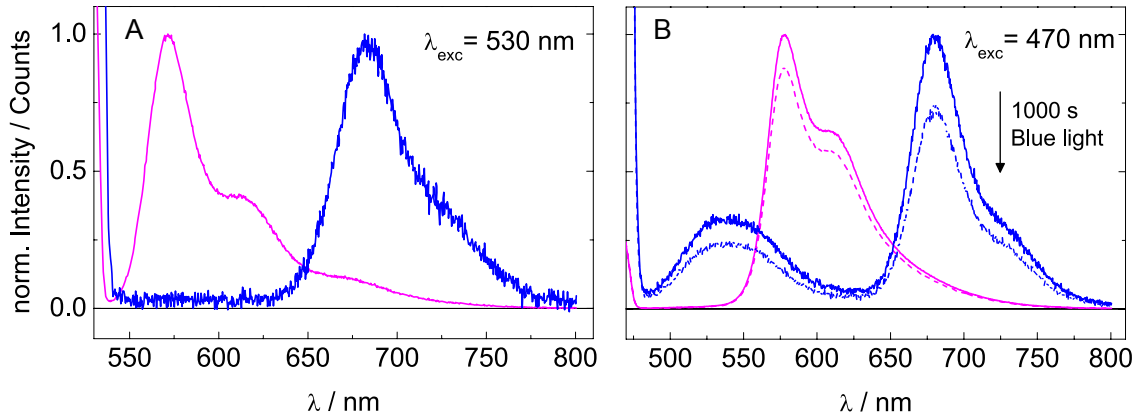

Figure 4.4.12 Normalized emission spectra of CrLOV1 A16C - Cy3 and CrLOV1 A16C - Cy5 with **A:** λ_{exc}=530 nm and **B:** λ_{exc}=470 nm. The spectra were monitored over 1000 s under continuous illumination. The first and the last spectrum of each sequence is shown.

$\lambda_{exc} = 530$ nm before and after 600 s continuous blue light irradiation. In contrast to CrLOV1-Cy3/Cy5, no spectral changes of the donor or acceptor emission could be observed contradicting the results obtained via SEC. Decreasing the concentration to 300 nM did not lead to any changes as well as adding donor-labeled CrLOV1 A16C in a 3:1 excess. The comparison of the CrLOV1 A16C Cy3 emission in the absence and in the presence of the acceptor Cy5 at equal concentrations (400 nM), however, indicates that blue light-independent FRET occurs in CrLOV1 A16C (Figure 4.4.13B) upon mixing of the solutions. It is evident from the FRET spectrum in the inset in Figure 4.4.13B that the donor emission decreases upon mixing of CrLOV1 A16C-Cy3 and CrLOV1 A16C-Cy5 while the acceptor emission increases. The kinetics of this process were determined in an analogous experiment like shown for CrLOV1-Cy3/Cy5 in Figure 4.4.6 with 100 ms time resolution. Accordingly, the decrease of donor emission and increase of acceptor emission occur on the timescale of minutes. E_{FRET} can be calculated to be around 0.15. Comparison of the FRET spectra before and after 1000 s of blue light irradiation does not show spectral changes.

4.4.4.3 His-tag impact

The SEC and emission measurements on unlabeled and labeled CrLOV1 and CrLOV1 A16C yielded significantly divergent results. Unlabeled CrLOV1 eluted in SEC at volumes corresponding to dimers and high molecular weight oligomers. Upon separation of the fractions the system re-equilibrated to the initial situation. Blue light illumination increased the amount of high molecular weight oligomers. In contrast, unlabeled CrLOV1 A16C eluted in SEC at volumes corresponding to dimers and with decreasing concentration to some extent as monomers. Blue light illumination shifted the system to the dimeric state only. The emission measurements of mixed CrLOV1-Cy3/Cy5 solutions showed a FRET in the range of 30 % due to mixing of the differently labeled LOV domains. In freshly prepared CrLOV1-Cy3/Cy5 samples blue light irradiation induced significant spectral changes indicating FRET. This

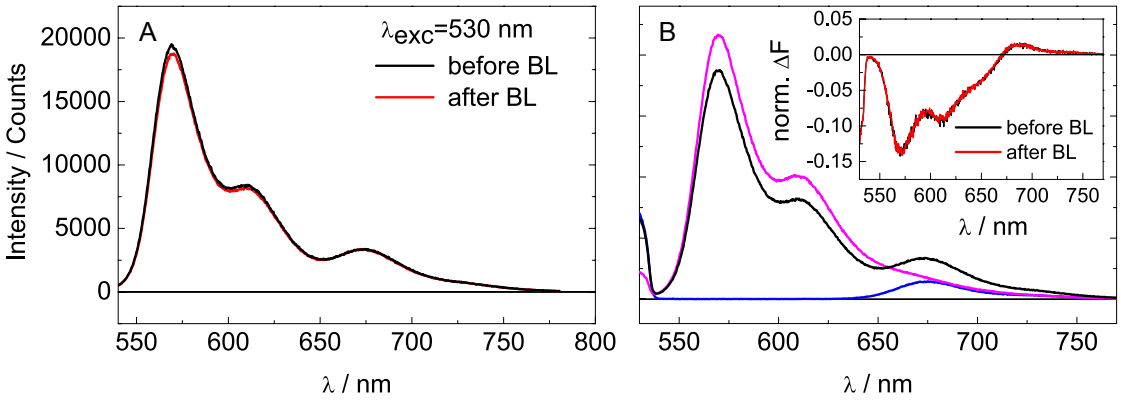

Figure 4.4.13 : **A:** Emission spectra of CrLOV1 A16C-Cy3/Cy5 before and after 1000 s blue light irradiation. **B:** Comparison of the emission spectra of CrLOV1 A16C - Cy3, CrLOV1 A16C - Cy5 and CrLOV1 A16C - Cy3 - Cy5 all containing the same concentration of each labeled protein (400 nM). **Inset:** FRET spectrum of CrLOV1 A16C-Cy3/Cy5 before and after 1000 s blue light irradiation. The spectra were obtained by subtraction of the emission spectra of CrLOV1 A16C - Cy3 and CrLOV1 A16C - Cy5 from the emission spectrum of CrLOV1 A16C-Cy3/Cy5 to eliminate the effect of homodimers and unlabeled LOV domains.

effect was not reversible and occurred only at low concentrations. CrLOV1 A16C-Cy3/Cy5 on the other hand only shows little FRET upon mixing of the solutions ($E_{FRET} = 0.15$) and no spectral changes upon blue light illumination of the sample. CrLOV1 and CrLOV1 A16C differ in two main points: i) The two surface cysteines, C32 and C83, were substituted by serines in CrLOV1 A16C in order to generate a site-specific labeling site at the N-terminus. Cysteines can form disulfide bonds, which might play a role in dimerization. ii) the two proteins were expressed in different expression vectors and carry divergent His-tag sequences at the N-terminus. It is know that His-tags can cause aggregation of proteins [174].

The gene encoding CrLOV1 A16C was cloned into the expression vector pTBSG [175]. This vector carries a N-terminal His-tag with six histidines, a fusion partner insertion site and a TEV (tobacco etch virus) protease cleavage site. The sequence is listed in Table 4.4 The His-tag adds an artificial extension of 24 amino acids to the natural 117 amino acids of CrLOV1 A16C.

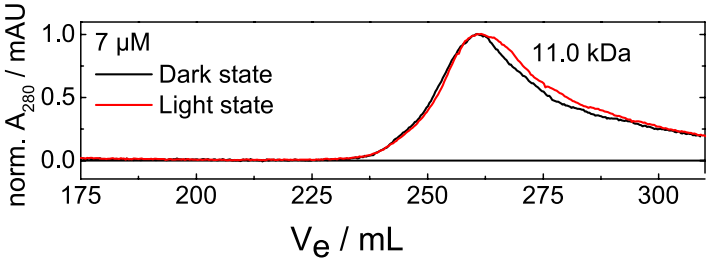

Figure 4.4.14 SEC of CrLOV1 A16C without purification tag in the dark and under continuous blue light illumination. The concentration of the injected samples was 7 µM.

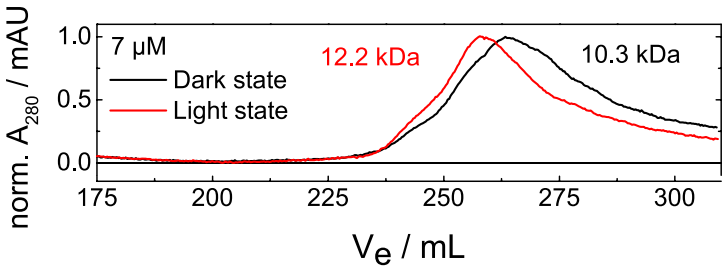

Figure 4.4.15 SEC of CrLOV1-28a in the dark and in the light state at a concentration of 7 µM.

This corresponds to 20 % of the total number of amino acids of the protein.
In order to test whether the artificial extension has an impact on the oligomeric state of CrLOV1 A16C the purification tag was cleaved with TEV protease. SEC was performed with cleaved CrLOV1 A16C in the dark and under continuous blue light illumination. Figure 4.4.14 shows the corresponding chromatogram. Due to the cleavage the amino acid sequence of CrLOV1 A16C was reduced to SNA-LOV and has a calculated molecular weight of 13.1 kDa. CrLOV1 A16C eluted with a single peak at 260 mL in SEC in both, dark and light state. The elution volume corresponds to a molecular weight of 11.0 kDa, which is consistent with the monomeric mass of CrLOV1 A16C. No light-induced oligomeric state changes were observed.

The natural surface cysteines, C32 and C83, were mutated in CrLOV1 A16C and it cannot be excluded that those were indispensable for dimer formation in CrLOV1. The purification tag of CrLOV1 does not provide any cleavage site and investigation of the cleaved protein was not possible with this construct. Therefore, the gene encoding for CrLOV1 was cloned into the very common expression vector pET-28a. This vector carries a N-terminal purification tag including six histidines and a thrombin cleavage site. The resulting protein will be designated as CrLOV1-28a. The mutation A16C was preserved in CrLOV1-28a as a potential labeling site.
SEC was performed with uncleaved CrLOV1-28a in the dark and under blue light conditions (Figure 4.4.15). Interestingly, CrLOV1 A16C-28a eluted with a single peak at 264 mL in the dark although the His-tag was not cleaved. The elution volume can be assigned to the CrLOV1-28a monomer. The calculated molecular weight is 15.1 kDa. Blue light illumination shifts the elution volume to 258 mL, which corresponds to 12.2 kDa. The shift of the elution peak between dark and light conditions can be explained by a shape change of the LOV domain upon adduct formation which could lead to a different migration behavior on the SEC column. However, also with the natural surface cysteines no light-induced oligomeric state changes could be observed in CrLOV1-28a.

In conclusion, the SEC results on cleaved CrLOV1 A16C and on uncleaved CrLOV1-28a indicate that the choice of the purification tag has huge impact on the oligomeric structure of these LOV1 domains. This will be discussed in detail in the discussion section.

Table 4.4 Expression vectors used for the expression of CrLOV1 and CrLOV1 A16C with the associated sequences of the purification tags.

Sample	Expression vector	Sequence of the purification tag
CrLOV1 A16C C32S C83S	pTBSG	MHHHHHH[a]STSVDLGT[b]-ENLYFQS[c]NA-LOV
CrLOV1	His-p2x	MHHHHHHHHHHHHEF-LOV
CrLOV1-28a	pET-28a	MGSSHHHHHHSSGLVPRGS[c]HM-LOV

[a] His-tag [b] fusion partner insertion site [c] cleavage site

4.4.5 Discussion

With our FRET study we addressed the question whether the LOV1 domain acts as a dimerization site of full-length CrPhot. CrLOV1 could only be labeled successfully with Cy3 and Cy5 NHS ester offering the problem that the specific labeling sites of the dyes are not known. Therefore, additionally, the mutant CrLOV1 A16C was generated, which carries a single labeling site at the N-terminus. The labeling reduces the adduct formation yield of the LOV domain, but the kinetics of adduct recovery are similar to unlabeled CrLOV1. We can exclude that only unlabeled proteins in the samples undergo adduct formation since CrLOV1 A16C does not contain any unlabeled LOV domains according to the results of mass spectrometry. In the case of CrLOV1 unlabeled LOV domains are present but due to our data and the high similarity between CrLOV1 and CrLOV A16C we assume that CrLOV1-Cy3 and CrLOV1-Cy5 are photo-active. The oligomeric state of both samples was investigated with SEC in the dark state and under blue light conditions. Potential protein-protein interactions were elucidated with the labeled proteins in emission measurements. Taken together, the results indicate that CrLOV1 does not act as a dimerization site of CrPhot.

4.4.5.1 FRET between FMN and the Cy dyes in CrLOV1 and CrLOV1 A16C

The emission spectra of the individual samples of labeled CrLOV1 and CrLOV1 A16C revealed a different behavior over time in dependence of the excitation wavelength. The spectra stayed constant over time when exciting the donor Cy3 at $\lambda = 530\,\text{nm}$. In contrast, excitation of the FMN chromophore at $\lambda = 470\,\text{nm}$ lead to a significant decrease of the emission intensity of the dyes and the flavin. The same behavior was already observed for labeled RsLOV. The decrease can be explained by FRET between the FMN and the Cy dyes. Due to the blue light irradiation of the samples the flavin-cysteinyl adduct is formed in the LOV domains. In the adduct state the flavin becomes non-fluorescent and the energy transfer from the FMN is interrupted. This in turn leads to the observed decrease of the emission

intensities. The fact that this emission decrease could not be detected in the photoinactive mutant CrLOV1 C57S labeled with Cy3 and Cy5 under the same conditions constitutes a further proof for FRET. Furthermore, the adduct formation yield is significantly decreased in labeled CrLOV1 and CrLOV1 A16C. This can as well be explained by FRET between FMN and the Cy dyes. It is known that upon excitation of the singlet state, the FMN incorporated in a LOV domain undergoes intersystem crossing to the triplet state from which the adduct is formed [30]. The energy transfer between FMN and the Cy dyes, however, occurs in the excited singlet state of FMN and therefore adds an additional deactivation channel to the S_1 state of FMN. This leads to reduced intersystem crossing and thus to a reduced adduct formation yield. The adduct formation yield was lower in the Cy3-labeled LOV domains than in the Cy5-labeled LOV domains for both, CrLOV1 and CrLOV1 A16C. This observation can be correlated with the E_{FRET} values calculated from the fluorescence decay times of unlabeled, Cy3- and Cy5-labeled samples. Since E_{FRET} of FMN-Cy3 is higher than the one of FMN-Cy5, the intersystem crossing should be in turn reduced stronger in Cy3-labeled CrLOV1 and CrLOV1 A16C than in the Cy5-labeled samples. Another hypothesis for the reduced adduct formation yield is that the Cy dyes do not only covalently bind to the designated amino acids, but also non-covalently attach to the protein surface via electrostatic interactions. It is easily conceivable that such an attachment could reduce the flexibility of the LOV domain, which yields in a reduced adduct formation. For labeled CrLOV1 A16C this hypothesis can be ruled out since only single-labeled LOV domains were observed in mass spectrometry and the calculated dye to protein ratio is 1:1 correlating with the single labeling site in CrLOV1 A16C. Assuming that CrLOV1 and CrLOV1 A16C have similar surface electrostatics due to their high sequence similarity it seems unlikely that non-covalently bound dyes play a significant role in CrLOV1. We can, however, not exclude completely that CrLOV1 has non-covalently bound Cy dyes attached to its surface.

4.4.5.2 His-tag artifacts

Upon mixing of Cy3- and Cy5-labeled samples CrLOV1 and CrLOV1 A16C both showed FRET at $\lambda = 530\,\text{nm}$ from Cy3 to Cy5 when comparing the Cy3/Cy5 mixtures with Cy3 and Cy5 alone at the same concentration. The effect is more significant for CrLOV1 with $E_{FRET} = 0.33$ than for CrLOV1 A16C with $E_{FRET} = 0.15$. Taking the results of the SEC measurements into account the FRET upon mixing can be explained by a re-equilibration between dimers and higher molecular weight oligomers in the case of CrLOV1 and between dimers and monomers in the case of CrLOV1 A16C. In contrast to RsLOV, no rapid exchange of subunits could be observed, the exchange occurs on the timescale of minutes in both, CrLOV1 and CrLOV1 A16C. Blue light illumination induced significant spectral changes of freshly prepared, 1:1 mixtures of CrLOV1-Cy3/Cy5. Adduct formation of the LOV domains resulted in 30 % FRET. These spectral changes, however, occur only at low concentrations and in fresh mixtures. SEC measurements showed an increase of the

high molecular oligomer fraction upon blue light in unlabeled samples.
CrLOV1 A16C-Cy3/Cy5, on the other hand, did not show any blue light-induced FRET under the tested conditions albeit a dimerization of CrLOV1 A16C upon blue light was observed in SEC on the unlabeled sample.
The critical differences between CrLOV1 and CrLOV1 A16C are the labeling sites of the dyes, the sequence and length of the His-tag and the mutation of the two surface cysteines in CrLOV1 A16C. It is known that His-tags can cause aggregation of proteins, inhibit protein activity or may alter the solubility [174, 176, 177]. But there is only very little knowledge about the mechanisms underlying these interactions between His-tags and target proteins. Carson *et al.* analyzed all crystal structures deposited in the PDB database until 2006 for their His-tag content [174]. They found that until then only approximately 6 % of all crystal structures in the database were crystallized with a His-tag. And in less than 1 % out of these 6 % the secondary structure of the His-tag was determined. Two third of these in total 29 crystal structures showed an unstructured His-tag, but the rest were helical.

Our results on CrLOV1 strongly suggest an impact of the His-tag on the oligomeric state of the LOV domains. CrLOV1 for instance was expressed with an exceptionally long His-tag consisting of 12 His. Our data suggest that this His-tag is responsible for the observed high molecular weight oligomers and also the dimer formation observed in SEC. Expression of the wild type-like CrLOV1-28a with a different His-tag including only 6 His suppressed the formation of the dimers and oligomers. Based on these findings, the FRET of CrLOV1-Cy3/Cy5 also needs to be attributed to the His-tag. Upon mixing of CrLOV1-Cy3 and CrLOV1-Cy5 the sample re-equilibrates between dimers and high molecular weight oligomers on a timescale of minutes. Interestingly, the re-equilibration is accelerated if the LOV domains are excited to the adduct state. The fact that the FRET efficiency is the same with and without blue light illumination indicates that adduct formation accelerates the equilibration of CrLOV1-Cy3/Cy5. This could be due to the conformational changes of CrLOV1 upon adduct formation. It is conceivable that the long His-tag mimics a flanking region like e.g. a Jα or A'α helix. Although CrLOV1 does not have a natural flanking helix, the propensity to influence an extension at the N- or C-terminus might be naturally imprinted in all LOV domains. To proof this hypothesis structure determination of CrLOV1 together with the His-tag via crystallization or NMR would be necessary.

The His-tag extension of CrLOV1 A16C includes 6 His but additionally a fusion partner insertion site. This not very common His-tag sequence also influences the oligomeric state of CrLOV1 A16C. The monomer-dimer equilibrium of CrLOV1 A16C observed in SEC is an artificial effect induced by the His-tag. This is supported by the fact, that no dimers can be observed after removal of the His-tag. Site-specific labeling at A16C apparently reduces the His-tag interactions. The FRET efficiency upon mixing of CrLOV1 A16C-Cy3 and CrLOV1 A16C-Cy5 is decreased by 50 % compared to labeled CrLOV1. Upon blue light illumination no spectral changes indicating FRET could be detected. This indicates that the blue light-induced

dimerization of CrLOV1 A16C is due to an artificial interaction of the His-tag, which is suppressed if Cys16 covalently binds a Cy dye.

In conclusion, the impact of the His-tags on the oligomeric state of CrLOV1 and CrLOV1 A16C is significant. One reason might be that a His-tag sequence of around 20 amino acids corresponds to approximately 20 % of the number of amino acids of a LOV domain. But it is noteworthy that the His-tags produced by the expression vectors His-p2x and pTBSG are not very common. The long His repeat in His-p2x seems to be responsible for the strong aggregation of CrLOV1. In the case of CrLOV1 A16C, only 6 His are repeated in the sequence but the additional fusion partner insertion site might also play a role in the interaction of the His-tag with the LOV core or with itself. The very common His-tag sequence produced by the expression vector pET-28a, however, did not influence the oligomeric state of CrLOV1.

4.4.5.3 CrLOV1 is a monomer in the dark and in the light state

After removal of the His-tag CrLOV1 A16C elutes with a single peak in SEC corresponding to the monomeric molecular weight of CrLOV1 A16C in the dark and under continuous blue light illumination. No blue light-induced changes of the oligomeric state can be observed. Determination of the crystal structure of Phot1-LOV1 of *Arabidopsis thaliana* showed that Cys261 located at the surface of the LOV domain is critical for the dimerization [137]. Cys261 in *A.thaliana* Phot1-LOV1 corresponds to Ser84 in CrLOV1, neighboring Cys83. The substitution of Cys83 with Ser in CrLOV1 A16C removed the potential dimerization site. But also in CrLOV1-28a with Cys83 present only monomers could be observed in SEC.

In summary, our data suggest that CrLOV1 does not act as a dimerization site of CrPhot. This is in line with the results of Fedorov *et al.* They determined the oligomeric state of CrLOV1 to be monomeric in SEC as well as in the crystal structure [76]. Furthermore, full-length CrPhot also elutes as a monomer in SEC in the dark and in the light state suggesting that CrLOV1 does not act as a dimerization site [145, 173]. Recently, a SAXS study on full-length CrPhot proposed that CrLOV1, CrLOV2 and the Ser/Thr kinase are organized in tandem with CrLOV1 and the kinase being located on opposite sides of CrLOV2 [145]. Upon blue light irradiation CrLOV1 moves away and possibly tilts relative to CrLOV2 and the kinase. The authors suggest that CrLOV1 thereby modifies the duration of the light-state of CrLOV2 via the blue light-induced conformational changes of CrPhot and is therefore an amplifier for the kinase photoactivation. CrLOV1 thereby possibly acts as a weight on the photoreaction of CrLOV2 and prevents the conformational change of CrLOV2. A dimerization of CrLOV1 would be in contradiction with the data obtained in this study [145].

This means that the function of CrLOV1 is different from other LOV1 domains of higher plants like e.g. Phot2-LOV1 of *A. thaliana*, which was found to be an attenuator of kinase photoactivation [130]. Although CrLOV1 shares a similarity

with LOV1 domains of higher plants regarding their amino acid sequences, they are divergent regarding the hinge region between LOV1 and LOV2 and the N-terminal extensions [145]. Furthermore, the LOV1 domains of higher plants are proposed to be in a dimeric form in *vivo* [128]. These differences might explain the distinct biological function between CrLOV1 and LOV1 domains of higher plants. Instead of acting as a dimerization site in CrPhot, it has been proposed that CrLOV1 in tandem with CrLOV2 interacts with a so far unidentified partner protein in a light-dependent manner [145].

4.5 Conclusions

We investigated the LOV-LOV interactions of the short LOV domain RsLOV and of Phot CrLOV1 using FRET. In the dark state RsLOV exists as an equilibrium of monomers and dimers. Our FRET experiments revealed that the dark state dimers rapidly exchange their subunits on the second timescale. The monomer-dimer equilibrium is concentration-dependent with $K_D \sim 3.0–7.0\,\mu M$. Upon blue light excitation, RsLOV undergoes adduct formation which is linked to dissociation of the dimers. Our data show that redimerization in the dark occurs on a much slower timescale than adduct recovery. This in turn indicates that the C- and potentially the N-terminal flanking helices undergo conformational changes upon activation of the LOV domain, which might play a role in RsLOV signaling. Reversion of these conformational changes to reconstitute the dimerization surface apparently is slower than conversion of the adduct state.
CrLOV1, on the other hand, did not show any light-induced oligomeric state changes but is a monomer in the dark and in the light state. Initially observed high molecular weight oligomers and dimers can be attributed to artifacts caused by the His-tag and could be eliminated by removing the His-tag. We conclude therefore that CrLOV1 does not act as a dimerization site of full-length Phot.

5 Experimental

5.1 Microbiological methods

5.1.1 Bacterial strains and plasmids

Table 5.1 Genotypes of the bacterial strains used in this work.

***E. coli* strain**	**Genotype**	**Reference**
DH5α	*supE44* Δ*(lacZYA-argF)*U196 (Φ80Δ*lacZM15*) *hsdR17 recA1 endA1 gyrA96 thi-1 relA1*	Woodcock *et al.*, 1989 [178]
BL21(DE3)	F$^-$ *ompT hsdS$_B$(r$_B$$^-m_B$$^-$) gal dem* (λ*Its857 indI Sam7 nin5 lavUV5*-T7*gene1*)	Studier and Moffatt, 1986 [179]

Table 5.2 Plasmids used in this work.

Strain	**Genotype**	**Reference**
His-p2x	Expression vector amp^R, *tac* - promoter, *lac* operator, derived from pMal-p2x: -*malE*, 12 x His - tag (N)	[133]
pET-28a(+)	Expression vector kan^R, T7 promoter, *lac* operator, 6 x His - tag (N), protease thrombin, T7 tag (N)	Novagen
pTBSG	Expression vector amp^R, T7 promoter, *lac* operator, protease TEV, 6 x His - tag (N), derived from pMCSG7 [180]	[175]

5.1.2 Preparation of chemical-competent cells

50 mL Lysogeny-Broth (LB) medium containing 2 % (v/v) Mg^{2+}-mix were inoculated with an *E.coli* overnight starter culture to $OD_{600} = 0.05$ and incubated at 37 °C and 110 rpm until $OD_{600} = 0.5$–0.7. The cells were harvested by centrifugation (15 min, 5000 rpm, 4 °C, Allegra® X–30R, Beckman Coulter, rotor F0850), the cell pellet was resuspended in 50 mL chilled TMF buffer and stored on ice for 1 h. The cells were harvested (15 min, 4000 rpm, 4 °C) and resuspended in a mixture of 4 mL TMF buffer and 1 mL sterile glycerol. Aliquots of 100 µL were frozen in liquid nitrogen and stored at −80 °C.

Mg^{2+}-mix:

500 mM $MgCl_2$
500 mM $MgSO_4$

TMF buffer:

100 mM $CaCl_2$
50 mM $RbCl_2$
40 mM $MnCl_2$

5.1.3 Heat shock transformation

The transformation of *E.coli* bacteria was performed following a modified protocol of [181]. 100 µL chemical-competent *E.coli* cells were thawed on ice and mixed with 1 µL plasmid DNA or 6 µL PCR reaction mix. The competent cell/DNA mixture was placed on ice for 30 min and subsequently heat shocked for 90 s at 42 °C in a heating block. After additional 5 min on ice, 900 µL SOC medium was added and the mixture was incubated for 1 h at 37 °C and 300 rpm. After centrifugation for 2 min at 9700 rpm (5418, Eppendorf, rotor FA-45-18-11), the cells were streaked on LB agar plates containing an appropriate antibiotic and incubated overnight at 37 °C.

5.1.4 Bacteria growth

5.1.4.1 Growth media:

- **Lysogeny-Broth (LB) medium**

1 % (w/v) Tryptone
0.5 % (w/v) Yeast extract
1 % (w/v) NaCl

Solid LB medium for LB agar plates was prepared by adding 1.5 % (w/v) agar to the LB solution. The selective antibiotic Ampicillin ($c = 100\,\mu g/mL$) or Kanamycin ($c = 30\,\mu g/mL$) was added after autoclaving at a temperature of $\leq 50\,°C$.

- **Super Optimal broth with Catabolite repression (SOC) medium**

2 % (w/v) Tryptone
0.5 % (w/v) Yeast extract
10 mM NaCl
2.5 mM KCl
10 mM $MgCl_2$
10 mM $MgSO_4$
20 mM Glucose

5.1.4.2 Growth of *E.coli* liquid cultures

A single colony of transformed *E.coli* cells harboring the respective plasmid from subsection 5.1.3 was used to inoculate a 50 mL LB starter culture containing the appropriate antibiotics. The culture was grown overnight at 37 °C, 120 rpm. This starter culture was used to inoculate a bigger volume of medium for gene induced protein expression.

5.1.4.3 Induced gene expression in *E.coli*

LB medium (30 µg/mL Kanamycin or 100 µg/mL Ampicillin) was inoculated with the starter culture to yield an $OD_{600} = 0.05$. The cell culture was grown at 30 °C, 120 rpm up to an $OD_{600} = 0.4$–0.6. After incubation at 18 °C, 120 rpm for 1 h the protein expression was induced with 0.3 mM isopropylthiogalactoside (IPTG, final concentration). The cells were harvested after 16–17 h at 18 °C, 120 rpm by centrifugation (20 min, 4255 g, 4 °C, Allegra® X - 30R, Beckman Coulter, rotor SX 4400). The cell pellet was resuspended in lysis buffer, frozen in liquid nitrogen and stored at −80 °C.

5.2 Molecular biological methods

5.2.1 Polymerase chain reaction (PCR)

PCR is a technique used to selectively amplify specific DNA fragments in a mixture of DNA molecules *in vitro*. PCR requires a thermostable DNA polymerase, a template DNA for amplification, two complementary oligonucleotide primers, DNA

polymerase buffer and a dNTP (desoxynucleotide triphosphate) mix. All PCR reactions were performed in a gradient PCR cycler (peQSTAR 96 Universal Gradient, peQlab). In this work, PCR was used for site-directed mutagenesis.

5.2.1.1 Site-directed mutagenesis

In order to introduce point mutations in a particular DNA sequence, the PCR reaction mixture in Table 5.3 was prepared and PCR was performed in a PCR cycler according to the program in Table 5.4. The synthetic oligonucleotide primers (see Table 5.5) contain the desired mutation and are complementary to the template DNA neighboring the mutation site. After hybridization with the DNA, the single strand primer is extended using a DNA polymerase. The new double strand DNA then contains the desired mutation and is further amplified. In this work a proofreading *Pfu* DNA polymerase (2.5 U/µL, Thermo Scientific) was used.

Table 5.3 PCR reaction mixture used for site directed mutagenesis.

Component	Concentration / Volume
Pfu buffer+$MgSO_4$	1 x
dNTP mix	0.2 mM
Template DNA	50 pg–1 µg
Primer-s[a]	0.4 pmol/µL
Primer-as[b]	0.4 pmol/µL
Pfu polymerase	2.5 U
bidestilled H_2O	ad 50 µL

[a] s: sense [b] as: anti-sense

Table 5.4 PCR program used for site directed mutagenesis.

#	T/ °C	Time	Step	Number of cycles
1.	95	1 min	initial denaturation	1
2.	95	30 s	denaturation	16 x
3.	T_m−5–10	1 min	primer annealing	16 x
4.	72	2 min/kbp	elongation	16 x
5 .	72	5 min	final elongation	1

Subsequently, the PCR reaction mixtures were digested with the methylation-sensitive restriction endonuclease *Dpn*I (see subsubsection 5.2.1.2) and 6 µL of the digested mixture were transformed in *E.coli* DH5α cells. The transformed cells were grown in

a starter culture overnight (subsubsection 5.1.4.2) followed by isolation of the plasmid DNA (subsection 5.2.4). The results of site-directed mutagenesis were verified via DNA sequencing (SeqLab GmbH).

5.2.1.2 *Dpn*I digestion

2 µL of the PCR reaction mixtures were mixed with 2 µL FastDigest *Dpn*I (Thermo Scientific), 2 µL 10 x FastDigest buffer *Dpn*I (Thermo Scientific) and bidestilled H_2O was added to a final volume of 20 µL. The samples were incubated 5 min at 37 °C.

5.2.2 Oligonucleotides

Synthetic oligonucleotides used for PCR reactions were purchased lyophilized and HPLC purified from Thermo Fisher Scientific GmbH. All oligonucleotides were dissolved in bidestilled water with a final concentration of 10 pmol/µL. The appropriate volume was given by the manufacturer.

Table 5.5 Oligonucleotide primers used for PCR reactions.

Name	**Sequence** (5 → 3)
pMal-CrLOV1 - s [1]	GAAACAGCCAGTCCGTTTAG
pMal-CrLOV1 - as [1]	GCGGGCCTCTTCGCTATTAC
CrLOV1 - F41Y - s	CAGCGAGGGGTATTa[2]TGCCATGAC
CrLOV1 - F41Y - as	GTCATGGCAtAATACCCCTCGCTG
CrLOV1 - C57S - s	GTGCTTGGTCACAACaGCCGCTTCCT
CrLOV1 - C57S - as	AGGAAGCGGCtGTTGTGACCAAGCAC
CrLOV1 - C57A - s	CTTGTTCACAACgcgCGCTTCCTC
CrLOV1 - C57A - as	GAGGAAGCGcgcGTTGTGACCAAG
CrLOV1 - C57G - s	gGCCGCTTCCTCCAAGGCGAGGGCACGGACCCCAA
CrLOV1 - C57G - as	CTTGGAGGAAGCGGCcGTTGTGACCAAGCACCTCATCGG

[1] s: sense primer; as: antisense primer [2] The mutated DNA bases in the specific codons are highlighted by small letters.

5.2.3 Gene synthesis

5.2.3.1 CrLOV1 A16C C32S C83S

The DNA sequence encoding the LOV1 domain (amino acids 16–133) of *C. reinhardtii* phototropin were optimized in codon usage for *E.coli*. The two surface Cys, C32 and C83, were replaced by serins and alanine 16 was mutated to Cys in order to generate a selective labeling site. The sequence was synthesized *de novo* and cloned into the *Nde*I and *Bam*HI site of the expression vector pTBSG in such a way that the protein carries a N-terminal His-tag and a tobacco etch virus (TEV) protease cleavage site. pTBSG is derived from the LIC expression vector pMCBS7 [182]. For further information about the vector see Gao and co-workers [175].

5.2.3.2 RsLOV

The gene encoding RsLOV (*R. sphaeroides* 17025) was synthesized *de novo* by eurofins MWG Operon (Eurofins Genomics GmbH) and cloned into the expression vector pET-28a(+) (Novagen) in frame with the restriction sites *Nde*I and *Eco*RI in such way, that it carries a His-tag and a Thrombin cleavage site at the N-terminus.

5.2.3.3 CrLOV1-28a

The gene encoding CrLOV1 (amino acids 16-133) with the mutation A16C was synthesized *de novo* by eurofins MWG Operon (Eurofins Genomics GmbH) and cloned into the expression vector pET-28a(+) (Novagen) in frame with the restriction sites *Nde*I and *Sal*I in such way, that it carries a N-terminal His-tag and a Thrombin cleavage site.

5.2.4 Isolation of plasmid DNA

Isolation of plasmid DNA was performed using the Roti®-Prep Plasmid MINI kit (Carl Roth GmbH + Co. KG) according to manufacturere's instructions using the supplied buffer solutions with the exception that the DNA was eluted with bidestilled water to a final volume of 50 µL.

5.2.5 Agarose gel electrophoresis

The gel matrix was prepared by adding 1 % (w/v) agarose to 0.5 X TBE buffer. The mixture was heated until the agarose completely dissolved. 0.1 µL ethidium bromide solution was added per mL gel matrix to visualize the DNA under UV light after the electrophoretic separation. The gel matrix was poured into a horizontal gel tray with a well comb in place (agarose gel system: Sub-Cell System, Bio-Rad).
The DNA samples were mixed with 0.1 volumes of 10 x DNA loading buffer and

incubated for 10 min at room temperature prior to loading them on the gel. Electrophoresis was performed at ∼200 V in 0.5 x TBE buffer.

Tris-borate-EDTA (TBE) buffer (pH 8.3):

89 mM Tris-HCl
89 mM boric acid
2.5 mM EDTA

10 x DNA loading buffer:

100 mM EDTA
30 % (v/v) glycerol
1 % (w/v) SDS

Ethidium bromide dye solution:

0.5 % (w/v) ethidium bromide

DNA molecular weight ruler:

"GeneRuler^{TM} 1 kb DNA Ladder", Thermo Fisher Scientific
0.25; 0.5; 0.75; 1.0; 1.5; 2.0; 2.5; 3.0; 3.5; 4.0; 5.0; 6.0; 8.0; 10.0 kb

5.3 Proteinbiochemical methods

5.3.1 Cell lysis and protein extraction

The frozen, resuspended cells obtained from protein expression (see subsubsection 5.1.4.3) were slowly thawed on ice. The cells were disrupted by sonication (permanent sonication, 15 min, 60 % power) using a sonicator (Sonopuls HD 2070 with probe MS73, Bandelin Electronic). An ice-cooled rosett cell was used to guarantee an intense and uniform sonication of the sample. Subsequently the cell debris was collected by centrifugation (20 min, 13682 g, 4 °C, Allegra® X - 30R, Beckman Coulter, rotor F 0850). The supernatant was additionally treated by ultracentrifugation (60 min, 45000 g, 4 °C, Ultracentrifuge TGA, Kontron Instruments, rotor TFT 45.95) and afterwards filtrated (Rotilabo® syringe filters, 0.45 µm, Carl Roth GmbH + Co. KG).

5.3.2 Protein purification via immobilized metal ion affinity chromatography (IMAC)

All proteins used in this work carry a His-tag and are therefore suitable for purification via IMAC. The His-tag interacts specifically with metal ions immobilized on a stationary phase by chelation. IMAC was performed in the dark at 4 °C using gravity flow columns with a bed volume of 49 mL (Liquid Chromatography Columns,

Sigma Aldrich). The columns were equipped with 3–5 mL Ni-NTA (Nitrilotriacetic acid) resin (Ni-NTA Superflow, 50 % suspension in ethanol, Qiagen GmbH). In a first step, the column was equilibrated with a 4-fold bed volume of lysis buffer. All solutions were pumped through the column using a peristaltic pump (ecoline VC-360, Ismatec) in order to generate a continuous flow. After equilibration, the protein solution from subsection 5.3.1 was applied to the column. The immobilized protein on the column was washed with a 10-fold bed volume of washing buffer supplied with 10 mM imidazole. The protein was eluted from the column using a 5-fold bed volume of elution buffer with increasing imidazole concentration (from 100 mM to 500 mM) collecting fractions of 2–3 mL. In order to remove the imidazole, the protein fractions were dialyzed four times against 1 L dialysis buffer in the dark, at 4 °C.

5.3.3 Buffers

For all CrLOV1 proteins sodium phosphate buffers (PB) were used. The proteins were stored in dialysis buffer after the purification process. All the experiments were conducted in dialysis buffer unless indicated otherwise.

Lysis Buffer:

50 mM Na_2HPO_4 (anhydrous)/NaH_2PO_4
300 mM NaCl
pH 8.0

Washing Buffer:

50 mM Na_2HPO_4 (anhydrous)/NaH_2PO_4
300 mM NaCl
10 mM imidazole
pH 8.0

Elution Buffer:

50 mM Na_2HPO_4 (anhydrous)/NaH_2PO_4
300 mM NaCl
100 mM–500 mM imidazole
pH 8.0

Dialysis Buffer:

10 mM Na_2HPO_4 (anhydrous)/NaH_2PO_4
10 mM NaCl
pH 8.0

In the case of RsLOV Tris(hydroxymethyl)aminomethane (Tris)-based buffers were used. RsLOV was stored in the dialysis buffer and the experiments were conducted in the same buffer unless indicated otherwise.

Lysis and Washing Buffer:

50 mM Tris-HCl
300 mM NaCl
10 mM imidzaole
pH 8.5

Elution Buffer:

50 mM Tris-HCl
300 mM NaCl
100 mM–500 mM imidzaole
pH 8.5

Dialysis Buffer:

50 mM Tris-HCl
150 mM NaCl
pH 8.5

5.3.4 His-tag cleavage

5.3.4.1 Thrombin cleavage

The eluted protein was concentrated and treated with Thrombin connected to a His-tag overnight at 4 °C (Thrombin CleanCleave^{TM} Kit, Sigma-Aldrich). The cleaved target protein was separated from uncleaved protein and cleaved His-tag via IMAC, concentrated and stored in dialysis buffer.

5.3.4.2 Tobacco etch virus (TEV) protease cleavage

TEV protease (Sigma-Aldrich) was added to 1–2 mg of target protein at a protease to target protein ratio of 1:100 (w/w). The samples were dialyzed in 25 mM Tris-HCl, pH 8.0, 150 mM NaCl and 14 mM β-mercaptoethanol at 4 °C for 16 hours. The cleaved target protein was separated from uncleaved protein and cleaved His-tag via IMAC, concentrated and stored in PB, pH 8.0.

5.3.5 Sodium dodecyl sulfate polyacrylamide gel electrophoresis (SDS-PAGE)

Protein separation via SDS-PAGE was performed under denaturing conditions with a discontinuous gel system according to a modified protocol of Laemmli [183]. For electrophoresis a 4 % stacking gel and a 15 % separation gel (the composition of the gels is described below) were prepared and placed into a vertical electrophoresis system (Twin S, PeqLab). The samples were mixed with SDS sample buffer and denatured at 99 °C for 10 min. The samples were loaded onto the gel with a volume

of 15 µL per pocket. Electrophoresis was performed at 150–200 V until the tracking dye reached the bottom of the gel. Following electrophoresis, the gels were stained with Coomassie Brilliant Blue for 1 h at room temperature with gentle shaking and afterwards washed with H_2O. For documentation the gels were visualized using a gel documentation system (Quantity One Version 4.0.3, Bio-Rad).

- **10 x SDS sample buffer:**
  0.5 M Tris-HCl (pH 8.8)
  23 % (v/v) glycerol
  10 % (w/v) SDS
  1 M dithiotreitol (DTT)
  0.1 % (w/v) bromophenol blue
- **Acrylamide gels:**
  1.5 M/0.5 M Tris-HCl pH 8.8/pH 6.8 (separating gel/stacking gel)
  0.1 % (w/v) SDS
  15 %/4 % acrylamide/bisacryamide (29:1) (separating gel/stacking gel)
- **5 x SDS-PAGE buffer:**
  0.12 M Tris-HCl (pH 8.3)
  1 M glycerol
  0.5 % (w/v) SDS
- **Coomassie Brilliant Blue Staining:**
  0.12 % (w/v) Coomassie Brilliant Blue
  10 % (w/v) ammonium sulfate
  10 % (v/v) 85 % phosphoric acid
  20 % (v/v) methanol
- **Molecular weight standard**
  Protein-Marker I, VWR Peqlab
  14.4, 18.4, 25.0, 35.0, 45.0, 66.2, 116.0 kDa

5.3.6 Size exclusion chromatography (SEC)

SEC was performed using an ÄKTA purifier column chromatography system with two different colums: a Superdex 200 26/60 and a Superdex 75 10/300 (all from GE Healthcare). The first column was used for measurements at a concentration of 7 µM, the second one for those at 50 µM and 100 µM. Potassium phosphate buffer (50 mM potassium phophate, 300 mM KCl, pH 7.5) was used for all SEC runs. For dark state measurements, the protein samples were incubated in the dark overnight at 4 °C and aliquots of 2 mL with a concentration of 7 µM or of 250 µL with a concentration of 50 µM or 100 µM were injected to the column. For light state measurements the protein samples were illuminated with blue light for 1 min prior to injection and the column was continuously illuminated with two blue LEDs (Luxeon III emitter LXHL-PBO9, Philips, 300 mW at 460 nm) during the measurement.

The absorbance of the eluted samples was measured at 280 nm. The Superdex 200 column was calibrated with a marker kit for protein molecular weights (*MWGF200*, Sigma Aldrich) including cytochrome c (12.4 kDa), carbonic anhydrase (29 kDa), albumin (66 kDa) and alcohol dehydrogenase (150 kDa). The Superdex 75 was calibrated using a low molecular weight calibration kit (Gel Filtration Calibration LMW, GE Healthcare) including aprotinin (6.5 kDa), ribonuclease A (13.7 kDa), carbonic anhydrase (29.0 kDa), ovalbumin (43.0 kDa) and conalbumin (75 kDa).

5.3.7 Labeling with the cyanine dyes Cy3 and Cy5

5.3.7.1 Labeling with Cy3/Cy5 maleimide ester

To minimize oxidation of thiols, the buffers used for the labeling reaction were degassed using argon. The protein solutions were gently degassed by dialysis against degassed buffer to prevent precipitation of the protein. All steps during the labeling reaction were carried out under argon. Proteins to be conjugated were dissolved in PB (10 mM sodium phosphate, 10 mM NaCl, pH 7.2) at a concentration of 1 mg/mL. The protein solutions were left for 30 min at room temperature. A 100 molar excess of tris - (2-carboxyl) phosphine (TCEP) was added to reduce the protein prior to labeling. The solution was mixed thoroughly and incubated for 10 min at room temperature. The dye solutions were prepared by adding 50 µL anhydrous dimethyformamide (DMF) to one pack of either Cy3 or Cy5 maleimide ester (GE Healthcare). The dye solution was added to the reduced protein solution, mixed and incubated at room temperature for two hours with additional mixing every 30 min. The protein/dye mix was further incubated over night at 4 °C.
The labeled proteins were separated from the excess, unconjugated dye by gel permeation chromatography using PD-10 columns (Econo-Pac 10DG columns, Bio-Rad). The columns were equlibrated with PB (10 mM Sodium Phosphate, 10 mM NaCl, 0.01 % NaN_3, pH 8.0) and the labeled proteins were eluted using the same buffer. The proteins were purified further by dialysis. The success of the labeling reaction was checked via mass spectrometry.

5.3.7.2 Labeling with Cy3/Cy5 N-Hydroxysuccinimide (NHS) ester

Proteins to be conjugated were dissolved in 0.1 M sodium carbonate buffer (pH 9.3) at a concentration of 1 mg/mL. 1 mL of the protein solution was added to one vial of either Cy3 or Cy5 NHS ester and the solution was mixed thoroughly. The protein/dye mixture was incubated for 30 min at room temperature with additional mixing every 10 min. The protein/dye mix was further incubated over night at 4 °C. Purification and removal of excess dye were performed in an identical way like described for labeling with maleimide esters.

5.4 Chemicals

Alfa Aesar:

Nickel(II) chloride hexahydrate, 98 %

AppliChem Panreac:

Sodium dodecyl sulfate (SDS), ultrapure

Becton, Dickinson and Company:

Bacto-Agar (Pancreatic Digest of Casein)
Bacto-Tryptone
Bacto-Yeast-Extract (Extract of Autolysed Yeast)

Carl Roth:

Agarose, Roti®garose, NEEO ultra-quality
Boric acid, ≧ 99.8 %
Bromophenol blue, for electrophoresis
Ethidium bromide, ≧ 98 %
Isopropyl-β-D-1-thiogalactopyranoside (IPTG), ≧ 99 %
Kanamycin, ≧ 750 I.E./mg
L-Tryptophane, ≧ 98.5 %
N,N,N',N'-Tetramethylethyleendiamine (TEMED), 99 %
Tris-(2-carboxyethyl)-phosphine (TCEP), ≧ 98 %

Fluka BioChemika:

Riboflavin 5'-monophosphate sodium salt hydrate, 85 % HPLC grade

GE Healthcare:

Cy™5 Maleimide Mono-reactive Dye
Cy™3 Maleimide Mono-reactive Dye
Cy™5 Mono-reactive Dye
Cy™3 Mono-reactive Dye
Gel filtration Calibration LMW kit

peqLab Biotechnologie:

peqGold Protein-Marker I

Qiagen:

Ni-NTA Superflow (50 % suspension)

Sigma-Aldrich:

Acrylamide/ Bis-acrylamide (29:1)
Ampicillin sodium salt, ≧ 91 %
Dialysis tubes, cellulose, size: 23 mm, cut-off: ≧ 12400 Da
Dimethyl sulfoxide (DMSO), ≧ 99.9 %

Ethylenediaminetetraacetic acid (EDTA), 95 %
HEPES, ≧ 99.5 %
Imidazole, ≧ 99 %
MWGF200 marker kit
Sodium azide, ≧ 99.5 %
L-Tyrosine, ≧ 98 %
Rubidium chloride, ≧ 99 %

Thermo Fisher Scientific:

10 x *Pfu* Puffer with 20 mM $MgSO_4$
10 mM dNTP mix
*Dpn*I, 10 U[1]/µL
GeneRuler™ 1 kb DNA Ladder, 0.5 µg/µL
Pfu DNA Polymerase, 2.5 U/µL

USB Corporation

Tris(hydroxymethyl)aminomethane (Tris), analytical grade

VWR Chemicals:

NaCl, analytical grade

All other chemicals were purchased from Merck.

5.5 Spectroscopy

5.5.1 UV/Vis absorption spectroscopy

UV/Vis spectra were recorded with a Lambda 9a spectrometer (Perkin Elmer) at 20 °C in a temperature-controlled cuvette holder. For adduct recovery kinetics the samples were irradiated for 500 ms with two intense blue light LEDs (Luxeon III emitter LXHL-PBO9, Philips, 300 mW at 460 nm) orthogonal to the optical path of the spectrometer. Kinetic traces were recorded at 475 nm in the dark after blue light illumination.

5.5.2 Transient absorption (TA) spectroscopy

Transient absorption spectroscopy in the µs-timerange was performed with a streak camera setup (C7700, Hamamatsu Photonics). The samples were excited at 447 nm via an OPO pumped by a Nd:YAG laser (Surelite II, Continuum) with a pulse width of 8 ns. The pulse energy was adjusted to be 8–10 mJ per pulse in front of the cuvette. A fused silica flow cuvette with 2 mm optical path length for excitation and

[1] unit of the enzyme activity. 1 U = 1 enzymatic Unit. One U is defined as the amount of the enzyme that catalyzes the conversion of 1 µmol of substrate per minute [184].

10 mm path length for probe light was used. The samples were pumped through the cuvette during the measurement using a peristaltic pump (LKB Pump P-1, Pharmacia Biosystems) in order to exchange the sample volume between two excitation cycles. The overall sample volume per measurement was around 10 mL with an optical density of approximately 0.5 at 450 nm. Each measurement was performed as a sequence of 100 excitation cycles with one cycle consisting of four individual streak images: $I_{L,P}$, I_D, I_P, I_D. With $I_{L,P}$ being an image with laser and probe light on, I_D being the dark spectrum and I_P referring to probe light on only.

The 2D TA data were analyzed by global lifetime analysis with the following model:

$$\Delta A(t,\lambda) = \left(D_0(\lambda)\delta(t) + \sum_{j=1}^{N} D_j(\lambda)\exp(-\kappa_j t) \right) \otimes g_{app}(t - t_0)$$

where $\otimes g_{app}(t-t_0)$ indicates convolution with the apparatus function approximated by a Gaussian, $\delta(t)$ is the Dirac delta function, and N is the number of decay components considered. The result of this fit are the rate constants $\kappa_j = 1/\tau_j$ and the corresponding decay associated difference spectra (DADS) $D_j(\lambda)$. The spectrum $D_0(\lambda)$ accounts for the contribution of fluorescence and scattered laser light. These contributions are not resolved. Further details about the setup and data analysis are described in Kutta *et al.* [185].

5.5.2.1 Spectral fitting of DADS

Spectral fitting of the D_2 of *Cr*LOV1-F41Y, *Cr*LOV1-F41Y/C57A and *Cr*LOV1-F41Y/C57S was performed using a least-square algorithm without any constraints. A linear combination of the reference spectra FMNox, $FMNH^{\bullet}$, $FMN^{\bullet-}$ and $TyrO^{\bullet}$ was used to calculate the model spectra and the coefficients were optimized.

The reference spectrum of $FMNH^{\bullet}$ was generated in a steady-state illumination experiment of a 40 μM solution of *Cr*LOV1 C57G in the presence of 10 mM β-mercaptoethanol (BME) in 10 mM sodium phosphate buffer (10 mM NaCl, pH 8.0). The solution was dialyzed against degassed buffer prior to illumination in order to remove the oxygen. This *Cr*LOV1 C57G sample was illuminated with two blue LEDs (Luxeon III emitter, LXHL-PB09, Philips, 300 mW at 460 nm) and spectral changes were monitored via UV/Vis until the spectrum stayed constant. In order to obtain the difference spectrum, the ground state spectrum, FMNox, was subtracted. This is possible since the relative amplitudes of both spectra are known from the isosbestic point at 500 nm.

The reference spectrum of $FMN^{\bullet-}$ minus FMNox was generated by flash photolysis of a 40 μM solution of *Cr*LOV1 C57S in the presence of 10 mM BME and oxygen in 10 mM sodium phosphate buffer (10 mM NaCl, pH 8.0). It is known that under these conditions the long-lived DADS ($\tau \gg 500\,\mu$s) is the SADS (species associated difference spectrum) of the FMN radical anion [47].

For the reference spectrum of $TyrO^{\bullet}$, FMN was dissolved in 10 mM sodium phosphate buffer, pH 8.0 supplemented with 10 mM NaCl at a concentration of 40 μM, resulting in an optical density of 0.5 at 450 nm. To this solution either L-Tyr or L-Cys was added at a concentration of 100 mM. TA was measured on a 20 μs (Tyr) or on a 10 μs (Cys) time window. The difference spectrum of the $TyrO^{\bullet}$ radical was thus obtained as the difference of the spectra from the Tyr and Cys experiments, scaled to the same ground state bleach of FMNox at 450 nm.

5.5.3 Time-correlated single photon counting (TCSPC)

The fluorescence lifetimes of the excited S_1 states were determined by TCSPC with a time resolution in the ns-range at room temperature. The samples were excited at 443 nm or at 280 nm with pulsed LEDs (NanoLED-450 or NanoLED-280, Horiba Jobin Yvon, $\lambda_{max} = 443$ nm, FDHM = 1.1 ns, FWHM = 27 nm, $\omega = 100$ KHz) and the emission was observed in a 90° geometry relative to the excitation path at 495 nm with a photomultiplier tube (PMT). The electronic signal was processed digitally resulting in histograms representing the fluorescence decay curves of the samples. The response function of the LED was detected separately at 450 nm or 280 nm close to λ_{max}.

Analysis of TCSPC data:
The duration of the excitation pulse of the LED cannot be neglected when determining fluorescence lifetimes in the ns time-range via TCSPC. Therefore, the measured data correspond to the fluorescence decay function, *f(t)*, convoluted with the response function of the LED, *g(t)*.

$$f(t) = \int_{-\infty}^{t} g(t')\, f_{model}\,(t - t')\, dt' = \sum_{i=1}^{N} A_i \int_{-\infty}^{t} g(t') \exp\left(-k_i(t - t')\right) dt' \qquad (5.1)$$

Analysis of these data was performed using home-written software, which uses a sum of N exponential functions as model function $f_{model}(t)$. The square deviation between *f(t)* and the data is minimized, taking the experimental instrument response for *g(t)*. The program makes efficient use of the fact that all data points are equidistant. The results of the fit are amplitudes A_i and rate constants k_i.
The fluorescence lifetimes of CrLOV1-Cy3 and CrLOV1-Cy5 were determined by analyzing the data with a maximum entropy method. Also for this analysis, the response function of the LED was used as response function. The maximum entropy analysis yielded a distribution function with the rate constant, k, plotted versus the probability of k with two well separated peaks in each case. The maximum values of these peaks (with logarithmic scale of k) correspond to the fluorescence rate constants of CrLOV1-Cy3 and CrLOV1-Cy5, respectively. The fluorescence lifetimes are the inverse rate constants. The fraction of the components were calculated via the ratio of the integrals of the peaks.

The fluorescence lifetimes of the F41Y mutants and labeled and unlabeled RsLOV (described in chapter 2 and 4) were determined at room temperature via TCSPC using a different system - the PicoHarp 300 system (PicoQuant) - because a higher time resolution was required. The samples were excited at 378 nm with a pulsed laser diode (Pico Brite, Horiba Scientific, PB-375L $\pm$ 7 nm, $\lambda_{max} = 378$ nm, pulse width < 100 ps, $\omega = 2$ MHz). Emission was detected at 510 nm in a 90 ° geometry relative to the excitation path with a photomultiplier tube. The response function of the excitation source (IRF) was detected separately at 376 nm. Data analysis was performed with the FluoFit software version 4.5 (PicoQuant) using an exponential model with reconvolution for compensating IRF effects.

5.5.4 Determination of fluorescence quantum yields, Φ_F

Measurements of the fluorescence quantum yields, Φ_F, at room temperatures were performed with a C9920-02 (Hamamatsu Photonics) integrating sphere system with an error of ± 5 %. The samples were excited at $\lambda_{exc} = 450$ nm.

5.5.5 Emission measurements

Emission spectra of the Cy3/Cy5 labeled LOV domains were measured using a setup consisting of two LEDs for excitation of the samples and an imaging spectrograph with a 300 lines/mm grating (Newport, Oriel MS 260i) coupled to a CCD camera (Andor Technology, DB401-UV) as detection unit. For excitation a green and a blue LED was available (Alustar, 1 W, 3 °, Edison Ledxons with $\lambda_{max} = 470$ nm and $\lambda_{max} = 525$ nm), for either exciting the Cy3 dye or the FMN chromophore. Bandpass filters were adjusted in front of each LED to achieve a reduced FWHM (FB 430-10, center wavelength $\lambda = 430$ nm, FWHM 10 ± 2 nm and FB 530-10, center wavelength $\lambda = 530$ nm FWHM 10 ± 2 nm, Thorlabs). Emission spectra were recorded at room temperature either as steady-state or as time-resolved spectra, with a ms to s time resolution.

5.5.6 Stopped-flow measurements

Stopped-flow measurements of RsLOV-Cy3/Cy5 were performed with the SX20 system from Applied Photophysics. The samples were excited at 540 nm with a 150 W Xe-Lamp coupled to a monochromator. RsLOV-Cy3 and RsLOV-Cy5 were prepared with a flavin concentration of 0.5 µM. The samples were mixed in a 1:1 ratio in the mixing chamber to yield a total volume of 400 µL. The emission was detected either at 595 nm for Cy3 emission or at 690 nm for Cy5 emission with a PMT. For each detection channel a bandpass filter was adjusted in front of the PMT (Cy3 emission: ET595/50, CWL: 595 nm, FWHM: 50 nm and Cy5 emission: ET690/50, CWL: 50 nm, FWHM: 50 nm, both purchased from Chroma Technology Corp). The

time-resolution of the experiment was 7 ms. The data were collected with the Pro-Data SX software (Applied Photophysics).

5.6 Theoretical methods

This section refers to the theoretical methods used in chapter 2. They were performed by Ivan Stambolic.

5.6.1 Modeling

For protein structure predictions MODELLER version 9.11 software package [186] was used, employing homology modelling method (comparative modelling). The model of each mutant has been generated based on the crystal structure of native CrLOV1 (pdb code: 1N9L, determined by Fedorov *et al.* [76]), with required point mutations: F41Y, F41Y/C57A, F41Y/C57S and F41Y/C57G.

5.6.2 Molecular dynamics (MD) simulations

To resolve the behavior of *Cr*LOV and its mutants at a molecular level, MD trajectories were generated using the GROMACS version 4.6.5 software package with the GROMOS 96-43a1 forcefield [187]. This forcefield has been shown to reliably reproduce experimental results on various protein-solution systems [188, 189]. For the simulations full particle-mesh-Ewald (PME) electrostatics were used with a Coulomb cutoff of 0.9 nm. Van der Waals interactions were computed with a cutoff of 1.4 nm. Proteins were put in a cubic box with the distance between the edge of the box and closest protein atom set to 1.0 nm. To neutralize the system, 2 sodium ions were placed at random positions within the cubic box. The systems were equilibrated for 5 ns using the NPT ensemble at 300 K and 1 bar, where all parts of the system were coupled to the Nosé-Hoover-thermostat and the Parrinello-Rahman barostat [190]. Following the equilibration phase, a production run of 20 ns non-invasive thermostating [191] was performed in which the protein and the FMN were decoupled from the thermostat, while the solvent and ions remained coupled. The non-invasive method allows the protein to follow its natural dynamics and sample configurations which are far from the equilibrium. For the numerical integration of the equations of motion, we have used the Leap-frog integrator with a timestep of 2 fs.

6 Summary

Light-, oxygen-, voltage-sensitive domains act as the photosensory units of a great number of organisms in nature. The absorption of blue light by their FMN chromophore constitutes the primary event of the photoreceptor activation. The light trigger is transduced into a physiological signal and is propagated downstream to effector domains or induces interactions with signaling partners.
This thesis is focused on two aspects of LOV domains. The first two chapters deal with the photochemistry of the flavin chromophore upon light excitation. The main emphasis thereby lies on the design of LOV mutants with a modified flavin reactivity towards electron transfer reactions. This not only contributes to the fundamental understanding of the factors which control the photochemistry of flavin blue light sensors, but might also lead to the development of novel applications of LOV domains. The second part of this thesis focuses on the intermolecular interactions of LOV domains which are thought to be directly linked to the signaling pathway of LOV domains. In the following an overview of the results is given in the scope of this thesis. It is noted that parts of these summaries are extracted from the abstracts of [31, 192]

Electron transfer in mutated LOV domains of *C. reinhardtii*

Adduct formation as the primary activation step is strictly conserved among LOV domains. While the reaction mechanisms of the flavin blue light photoreceptors cryptochrome and BLUF implicate electron transfer reactions, no other photoreaction than adduct formation has been reported for LOV domains.

In chapter 2 the question was addressed whether the reaction type of flavin in a LOV domain can be influenced by the introduction of the electron donor Tyr. Therefore, the LOV1 domain of *C. reinhardtii* was used as a template and Phe41 was substituted with Tyr. The mutation did not significantly alter the electronic properties of FMN nor the structure of the protein. Adduct formation, however, cannot be observed in CrLOV1 F41Y although the reactive Cys is present. Instead, electron transfer accompanied by proton transfer occurs from the introduced Tyr to FMN, most likely suppressing covalent bond formation between Cys57 and FMN. For comparison, the reactive Cys was additionally mutated to Ser and Ala. Excitation of these mutants also results in the photoreduction of FMN similar to CrLOV1 F41Y corroborating the role of Tyr41 to act as an electron donor. The electron transfer can occur either via the excited singlet state or, as a competitive reaction, follow

the triplet pathway. In any case, protonation is essential for the radical stability exemplified by CrLOV1 F41Y/C57G. This mutant lacks a suitable proton donor and as a consequence, no stabilized radicals can be observed.
On the one hand, our results obtained for CrLOV1 F41Y have implications for the adduct mechanism of the wild type strongly hinting towards the radical-pair mechanism. On the other hand, this photoreductive pathway resembles the flavin photoreactivity observed in other photoreceptors, e.g. BLUF domains or cryptochromes. These proteins are increasingly used as templates for optogenetic tools and reporter proteins. Identifying key parameters to engineer the flavin photoreactivity in a protein environment contributes significantly to this development.

Reengineering the flavin photochemistry in iLOV

It has long been assumed that adduct formation is absolutely essential for signaling of LOV domains. But recently, it has been shown that LOV photoreceptor variants devoid of the photo-active cysteine can elicit a functional response upon light irradiation. Thereby, photoreduction of the flavin chromophore to the neutral semiquinone is sufficient for signal transduction, suggesting that signaling hinges only on flavin protonation, which is a feature of both the native flavin-cysteine adduct and the neutral semiquinone. LOV domains lacking the reactive cysteine are usually non-photoreducible under aerobic conditions and in the absence of external electron donors.

In chapter 3, the flavin photochemistry of iLOV was reengineered towards efficient photoreduction under aerobic conditions. The naturally non-photoreducible and photo-inactive iLOV protein was chosen as a target protein. Following a rational approach, Q489 was substituted by an aspartate residue in iLOV in order to introduce a proton donating functional group in the vicinity of the flavin chromophore. In contrast to parental iLOV, the mutant iLOV Q489D showed efficient photoreduction upon blue light irradiation. The resulting flavin neutral semiquinone radical, $FMNH^{\bullet}$, is remarkably long-lived. The proton transfer of D489 to the flavin is essential for this stability. Efficient photoreduction can be observed in a pH range from 3 to 9 due to a pK_a shift of D489 from 3.9 for free aspartate to over 6.0 in iLOV. MD simulations showed that iLOV is still (at least partially) protonated at pH 7.0. Transient absorption spectroscopy revealed that $FMNH^{\bullet}$ is formed via the excited triplet state. The counter-radical could be identified to be the only Trp, W467. The presence of a stable radical pair in iLOV Q489D is corroborated by EPR spectroscopy at low temperatures. Interestingly, the EPR data also indicate the presence of a radical pair in parental iLOV, but only at 77 K and with a lower amplitude than observed for iLOV Q489D. A mutational approach implies that multiple Trp/Tyr residues can participate in the electron transfer pathway of iLOV Q489D. Substitution of Tyr416, Tyr459 or Tyr484 by redox-inert Phe does not change the photoreduction yield in iLOV Q489D. On the other hand, a significant reduction can be observed for iLOV Q489D W467F. In this case, a Tyr constitutes the counter-radical of $FMNH^{\bullet}$

replacing the actual electron donor W467 in iLOV Q489D.
The results on iLOV Q489D provide strong evidence that a Trp residue, which is highly conserved in all LOV proteins, constitutes the electron donor for flavin photoreduction. But also highly conserved tyrosine residues could act as electron donors in iLOV Q489D although with less efficiency compared to the Trp. This suggests that the propensity for photoreduction is evolutionary imprinted in all LOV domains. These findings highlight the possibility that todays' adduct-forming LOV photoreceptors evolutionary derive from ancestral redox-active flavoproteins.

Investigation of the intermolecular interactions of LOV domains

LOV-LOV interactions are thought to be directly linked to the biological function of LOV-harboring proteins. In chapter 4, size exclusion chromatography and FRET-based fluorescence spectroscopy were used as tools to investigate interdomain interactions of the short LOV domain from *R. sphaeroides* and the LOV1 domain from CrPhot. The LOV domains were labeled with the fluorescent dyes Cy3 and Cy5, respectively. Both dyes did not only interact with each other to form a FRET pair but also with the FMN chromophore of the LOV domains. A high FRET efficiency could be calculated for the pairs FMN-Cy3 and FMN-Cy5. As a consequence, the adduct formation yield of the labeled LOV domains was reduced.

RsLOV exists as a mixture of monomers and dimers in the dark state. Upon blue light, the equilibrium shifts to monomers only. FRET measurements of dark-state RsLOV revealed that the monomers and dimers exchange rapidly on the second timescale. Concentration-dependent measurements allowed to determine the dissociation constant, K_D, to be around 3 µM. Upon blue light excitation, RsLOV forms the adduct state. Concomitantly, conformational changes of the flanking HTH-motif and/or the aα-helix occur. Our FRET measurements showed, that recovery of the adduct state occurs on a faster timescale than reversion of the conformational changes. This finding has implications for the signaling mechanism of RsLOV. The light-state conformation of RsLOV, which potentially interacts with a signaling partner, is prolonged beyond the lifetime of the adduct.

The second part of chapter 4 addresses the question whether CrLOV1 acts as a dimerization site of CrPhot. According to our SEC measurements, CrLOV1 exists as a mixture of dimers and high molecular weight oligomers in solution. Upon light excitation, the equilibrium shifts to higher molecular weights. This behavior could be confirmed in the emission measurements of CrLOV1-Cy3/Cy5 mixtures in the form of blue light-induced FRET. This effect could, however, only be observed at low concentrations and in freshly prepared samples. Further investigations with CrLOV1 A16C, a mutant with a selective labeling site at the N-terminus, showed a different behavior. Unlabeled CrLOV1 A16C eluted as a concentration-dependent mixture of monomers and dimers in SEC. Upon blue light, the equilibrium shifted to the dimeric side. On the other hand, emission measurements of CrLOV1 A16C-Cy3/Cy5 did

not show any blue light-induced FRET. The contradictory results of CrLOV1 and CrLOV1 A16C could be explained by artificial interactions caused by the His-tags. CrLOV1 and CrLOV1 A16C were expressed with different and uncommon vectors resulting in very long and unusual His-tag sequences. Removal of the His-tags or substitution with commonly used His-tag sequences resulted in monomeric CrLOV1 in the dark and in the light state. This strongly suggests that the LOV1 domain does not act as a dimerization site of Phot from *C. reinhardtii*. Interestingly, the His-tag of CrLOV1, including 12 His, induced artificial oligomeric state changes upon blue light excitation. This indicates that the ability to influence flanking regions - even artificial ones - connected to the LOV core might be an intrinsic property of all LOV domains.

A Appendix

A.1 Singular value decomposition (SVD) and deconvolution of time sequences of the steady-state UV/Vis spectra of iLOV-Q489D at pH 7.2

The data from bleaching and recovery experiments consist of a sequence of spectra measured at different times. These data were arranged into a matrix **D** of size N by M (with M≤N) and analyzed by singular value decomposition (SVD),

$$\boldsymbol{D} = \mathbf{U}\mathbf{W}\mathbf{V}^{\dagger} = \sum_{k=1}^{M} \mathbf{u}^{(k)} w_k \mathbf{v}^{(k)\dagger} \tag{A.1}$$

Here, the orthogonal and normalized vectors **u** and **v** are the columns of the matrices **U** and **V** and form a basis in the space of spectra and concentration time profiles, respectively. $\mathbf{V}^{\dagger}$ indicates a transposed matrix, $\mathbf{v}^{\dagger}$ a row-vector. The matrix elements w_k of the diagonal matrix **W** are positive and arranged in descending order. Subsequently, a sequence of approximations $\mathbf{A}^{(K)}$ to the data matrix is formed

$$\mathbf{A}^{(K)} = \sum_{k=1}^{K} \mathbf{u}^{(k)} w_k \mathbf{v}^{(k)\dagger} \; ; \; K = 1, 2, 3... \tag{A.2}$$

and compared to the original data matrix

$$\sigma^{(K)} = \sqrt{\|\mathbf{D} - \mathbf{A}^{(K)}\|/NM} \tag{A.3}$$

A plot of $\sigma^{(K)}$ vs K indicates how many components K make a significant contribution to the data. In all our experiments we found K = 2, with the third components contributing less than 1 % of the first two.
The reduced data matrix $\mathbf{A}^{(2)}$ was then decomposed into the product of two spectra and two concentration time profiles,

$$\mathbf{A^{(2)}} = \mathbf{S}\mathbf{C}^{\dagger} = \mathbf{U}\mathbf{W^{(2)}}\mathbf{X}\mathbf{Y}\mathbf{V}^{\dagger} \tag{A.4}$$

Here, $\mathbf{S}$ is a matrix with two columns containing the species spectra, $\mathbf{C}$ is a matrix with two columns containing the concentration-time profiles of the two species, $\mathbf{W}^{(2)}$ contains only the first two diagonal elements of the matrix $\mathbf{W}$, and $\mathbf{X}$ and $\mathbf{Y}$ are 2x2 matrices with $\mathbf{XY} = \mathbf{1}$. Since only one species (i.e. the neutral radical) absorbs at 615 nm, we take the corresponding row of $\mathbf{A}^{(2)}$ as the concentration profile of this species, i.e.

$$\mathbf{c^{(2)}} = \alpha \mathbf{A}^{(2)}(\lambda_{615}, t) \tag{A.5}$$

Were α is a scaling factor that determines the yield of the reaction at the final time. The concentration of the other species (i.e. the oxidized flavin) is defined by $c^{(1)} + c^{(2)} = 1$. The matrix $\mathbf{Y}$ is then calculated according to

$$\mathbf{C}^{\dagger} = \mathbf{Y}\mathbf{V}^{\dagger} \rightarrow \mathbf{Y} = \mathbf{C}^{\dagger}\mathbf{V} \tag{A.6}$$

due to the orthogonality of the matrix $\mathbf{V}$. Inversion of $\mathbf{Y}$ gives the matrix $\mathbf{X}$ and the species spectra according to

$$\mathbf{S} = \mathbf{U}\mathbf{W^{(2)}}\mathbf{X} \tag{A.7}$$

The only adjustable parameter in this procedure is the scaling factor α. If α is too small, the calculated spectrum of species 2 will have negative intensity in the region of strong absorption of species 1, if α is too large, the peaks of species 1 will also appear in the spectrum of species 2.

A.2 Model for the dimerization of RsLOV

The model described here was used to determine the dissociation constant, K_D, of RsLOV. The corresponding data are shown in chapter 4, Figure 4.3.10.

We consider a system composed of donor-labeled LOV domains (D), acceptor-labeled LOV domains (A) and unlabeled LOV domains (N). The total concentrations of these units in the samples are c_D, c_A and c_N, and the total concentration of all LOV domains is $c_0 = c_D + c_A + c_N$. Species of the same kind can form dimers with the equilibrium constant K:

$$K = \frac{[\mathrm{D}]^2}{[\mathrm{DD}]} = \frac{[\mathrm{A}]^2}{[\mathrm{AA}]} = \frac{[\mathrm{N}]^2}{[\mathrm{NN}]} \tag{A.8}$$

where [D] is the concentration of donor-labeled monomers, [DD] the concentration of dimers consisting of donor-labeled RsLOV, and so on. We assume that the label does not influence the dimerization mechanism. The corresponding equilibrium constants for mixed dimers are then

$$\frac{K}{2} = \frac{[\mathrm{D}][\mathrm{A}]}{[\mathrm{DA}]} = \frac{[\mathrm{N}][\mathrm{A}]}{[\mathrm{NA}]} = \frac{[\mathrm{N}][\mathrm{D}]}{[\mathrm{ND}]} \tag{A.9}$$

The factor 1/2 in Equation A.9 ensures that in a mixture with equal amounts of [A] and [D] the concentration [AD] is twice that of [DD], as required by combinatorial statistics. The concentrations of these monomers and dimers are related to the total concentrations of LOV units by:

$$\begin{aligned} c_A &= 2[\mathrm{AA}] + [\mathrm{A}] + [\mathrm{NA}] + [\mathrm{DA}] \\ c_D &= 2[\mathrm{DD}] + [\mathrm{D}] + [\mathrm{ND}] + [\mathrm{DA}] \\ c_N &= 2[\mathrm{NN}] + [\mathrm{N}] + [\mathrm{ND}] + [\mathrm{NA}] \end{aligned} \tag{A.10}$$

Equation A.8-A.10 are 9 equations that can be solved for the 9 unknown concentrations [N], [A],... in terms of the total concentrations c_D, c_A and c_N.

As a reference system we consider a sample that contains only donor-labeled and unlabeled LOV domains with total concentrations c'_D and c'_N. We assume that all donor units in monomers or dimers not containing an acceptor yield fluorescence with the same quantum yield, Φ_D, whereas in the mixed dimers DA the quantum yield is $\Phi_D(1\text{-}E)$, where E is the FRET efficiency. The fluorescence intensity following excitation into the donor absorption band is then for each sample:

$$F = \Phi_D \, (c_D - E[\mathrm{DA}]) \tag{A.11}$$

$$F' = \Phi_D \, c'_D \tag{A.12}$$

When the reference sample is prepared such that $c_D = c\,'_D$, the relative change in donor emission in the mixture is

$$S = \frac{F' - F}{F'} = E[\mathrm{DA}] = \frac{E c_A}{4\, c_0} \left(\frac{K}{c_0} - \sqrt{\frac{K}{c_0} \left(\frac{K}{c_0} + 8 \right)} + 4 \right) \tag{A.13}$$

A fit of Equation A.13 to the data $S(c_0)$ in chapter 4, Figure 4.3.10 yields the equilibrium constant K and the amplitude $\mathrm{E}c_A/c_0$. In chapter 4, Figure 4.3.10, K is referred to as the dissociation constant K_D, Ec_A/c_0 as $\mathrm{E_{FRET}max}$ and $E[\mathrm{AD}]$ as $\mathrm{E_{FRET}}$. Equation A.13 is hence expressed as:

$$\mathrm{E_{FRET}} = \frac{\mathrm{E_{FRET}max}}{4} \left(\frac{K_D}{c_0} - \sqrt{\frac{K_D}{c_0} \left(\frac{K_D}{c_0} + 8 \right)} + 4 \right) \tag{A.14}$$

Bibliography

[1] W. Schmidt: *Bluelight Physiology*. Bioscience **34**, 698 (1984).

[2] S. Poggioli: *Della influenza che ha il raggio magnetico sulla vegetatione delle piante*. Bol. – Coi Tipi di Annesio Nobili Opusc Sci. Fasc I 9–23 (1817).

[3] J. Sachs: *Wirkungen farbigen Lichts auf Pflanzen*. Bot. Zeitung **22**, 353 (1864).

[4] C. Darwin: *The Power of Movement in Plants*. London, UK (1880).

[5] W. R. Briggs. *BLUE/UV-A RECEPTORS: HISTORICAL OVERVIEW*, 171–197. Springer Netherlands, Dordrecht (2006).

[6] M. Ahmad und A. R. Cashmore: *HY4 gene of A. thaliana encodes a protein with characteristics of a blue-light photoreceptor*. Nature **366**, 162 (1993).

[7] E. Huala, P. W. Oeller, E. Liscum *et al.*: *Arabidopsis NPH1: A Protein Kinase with a Putative Redox-Sensing Domain*. Science **278**, 2120 (1997).

[8] J. M. Christie, P. Reymond, G. K. Powell *et al.*: *Arabidopsis NPH1: A Flavoprotein with the Properties of a Photoreceptor for Phototropism*. Science **282**, 1698 (1998).

[9] S. Masuda und C. E. Bauer: *AppA is a blue light photoreceptor that antirepresses photosynthesis gene expression in Rhodobacter sphaeroides*. Cell **110**, 613 (2002).

[10] W. R. Briggs und J. M. Christie: *Phototropins 1 and 2: versatile plant blue-light receptors*. Trends Plant Sci. **7**, 204 (2002).

[11] J. A. Jarillo, H. Gabrys, J. Capel *et al.*: *Phototropin-related NPL1 controls chloroplast relocation induced by blue light*. Nature **410**, 952 (2001).

[12] M. Iseki, S. Matsunaga, A. Murakami *et al.*: *A blue-light-activated adenylyl cyclase mediates photoavoidance in Euglena gracilis*. Nature **415**, 1047 (2002).

[13] K. Huang, T. Merkle, und C. F. Beck: *Isolation and characterization of a Chlamydomonas gene that encodes a putative blue-light photoreceptor of the phototropin family*. Physiol. Plant. **115**, 613 (2002).

[14] A. C. Froehlich, Y. Liu, J. J. Loros *et al.*: *White Collar-1, a circadian blue light photoreceptor, binding to the frequency promoter*. Science **297**, 815 (2002).

[15] R. Kort, W. D. Hoff, M. Van West *et al.*: *The xanthopsins: a new family of eubacterial blue-light photoreceptors*. EMBO J. **15**, 3209 (1996).

[16] M. Gomelsky und G. Klug: *BLUF: a novel FAD-binding domain involved in sensory transduction in microorganisms*. Trends Biochem. Sci. **27**, 497 (2002).

[17] J. M. Christie, M. Salomon, K. Nozue *et al.*: *LOV (light, oxygen, or voltage) domains of the blue-light photoreceptor phototropin (nph1): Binding sites for the chromophore flavin mononucleotide*. Proc. Natl. Acad. Sci. **96**, 8779 (1999).

[18] D. E. Somers, T. F. Schultz, M. Milnamow *et al.*: *ZEITLUPE Encodes a Novel Clock-Associated PAS Protein from Arabidopsis*. Cell **101**, 319 (2000).

[19] D. J. Kliebenstein, J. E. Lim, L. G. Landry *et al.*: *Arabidopsis UVR8 Regulates Ultraviolet-B Signal Transduction and Tolerance and Contains Sequence Similarity to Human Regulator of Chromatin Condensation 1*. Plant Physiol. **130**, 234 (2002).

[20] P. H. Quail, M. T. Boylan, B. M. Parks *et al.*: *Phytochromes: Photosensory Perception and Signal Transduction*. Science **268**, 675 (1995).

[21] J. L. Spudich, C.-S. Yang, K.-H. Jung *et al.*: *Retinylidene Proteins: Structures and Functions from Archaea to Humans*. Annu. Rev. Cell Dev. Biol. **16**, 365 (2000).

[22] B. L. Taylor und I. B. Zhulin: *PAS Domains: Internal Sensors of Oxygen, Redox Potential, and Light*. Microbiol. Mol. Biol. Rev. **63**, 479 (1999).

[23] S. M. Harper, L. C. Neil, und K. H. Gardner: *Structural Basis of a Phototropin Light Switch*. Science **301**, 1541 (2003).

[24] M. H. Hefti, K.-J. Françoijs, S. C. de Vries *et al.*: *The PAS fold*. Eur. J. Biochem. **271**, 1198 (2004).

[25] A. Losi und W. Gärtner: *Solving Blue-light Riddles: New Lessons from Flavin-binding LOV Photoreceptors*. Photochem. Photobiol. (2016).

[26] V. Massey: *The Chemical and Biological Versatility of Riboflavin*. Biochem. Soc. Trans. **28**, 283 (2000).

[27] T. Tomiki und N. Saitou: *Phylogenetic Analysis of Proteins Associated in the Four Major Energy Metabolism Systems: Photosynthesis, Aerobic Respiration, Denitrification, and Sulfur Respiration*. J. Mol. Evol. **59**, 158 (2004).

[28] E. Herman, M. Sachse, P. G. Kroth *et al.*: *Blue-Light-Induced Unfolding of the Jα Helix Allows for the Dimerization of Aureochrome-LOV from the Diatom Phaeodactylum tricornutum*. Biochemistry **52**, 3094 (2013).

[29] J. P. Zayner und T. R. Sosnick: *Factors that control the chemistry of the LOV domain photocycle*. PLoS One **9**, e87074 (2014).

[30] T. Kottke, J. Heberle, D. Hehn *et al.*: *Phot-LOV1: Photocycle of a Blue-Light Receptor Domain from the Green Alga Chlamydomonas reinhardtii*. Biophys. J. **84**, 1192 (2003).

[31] B. Kopka, K. Magerl, A. Savitsky *et al.*: *Reengineering flavin photochemistry: Electron and proton transfer pathways in a light, oxygen, voltage (LOV) photoreceptor devoid of the photoactive cysteine - ready to submit* (2017).

[32] S. Crosson und K. Moffat: *Structure of a flavin-binding plant photoreceptor domain: Insights into light-mediated signal transduction*. Proc. Natl. Acad. Sci. **98**, 2995 (2001).

[33] J. T. M. Kennis, S. Crosson, M. Gauden *et al.*: *Primary reactions of the LOV2 domain of phototropin, a plant blue-light photoreceptor*. Biochemistry **42**, 3385 (2003).

[34] T. E. Swartz, S. B. Corchnoy, J. M. Christie *et al.*: *The Photocycle of a Flavin-binding Domain of the Blue Light Photoreceptor Phototropin*. J. Biol. Chem. **276**, 36493 (2001).

[35] E. Schleicher, R. M. Kowalczyk, C. W. M. Kay *et al.*: *On the reaction mechanism of adduct formation in LOV domains of the plant blue-light receptor phototropin*. J. Am. Chem. Soc. **126**, 11067 (2004).

[36] K. Lanzl, M. v. Sanden-Flohe, R.-J. Kutta *et al.*: *Photoreaction of mutated LOV photoreceptor domains from Chlamydomonas reinhardtii with aliphatic mercaptans: implications for the mechanism of wild type LOV*. Phys. Chem. Chem. Phys. **12**, 6594 (2010).

[37] C. Bauer, C.-R. Rabl, J. Heberle *et al.*: *Indication for a radical intermediate preceding the signaling state in the LOV domain photocycle*. Photochem. Photobiol. **87**, 548 (2011).

[38] S. Crosson und K. Moffat: *Photoexcited Structure of a Plant Photoreceptor Domain Reveals a Light-Driven Molecular Switch*. Plant Cell Online **14**, 1067 (2002).

[39] D. Nozaki, T. Iwata, T. Ishikawa *et al.*: *Role of Gln1029 in the Photoactivation Processes of the LOV2 Domain in Adiantum Phytochrome3*. Biochemistry **43**, 8373 (2004).

[40] D. Matsuoka, T. Iwata, K. Zikihara *et al.*: *Primary Processes During the Light-signal Transduction of Phototropin*. Photochem. Photobiol. **83**, 122 (2007).

[41] A. I. Nash, W.-H. Ko, S. M. Harper *et al.*: *A conserved glutamine plays a central role in LOV domain signal transmission and Its duration*. Biochemistry **47**, 13842 (2008).

[42] B. D. Zoltowski und K. H. Gardner: *Tripping the Light Fantastic: Blue-Light Photoreceptors as Examples of Environmentally Modulated Protein-Protein Interactions*. Biochemistry **50**, 4 (2011).

[43] B. D. Zoltowski, C. Schwerdtfeger, J. Widom *et al.*: *Conformational Switching in the Fungal Light Sensor Vivid*. Science **316**, 1054 (2007).

[44] A. T. Vaidya, C.-H. Chen, J. C. Dunlap *et al.*: *Structure of a light-activated LOV protein dimer that regulates transcription in Neurospora crassa.* Sci. Signal. **4**, ra50 (2011).

[45] K. S. Conrad, C. C. Manahan, und B. R. Crane: *Photochemistry of flavoprotein light sensors.* Nat. Chem. Biol. **10**, 801 (2014).

[46] S. T. Glantz, E. J. Carpenter, M. Melkonian *et al.*: *Functional and topological diversity of LOV domain photoreceptors.* Proc. Natl. Acad. Sci. **113**, E1442 (2016).

[47] R. J. Kutta, K. Magerl, U. Kensy *et al.*: *A search for radical intermediates in the photocycle of LOV domains.* Photochem. Photobiol. Sci. **14**, 288 (2015).

[48] M. H. V. Huynh und T. J. Meyer: *Proton-coupled electron transfer.* Chem. Rev. **107**, 5004 (2007).

[49] V. Dragnea, M. Waegele, S. Balascuta *et al.*: *Time-resolved spectroscopic studies of the AppA blue-light receptor BLUF domain from Rhodobacter sphaeroides.* Biochemistry **44**, 15978 (2005).

[50] M. Gauden, I. H. M. van Stokkum, J. M. Key *et al.*: *Hydrogen-bond switching through a radical pair mechanism in a flavin-binding photoreceptor.* Proc. Natl. Acad. Sci. **103**, 10895 (2006).

[51] S. Masuda: *Light detection and signal transduction in the BLUF photoreceptors.* Plant Cell Physiol. **54**, 171 (2013).

[52] S. Anderson, V. Dragnea, S. Masuda *et al.*: *Structure of a novel photoreceptor, the BLUF domain of AppA from Rhodobacter sphaeroides.* Biochemistry **44**, 7998 (2005).

[53] A. Jung, J. Reinstein, T. Domratcheva *et al.*: *Crystal Structures of the AppA BLUF Domain Photoreceptor Provide Insights into Blue Light-mediated Signal Transduction.* J. Mol. Biol. **362**, 717 (2006).

[54] H. Yuan, V. Dragnea, Q. Wu *et al.*: *Mutational and structural studies of the PixD BLUF output signal that affects light-regulated interactions with PixE.* Biochemistry **50**, 6365 (2011).

[55] K. Okajima, Y. Fukushima, H. Suzuki *et al.*: *Fate Determination of the Flavin Photoreceptions in the Cyanobacterial Blue Light Receptor TePixD (Tll0078).* J. Mol. Biol. **363**, 10 (2006).

[56] C. Bonetti, M. Stierl, T. Mathes *et al.*: *The role of key amino acids in the photoactivation pathway of the Synechocystis Slr1694 BLUF domain.* Biochemistry **48**, 11458 (2009).

[57] T. Mathes, I. H. M. van Stokkum, M. Stierl *et al.*: *Redox modulation of flavin and tyrosine determines photoinduced proton-coupled electron transfer and photoactivation of BLUF photoreceptors.* J. Biol. Chem. **287**, 31725 (2012).

[58] A. A. Gil, A. Haigney, S. P. Laptenok *et al.*: *Mechanism of the AppABLUF Photocycle Probed by Site-Specific Incorporation of Fluorotyrosine Residues: Effect of the Y21 pKa on the Forward and Reverse Ground-State Reactions.* J. Am. Chem. Soc. **138**, 926 (2016).

[59] H. Suzuki, K. Okajima, M. Ikeuchi *et al.*: *LOV-like flavin-cys adduct formation by introducing a cys residue in the BLUF domain of TePixD.* J. Am. Chem. Soc. **130**, 12884 (2008).

[60] C. W. M. Kay, E. Schleicher, A. Kuppig *et al.*: *Blue light perception in plants: Detection and characterization of a light-induced neutral flavin radical in a C450A mutant of phototropin.* J. Biol. Chem. **278**, 10973 (2003).

[61] E. F. Yee, R. P. Diensthuber, A. T. Vaidya *et al.*: *Signal transduction in light–oxygen–voltage receptors lacking the adduct-forming cysteine residue.* Nat. Commun. **6**, 10079 (2015).

[62] A. Lukacs, R. Brust, A. Haigney *et al.*: *BLUF domain function does not require a metastable radical intermediate state.* J. Am. Chem. Soc. **136**, 4605 (2014).

[63] A. Kotaki, M. Naoi, und K. Yagi: *Effect of Proton Donors on the Absorption Spectrum of Flavin Compounds in Apolar Media.* J. Biochem. **68**, 287 (1970).

[64] S. Salzmann, J. Tatchen, und C. M. Marian: *The photophysics of flavins: What makes the difference between gas phase and aqueous solution?.* J. Photochem. Photobiol. A Chem. **198**, 221 (2008).

[65] M. Sakai und H. Takahashi: *One-electron photoreduction of flavin mononucleotide: time-resolved resonance Raman and absorption study.* J. Mol. Struct. **379**, 9 (1996).

[66] F. Müller, M. Brüstlein, P. Hemmerich *et al.*: *Light-Absorption Studies on Neutral Flavin Radicals.* Eur. J. Biochem. **25**, 573 (1972).

[67] T. Kottke, B. Dick, R. Fedorov *et al.*: *Irreversible photoreduction of flavin in a mutated phot-LOV1 domain.* Biochemistry **42**, 9854 (2003).

[68] S.-H. Song, B. Dick, A. Penzkofer *et al.*: *Photo-reduction of flavin mononucleotide to semiquinone form in LOV domain mutants of blue-light receptor phot from Chlamydomonas reinhardtii.* J. Photochem. Photobiol. B Biol. **87**, 37 (2007).

[69] G. Nöll, G. Hauska, P. Hegemann *et al.*: *Redox Properties of LOV Domains: Chemical versus Photochemical Reduction, and Influence on the Photocycle.* ChemBioChem **8**, 2256 (2007).

[70] D. A. Proshlyakov: *UV optical absorption by protein radicals in cytochrome c oxidase.* Biochim. Biophys. Acta - Bioenerg. **1655**, 282 (2004).

[71] J. Torra, A. Burgos-Caminal, S. Endres *et al.*: *Singlet oxygen photosensitisation by the fluorescent protein Pp2FbFP L30M, a novel derivative of Pseu-*

domonas putida flavin-binding Pp2FbFP. Photochem. Photobiol. Sci. **14**, 280 (2015).

[72] T. K. Harris und G. J. Turner: *Structural Basis of Perturbed pKa Values of Catalytic Groups in Enzyme Active Sites*. IUBMB Life **53**, 85 (2002).

[73] R. Anandakrishnan, B. Aguilar, und A. V. Onufriev: *H++ 3.0: Automating pK prediction and the preparation of biomolecular structures for atomistic molecular modeling and simulations*. Nucleic Acids Res. **40**, 537 (2012).

[74] W. Holzer, A. Penzkofer, M. Fuhrmann *et al.*: *Spectroscopic characterization of flavin mononucleotide bound to the LOV1 domain of Phot1 from Chlamydomonas reinhardtii*. Photochem. Photobiol. **75**, 479 (2002).

[75] K. Yagi, N. Ohishi, K. Nishimoto *et al.*: *Effect of hydrogen bonding on electronic spectra and reactivity of flavins*. Biochemistry **19**, 1553 (1980).

[76] R. Fedorov, I. Schlichting, E. Hartmann *et al.*: *Crystal Structures and Molecular Mechanism of a Light-Induced Signaling Switch: The Phot-LOV1 Domain from Chlamydomonas reinhardtii*. Biophys. J. **84**, 2474 (2003).

[77] Schrödinger LCC. *The PyMOL Molecular Graphics System, Version 1.3* (2015).

[78] G. Lüdemann, I. A. Solov'yov, T. Kubar *et al.*: *Solvent driving force ensures fast formation of a persistent and well-separated radical pair in plant cryptochrome*. J. Am. Chem. Soc. **137**, 1147 (2015).

[79] J. J. Warren, J. R. Winkler, und H. B. Gray: *Redox properties of tyrosine and related molecules*. FEBS Lett. **586**, 596 (2012).

[80] S. Y. Reece und D. G. Nocera: *Proton-coupled electron transfer in biology: results from synergistic studies in natural and model systems*. Annu. Rev. Biochem. **78**, 673 (2009).

[81] I. A. Solov'yov, T. Domratcheva, A. R. M. Shahi *et al.*: *Decrypting cryptochrome: Revealing the molecular identity of the photoactivation reaction*. J. Am. Chem. Soc. **134**, 18046 (2012).

[82] I. A. Solov'yov, T. Domratcheva, und K. Schulten: *Separation of photo-induced radical pair in cryptochrome to a functionally critical distance*. Sci. Rep. **4**, 3845 (2014).

[83] R. D. Draper und L. L. Ingraham: *A Potentiometric Study of the Flavin Semiquinone Equilibrium*. Arch. Biochem. Biophys. **125**, 802 (1968).

[84] R. Y. Tsien: *THE GREEN FLUORESCENT PROTEIN*. Annu. Rev. Biochem. **67**, 509 (1998).

[85] D. M. Chudakov, M. V. Matz, S. Lukyanov *et al.*: *Fluorescent Proteins and Their Applications in Imaging Living Cells and Tissues*. Physiol. Rev. **90**, 1103 (2010).

[86] O. Shimomura, F. H. Johnson, und Y. Saiga: *Extraction, Purification and Properties of Aequorin, a Bioluminescent Protein from the Luminous Hydromedusan, Aequorea.* J. Cell. Comp. Physiol. **59**, 223 (1962).

[87] N. C. Shaner, G. H. Patterson, und M. W. Davidson: *Advances in fluorescent protein technology.* J. Cell Sci. **120**, 4247 (2007).

[88] T. Drepper, T. Eggert, F. Circolone *et al.*: *Reporter proteins for in vivo fluorescence without oxygen.* Nat Biotech **25**, 443 (2007).

[89] S. Chapman, C. Faulkner, E. Kaiserli *et al.*: *The photoreversible fluorescent protein iLOV outperforms GFP as a reporter of plant virus infection.* Proc. Natl. Acad. Sci. **105**, 20038 (2008).

[90] X. Shu, V. Lev-Ram, T. J. Deerinck *et al.*: *A Genetically Encoded Tag for Correlated Light and Electron Microscopy of Intact Cells, Tissues, and Organisms.* PLoS Biol **9**, e1001041 (2011).

[91] M. D. Davari, B. Kopka, M. Wingen *et al.*: *Photophysics of the LOV-Based Fluorescent Protein Variant iLOV-Q489K Determined by Simulation and Experiment.* J. Phys. Chem. B **120**, 3344 (2016).

[92] M. Wingen, J. Potzkei, S. Endres *et al.*: *The photophysics of LOV-based fluorescent proteins - new tools for cell biology.* Photochem. Photobiol. Sci. **13**, 875 (2014).

[93] J. M. Christie, K. Hitomi, A. S. Arvai *et al.*: *Structural tuning of the fluorescent protein iLOV for improved photostability.* J. Biol. Chem. **287**, 22295 (2012).

[94] W. Holzer, J. Shirdel, P. Zirak *et al.*: *Photo-induced degradation of some flavins in aqueous solution.* Chem. Phys. **308**, 69 (2005).

[95] M.-F. Jeng und H. J. Dyson: *Direct Measurement of the Aspartic Acid 26 pKa for Reduced Escherichia coli Thioredoxin by 13C NMR.* Biochemistry **35**, 1 (1996).

[96] P. T. Chivers, K. E. Prehoda, B. F. Volkman *et al.*: *Microscopic pKa Values of Escherichia coli Thioredoxin.* Biochemistry **36**, 14985 (1997).

[97] A. Iqbal, F. Gomes-Neto, C. A. Myiamoto *et al.*: *Dissection of the Water Cavity of Yeast Thioredoxin 1: The Effect of a Hydrophobic Residue in the Cavity.* Biochemistry **54**, 2429 (2015).

[98] M. H. M. Olsson, C. R. Søndergaard, M. Rostkowski *et al.*: *PROPKA3: Consistent Treatment of Internal and Surface Residues in Empirical pKa Predictions.* J. Chem. Theory Comput. **7**, 525 (2011).

[99] J. Van Durme, J. Delgado, F. Stricher *et al.*: *A graphical interface for the FoldX forcefield.* Bioinformatics **27**, 1711 (2011).

[100] R. Guerois, J. E. Nielsen, und L. Serrano: *Predicting Changes in the Stability of Proteins and Protein Complexes: A Study of More Than 1000 Mutations.* J. Mol. Biol. **320**, 369 (2002).

[101] Y. Kao, C. Saxena, T. He *et al.*: *Ultrafast Dynamics of Flavins in Five Redox States Ultrafast Dynamics of Flavins in Five Redox States.* J. Am. Chem. Soc. **130**, 13132 (2008).

[102] D. V. Bent und E. Hayon: *Excited State Chemistry of Aromatic Amino Acids and Related Peptides. I. Tyrosine.* J. Am. Chem. Soc. **97**, 2599 (1975).

[103] C. Aubert, P. Mathis, A. P. M. Eker *et al.*: *Intraprotein electron transfer between tyrosine and tryptophan in DNA photolyase from Anacystis nidulans.* Proc. Natl. Acad. Sci. **96**, 5423 (1999).

[104] S. Solar, N. Gtoff, P. S. Surdhar *et al.*: *Oxidation of Tryptophan and N-Methylindole by N3*, Br2*-, and (SCN)2*- Radicals in Light- and Heavy-Water Solutions: A Pulse Radiolysis Study.* J. Phys. Chem. **95**, 3639 (1991).

[105] H. Li, T. B. Melø, und K. Razi Naqvi: *Triplets, radical cations and neutral semiquinone radicals of lumiflavin and riboflavin: An overhaul of previous pump-probe data and new multichannel absolute absorption spectra.* J. Photochem. Photobiol. B Biol. **106**, 34 (2012).

[106] P. F. Heelis, B. J. Parsons, G. O. Phillips *et al.*: *A laser flash photolysis study of the nature of flavin mononucleotide triplet states and the reactions of the neutral form with amino acids.* Photochem. Photobiol. **28**, 169 (1978).

[107] M. Z. Hoffman und E. Hayon: *Pulse radiolysis study of sulfhydryl compounds in aqueous solution.* J. Phys. Chem. **77**, 990 (1973).

[108] X. Liu, L. Jiang, J. Li *et al.*: *Significant expansion of fluorescent protein sensing ability through the genetic incorporation of superior photo-induced electron-transfer quenchers.* J. Am. Chem. Soc. **136**, 13094 (2014).

[109] C. W. M. Kay, R. Feicht, K. Schulz *et al.*: *EPR, ENDOR, and TRIPLE Resonance Spectroscopy on the Neutral Flavin Radical in Escherichia coli DNA Photolyase.* Biochemistry **38**, 16740 (1999).

[110] G. Bleifuss, M. Kolberg, S. Pötsch *et al.*: *Tryptophan and Tyrosine Radicals in Ribonucleotide Reductase: A Comparative High-Field EPR Study at 94 GHz.* Biochemistry **40**, 15362 (2001).

[111] F. Lendzian, M. Sahlin, F. MacMillan *et al.*: *Electronic Structure of Neutral Tryptophan Radicals in Ribonucleotide Reductase Studied by EPR and ENDOR Spectroscopy.* J. Am. Chem. Soc. **118**, 8111 (1996).

[112] R. Pogni, M. C. Baratto, S. Giansanti *et al.*: *Tryptophan-Based Radical in the Catalytic Mechanism of Versatile Peroxidase from Bjerkandera adusta.* Biochemistry **44**, 4267 (2005).

[113] R. Pogni, M. C. Baratto, C. Teutloff *et al.*: *A Tryptophan Neutral Radical in the Oxidized State of Versatile Peroxidase from Pleurotus eryngii: A COMBINED MULTIFREQUENCY EPR AND DENSITY FUNCTIONAL THEORY STUDY.* J. Biol. Chem. **281**, 9517 (2006).

[114] T. Takui, K. Sato, D. Shiomi *et al.*: *FT Pulsed ESR/Electron Spin Transient Nutation (ESTN) Spec-Troscopy Applied to High-Spin Systems in Solids; Direct Evi-Dence of a Topologically Controlled High-Spin Polymer as Models for Quasi ID Organic Ferro-and Superpara-Magnets*. Mol. Cryst. Liq. Cryst. **279**, 155 (1996).

[115] D. M. Murphy: *Principles of pulse electron paramagnetic resonance. By A Schweiger and G Jeschke, Oxford University Press, UK, 2001, 578 pp. ISBN 0 19 850634 1*. J. Chem. Technol. Biotechnol. **79**, 103 (2004).

[116] D. Immeln, A. Weigel, T. Kottke *et al.*: *Primary Events in the Blue Light Sensor Plant Cryptochrome: Intraprotein Electron and Proton Transfer Revealed by Femtosecond Spectroscopy*. J. Am. Chem. Soc. **134**, 12536 (2012).

[117] K. Maeda, A. J. Robinson, K. B. Henbest *et al.*: *Magnetically sensitive light-induced reactions in cryptochrome are consistent with its proposed role as a magnetoreceptor*. Proc. Natl. Acad. Sci. **109**, 4774 (2012).

[118] T. Langenbacher, D. Immeln, B. Dick *et al.*: *Microsecond light-induced proton transfer to flavin in the blue light sensor plant cryptochrome*. J. Am. Chem. Soc. **131**, 14274 (2009).

[119] I. Chaves, R. Pokorny, M. Byrdin *et al.*: *The Cryptochromes: Blue Light Photoreceptors in Plants and Animals*. Annu. Rev. Plant Biol. **62**, 335 (2011).

[120] T. J. Wheeler, J. Clements, und R. D. Finn: *Skylign: a tool for creating informative, interactive logos representing sequence alignments and profile hidden Markov models*. BMC Bioinformatics **15**, 7 (2014).

[121] A. S. Halavaty und K. Moffat: *N- and C-terminal flanking regions modulate light-induced signal transduction in the LOV2 domain of the blue light sensor phototropin 1 from Avena sativa*. Biochemistry **46**, 14001 (2007).

[122] A. I. Nash, R. McNulty, M. E. Shillito *et al.*: *Structural basis of photosensitivity in a bacterial light-oxygen-voltage/helix-turn-helix (LOV-HTH) DNA-binding protein*. Proc. Natl. Acad. Sci. **108**, 9449 (2011).

[123] B. D. Zoltowski und B. R. Crane: *Light activation of the LOV protein vivid generates a rapidly exchanging dimer*. Biochemistry **47**, 7012 (2008).

[124] E. Herman und T. Kottke: *Allosterically Regulated Unfolding of the A'α Helix Exposes the Dimerization Site of the Blue-Light-Sensing Aureochrome-LOV Domain*. Biochemistry **54**, 1484 (2015).

[125] A. Möglich und K. Moffat: *Structural Basis for Light-dependent Signaling in the Dimeric LOV Domain of the Photosensor YtvA*. J. Mol. Biol. **373**, 112 (2007).

[126] M. Kasahara, M. Torii, A. Fujita *et al.*: *FMN Binding and Photochemical Properties of Plant Putative Photoreceptors Containing Two LOV Domains, LOV/LOV Proteins*. J. Biol. Chem. **285**, 34765 (2010).

[127] N. Suetsugu, F. Mittmann, G. Wagner *et al.*: *A chimeric photoreceptor gene, NEOCHROME, has arisen twice during plant evolution.* Proc. Natl. Acad. Sci. **102**, 13705 (2005).

[128] E. Kaiserli, S. Sullivan, M. A. Jones *et al.*: *Domain Swapping to Assess the Mechanistic Basis of Arabidopsis Phototropin 1 Receptor Kinase Activation and Endocytosis by Blue Light.* Plant Cell **21**, 3226 (2009).

[129] J. M. Christie, T. E. Swartz, R. A. Bogomolni *et al.*: *Phototropin LOV domains exhibit distinct roles in regulating photoreceptor function.* Plant J. **32**, 205 (2002).

[130] D. Matsuoka und S. Tokutomi: *Blue light-regulated molecular switch of Ser/Thr kinase in phototropin.* Proc. Natl. Acad. Sci. **102**, 13337 (2005).

[131] H.-Y. Cho, T.-S. Tseng, E. Kaiserli *et al.*: *Physiological Roles of the Light, Oxygen, or Voltage Domains of Phototropin 1 and Phototropin 2 in Arabidopsis.* Plant Physiol. **143**, 517 (2007).

[132] S. M. Harper, J. M. Christie, und K. H. Gardner: *Disruption of the LOV-Jα Helix Interaction Activates Phototropin Kinase Activity.* Biochemistry **43**, 16184 (2004).

[133] H. Guo, T. Kottke, P. Hegemann *et al.*: *The phot LOV2 domain and its interaction with LOV1.* Biophys. J. **89**, 402 (2005).

[134] K. Okajima: *Molecular mechanism of phototropin light signaling.* J. Plant Res. **129**, 149 (2016).

[135] M. Salomon, U. Lempert, und W. Rüdiger: *Dimerization of the plant photoreceptor phototropin is probably mediated by the LOV1 domain.* FEBS Lett. **572**, 8 (2004).

[136] M. Nakasako, T. Iwata, D. Matsuoka *et al.*: *Light-Induced Structural Changes of LOV Domain-Containing Polypeptides from Arabidopsis Phototropin 1 and 2 Studied by Small-Angle X-ray Scattering.* Biochemistry **43**, 14881 (2004).

[137] M. Nakasako, K. Zikihara, D. Matsuoka *et al.*: *Structural Basis of the LOV1 Dimerization of Arabidopsis Phototropins 1 and 2.* J. Mol. Biol. **381**, 718 (2008).

[138] E. Malzahn, S. Ciprianidis, K. Káldi *et al.*: *Photoadaptation in Neurospora by Competitive Interaction of Activating and Inhibitory LOV Domains.* Cell **142**, 762 (2010).

[139] F. Takahashi, D. Yamagata, M. Ishikawa *et al.*: *AUREOCHROME, a photoreceptor required for photomorphogenesis in stramenopiles.* Proc. Natl. Acad. Sci. **104**, 19625 (2007).

[140] U. Heintz und I. Schlichting: *Blue light-induced LOV domain dimerization enhances the affinity of Aureochrome 1a for its target DNA sequence.* Elife **5**, e11860 (2016).

[141] O. Hisatomi, Y. Nakatani, K. Takeuchi *et al.*: *Blue Light-induced Dimerization of Monomeric Aureochrome-1 Enhances Its Affinity for the Target Sequence*. J. Biol. Chem. **289**, 17379 (2014).

[142] Y. Nakatani und O. Hisatomi: *Molecular Mechanism of Photozipper, a Light-Regulated Dimerizing Module Consisting of the bZIP and LOV Domains of Aureochrome-1*. Biochemistry **54**, 3302 (2015).

[143] K. S. Conrad, A. M. Bilwes, und B. R. Crane: *Light-induced subunit dissociation by a light-oxygen-voltage domain photoreceptor from Rhodobacter sphaeroides*. Biochemistry **52**, 378 (2013).

[144] R. J. Kutta, E. S. A. Hofinger, H. Preuss *et al.*: *Blue-Light Induced Interaction of LOV Domains from Chlamydomonas reinhardtii*. ChemBioChem **9**, 1931 (2008).

[145] K. Okajima, Y. Aihara, Y. Takayama *et al.*: *Light-induced Conformational Changes of LOV1 (Light Oxygen Voltage-sensing Domain 1) and LOV2 Relative to the Kinase Domain and Regulation of Kinase Activity in Chlamydomonas Phototropin*. J. Biol. Chem. **289**, 413 (2014).

[146] E. Gaviola und P. Pringsheim: *Über den Einfluß der Konzentration auf die Polarisation der Fluoreszenz von Farbstofflösungen*. Zeitschrift für Phys. **24**, 24 (1924).

[147] T. Förster: *Zwischenmolekulare Energiewanderung und Fluoreszenz*. Ann. Phys. **437**, 55 (1948).

[148] P. G. Wu und L. Brand: *Resonance Energy Transfer: Methods and Applications*. Anal. Biochem. **218**, 1 (1994).

[149] R. M. Clegg: *Fluorescence resonance energy transfer*. Curr. Opin. Biotechnol. **6**, 103 (1995).

[150] J. R. Lakowicz: *Principles of fluorescence spectroscopy, Third Edition*. Springer US, Boston, MA (1999).

[151] R. Yasuda: *Imaging spatiotemporal dynamics of neuronal signaling using fluorescence resonance energy transfer and fluorescence lifetime imaging microscopy*. Curr. Opin. Neurobiol. **16**, 551 (2006).

[152] I. T. Li, E. Pham, und K. Truong: *Protein biosensors based on the principle of fluorescence resonance energy transfer for monitoring cellular dynamics*. Biotechnol. Lett. **28**, 1971 (2006).

[153] T. Förster: *Experimentelle und theoretische Untersuchung des zwischenmolekularen Übergangs von Elektronenanregungsenergie*. Zeitschrift für Naturforsch. A **4**, 321 (1949).

[154] T. Főrster: *10th Spiers Memorial Lecture. Transfer mechanisms of electronic excitation*. Discuss. Faraday Soc. **27**, 7 (1959).

[155] R. M. Clegg. *The History of Fret*, 1–45. Springer US, Boston, MA (2006).

[156] A. Periasamy und R. N. Day (Hg.): *Molecular imaging: FRET microscopy and spectroscopy*. Oxford University Press, Inc. (2005).

[157] L. a. Ernst, R. K. Gupta, R. B. Mujumdar *et al.*: *Cyanine dye labeling reagents for sulfhydryl groups*. Cytometry **10**, 3 (1989).

[158] R. B. Mujumdar, L. a. Ernst, S. R. Mujumdar *et al.*: *Cyanine dye labeling reagents: sulfoindocyanine succinimidyl esters*. Bioconjug. Chem. **4**, 105 (1993).

[159] A. Toutchkine, P. Nalbant, und K. M. Hahn: *Facile synthesis of thiol-reactive Cy3 and Cy5 derivatives with enhanced water solubility*. Bioconjug. Chem. **13**, 387 (2002).

[160] A.-K. Hendrischk, J. Moldt, S. W. Frühwirth *et al.*: *Characterization of an Unusual LOV Domain Protein in the α-Proteobacterium Rhodobacter sphaeroides*. Photochem. Photobiol. **85**, 1254 (2009).

[161] A.-K. Hendrischk, J. Moldt, S. W. Frühwirth *et al.*: *Characterization of an Unusual LOV Domain Protein in the α-Proteobacterium Rhodobacter sphaeroides*. Photochem. Photobiol. **85**, 1254 (2009).

[162] S. Metz, A. Jäger, und G. Klug: *Role of a short light, oxygen, voltage (LOV) domain protein in blue light- and singlet oxygen-dependent gene regulation in Rhodobacter sphaeroides*. Microbiology **158**, 368 (2012).

[163] D. J. Winzor und H. A. Scheraga: *Studies of Chemically Reacting Systems on Sephadex. I. Chromatographic Demonstration of the Gilbert Theory*. Biochemistry **2**, 1263 (1963).

[164] F. J. Stevens: *Analysis of protein-protein interaction by simulation of small-zone size-exclusion chromatography: application to an antibody-antigen association*. Biochemistry **25**, 981 (1986).

[165] P. Macheroux: *UV-Visible Spectroscopy as a Tool to Study Flavoproteins*. In G. A. Reid (Hg.): *Flavoprotein Protoc.*, Band 131, Kapitel 1, 1–7. Humana Press Inc., Totowa, New Jersey (1999).

[166] H. J. Gruber, C. D. Hahn, G. Kada *et al.*: *Anomalous Fluorescence Enhancement of Cy3 and Cy3.5 versus Anomalous Fluorescence Loss of Cy5 and Cy7 upon Covalent Linking to IgG and Noncovalent Binding to Avidin*. Bioconjug. Chem. **11**, 696 (2000).

[167] S. Preus, K. Kilså, F.-A. Miannay *et al.*: *FRETmatrix: a general methodology for the simulation and analysis of FRET in nucleic acids*. Nucleic Acids Res. **41**, e18 (2013).

[168] K. Huang und C. F. Beck: *Phototropin is the blue-light receptor that controls multiple steps in the sexual life cycle of the green alga Chlamydomonas reinhardtii*. Proc. Natl. Acad. Sci. **100**, 6269 (2003).

[169] C.-S. Im, S. Eberhard, K. Huang *et al.*: *Phototropin involvement in the expression of genes encoding chlorophyll and carotenoid biosynthesis enzymes and LHC apoproteins in Chlamydomonas reinhardtii.* Plant J. **48**, 1 (2006).

[170] J. Trippens, A. Greiner, J. Schellwat *et al.*: *Phototropin Influence on Eyespot Development and Regulation of Phototactic Behavior in Chlamydomonas reinhardtii.* Plant Cell **24**, 4687 (2012).

[171] A. Pfeifer, T. Mathes, Y. Lu *et al.*: *Blue Light Induces Global and Localized Conformational Changes in the Kinase Domain of Full-Length Phototropin.* Biochemistry **49**, 1024 (2010).

[172] M. A. Jones, K. A. Feeney, S. M. Kelly *et al.*: *Mutational Analysis of Phototropin 1 Provides Insights into the Mechanism Underlying LOV2 Signal Transmission.* J. Biol. Chem. **282**, 6405 (2007).

[173] Y. Aihara, T. Yamamoto, K. Okajima *et al.*: *Mutations in the N-terminal flanking region of the blue-light sensing domain LOV2 disrupt its repressive activity on the kinase domain in the Chlamydomonas phototropin.* J. Biol. Chem. (2012).

[174] M. Carson, D. H. Johnson, H. McDonald *et al.*: *His-tag impact on structure.* Acta Crystallogr. Sect. D **63**, 295 (2007).

[175] H. Qin, J. Hu, Y. Hua *et al.*: *Construction of a series of vectors for high throughput cloning and expression screening of membrane proteins from Mycobacterium tuberculosis.* BMC Biotechnol. **8**, 51 (2008).

[176] O. Kirillova, M. Chruszcz, I. A. Shumilin *et al.*: *An extremely SAD case: Structure of a putative redox-enzyme maturation protein from Archaeoglobus fulgidus at 3.4 A resolution.* Acta Crystallogr. **63**, 348 (2007).

[177] K. A. Majorek, M. L. Kuhn, M. Chruszcz *et al.*: *Double trouble - Buffer selection and his-tag presence may be responsible for nonreproducibility of biomedical experiments.* Protein Sci. **23**, 1359 (2014).

[178] D. Woodcock, P. Crowther, J. Doherty *et al.*: *Quantitative evaluation of Escherichia coli host strains for tolerance to cytosine methylation in plasmid and phage recombinants.* Nucleic Acids Res. **17**, 3469 (1989).

[179] F. W. Studier und B. A. Moffatt: *Use of bacteriophage T7 RNA polymerase to direct selective high-level expression of cloned genes.* J. Mol. Biol. **189**, 113 (1986).

[180] L. Stols, M. Gu, L. Dieckman *et al.*: *A new vector for high-throughput, ligation-independent cloning encoding a tobacco etch virus protease cleavage site.*. Protein Expr. Purif. **25**, 8 (2002).

[181] D. Hanahan: *Studies on transformation of Escherichia coli with plasmids.* J. Mol. Biol. **166**, 557 (1983).

[182] L. Dieckman, M. Gu, L. Stols *et al.*: *High Throughput Methods for Gene Cloning and Expression.* Protein Expr. Purif. **25**, 1 (2002).

[183] U. K. Laemmli: *Cleavage of Structural Proteins during the Assembly of the Head of Bacteriophage T4*. Nature **227**, 680 (1970).

[184] E. J. King und D. M. Campbell: *International enzyme units an attempt at international agreement*. Clin. Chim. Acta **6**, 301 (1961).

[185] R.-J. Kutta, T. Langenbacher, U. Kensy *et al.*: *Setup and performance of a streak camera apparatus for transient absorption measurements in the ns to ms range*. Appl. Phys. B **111**, 203 (2013).

[186] A. Šali und T. L. Blundell: *Comparative Protein Modelling by Satisfaction of Spatial Restraints*. J. Mol. Biol. **234**, 779 (1993).

[187] E. Lindahl, B. Hess, und D. van der Spoel: *GROMACS 3.0: a package for molecular simulation and trajectory analysis*. Mol. Model. Annu. **7**, 306 (2001).

[188] T. A. Soares, X. Daura, C. Oostenbrink *et al.*: *Validation of the GROMOS force-field parameter set 45A3 against nuclear magnetic resonance data of hen egg lysozyme*. J. Biomol. NMR **30**, 407 (2004).

[189] N. Todorova, F. S. Legge, H. Treutlein *et al.*: *Systematic Comparison of Empirical Forcefields for Molecular Dynamic Simulation of Insulin*. J. Phys. Chem. B **112**, 11137 (2008).

[190] D. Frenkel und B. Smit: *Understanding molecular simulation: from algorithms to applications*, Band 1. Academic press (2002).

[191] E. Peter, B. Dick, und S. A. Baeurle: *Mechanism of signal transduction of the LOV2-Jα photosensor from Avena sativa*. Nat. Commun. **1**, 122 (2010).

[192] K. Magerl, I. Stambolic, und B. Dick: *Switching from adduct formation to electron transfer in a light-oxygen-voltage domain containing the reactive cysteine - under review*. Phys. Chem. Chem. Phys. (2017).

Vielen Dank

Die vorliegende Arbeit wurde erst durch die Unterstützung und Hilfe möglich, die mir von vielen Seiten entgegengebracht worden ist. Dafür möchte ich mich bei allen aus tiefstem Herzen bedanken.

Mein besonderer Dank gilt Herrn Prof. Dr. Bernhard Dick für die Möglichkeit, meine Dissertation an seinem Lehrstuhl anzufertigen, die Überlassung des spannenden Themas, die intensive Betreuung, die vielen anregenden und interessanten Diskussionen und die stete Förderung des eigenständigen, wissenschaftlichen Denkens und Arbeitens.

Des Weiteren gilt mein Dank PD Dr. Tilman Kottke für die Übernahme des Zweitgutachtens, seinem Interesse an meiner Forschung und interessante und hilfreiche Diskussionen.

Ich bedanke mich bei Joachim Herman für die exzellente technische Assistenz, das unermüdliche Exprimieren und Aufreinigen von Proteinen und seinen großen Einsatz. In diesem Zusammenhang möchte ich mich auch bei den Mitgliedern des Lehrstuhls für Pharmazeutische und Medizinische Chemie II für die Benutzung ihrer Ultrazentrifuge und die große Hilfsbereitschaft bei fehlender Gerätschaft und Chemikalien und bei Problemen aller Art im (Bio)Laboralltag bedanken.

Ganz herzlich möchte ich mich bei Herrn Dr. Ulrich Krauß vom IMET am Forschungszentrum Jülich bedanken für die gute Zusammenarbeit beim iLOV Projekt, für die stete Hilfe bei biologischen Fragen und Problemen, für die vielen Diskussionen und die schönen Zeiten auf Konferenzen.

I would like to thank Prof. Carey K. Johnson and his group at the University of Kansas for the good collaboration including our transatlantic Skype-meetings and the opportunity to spend a research stay at his lab in Lawrence, KS.

My special thanks to Ivan Stambolic for the performance and analysis of the MD simulations, uncountable discussions about LOV domains and the good collaboration.

Mein Dank gilt Herrn Prof. Dr. Alkwin Slenzcka für die großzügige Nutzung seines Raman-Spektrographen für meine Messungen und die technische Unterstützung.

Ich bedanke mich bei der Arbeitsgruppe von Prof. Dr. Hartmut Yersin, im Speziellen bei Dr. N.-Larisa Mataranga-Popa, Dr. Thomas Hofbeck und Dr. Markus Leitl, für die große Hilfsbereitschaft bei Emissionsmessungen und organischer Synthese.

Eduard Hochmuth vom Lehrstuhl für Biochemie I (RNA-Biologie) danke ich für die Durchführung der Massenspektren meiner gelabelten LOV Domänen.

Ich bedanke mich bei Veronika Kropf vom Lehrstuhl für Biophysik für die Unterstützung bei den SEC-Messungen. In diesem Zusammenhang danke ich ebenfalls Florian Semmelmann vom Lehrstuhl für Biochemie II für seine Unterstützung bei SEC-Messungen, Stopped-Flow Messungen und seine stete Hilfsbereitschaft.

Mein Dank gilt allen momentanen und ehemaligen Mitgliedern des Lehrstuhls für Physikalische und Theoretische Chemie für die gute Zusammenarbeit, die entspannte Atmosphäre während all den Jahren, die fachlichen und nicht fachlichen Diskussionen und die Freundschaften, die daraus entstanden sind. Besonders bedanken möchte ich mich bei Fabian Brandl und Uwe Faltermeier für die gute Zusammenarbeit im Spektroskopielabor und die stete Hilfe bei technischen Problemen aller Art. Roger Kutta gilt mein Dank für die Unterstützung in der Anfangsphase meiner Promotion, für die vielen fachlichen Diskussionen und Anregungen und besonders die "freaky fridays".

Ich bedanke mich bei allen nicht-wissenschaftichen Mitarbeitern des Lehrstuhls für Physikalische und Theoretische Chemie für die gute Zusammenarbeit. Mein besonderer Dank gilt Andrea Nömeier für die Unterstützung bei allen administrativen Belangen, Madlene von Sanden für die technische Assistenz und Klaus Ziereis für den IT-Support.

Ich danke dem Graduiertenkolleg 1626 "Chemische Photokatalyse" für die Förderung meiner wissenschaftlichen Arbeit während meiner Promotion und die Möglichkeit, an Konferenzen und Tagungen teilzunehmen und meine Kenntnisse im Bereich Photokatalyse über den eigenen Tellerrand hinaus zu erweitern.

I would like to thank Ivan Stambolic and Dr. N.-Larisa Mataranga-Popa for their friendship, their support during the demanding phases of my PhD time, the coffee breaks and the good time over the years.

Ich danke meinen Leidensgenossinnen Hanna Bartling, Franziska Fendt, Veronika Kropf und Carina Koch. Eure Freundschaft hat unsere gemeinsame Studien- und Promotionszeit sehr bereichert.

Mein weiterer Dank gilt der Rakete für die unzähligen fachlichen und nicht-fachlichen Diskussionen, den guten Draht zur Physik-Fakultät, K & K, die schönen gemeinsamen Erlebnisse, die gemeinsamen Durststrecken und eure jahrelange Freundschaft.

Besonders möchte ich meinen Eltern danken. Sie haben mich während des Chemiestudiums und der Promotion immer bedingungslos unterstützt, dadurch vieles erst möglich gemacht und mich auch in schwierigen Zeiten motiviert.

Aus tiefstem Herzen möchte ich mich bei Dieter Vogel bedanken für seine stete Unterstützung, für seine Motivation in guten und besonders in schlechten Zeiten, für seine Rücksichtnahme in den letzten Monaten, fürs Korrekturlesen und all die kleinen und großen Momente in den letzten Jahren, die ohne ihn nicht möglich gewesen wären.